

- 6 138 518 95

U.O.V.S. BIBLIOTEK

o i a t T

HIERDIE EKSEMPLAAR MAG ONDER
GEEN OMSTANDIGHEDE UIT DIE
BIBLIOTEK VERWYDER WORD NIE



University Free State

34300000427603

Universiteit Vrystaat

**THE CHARACTERISATION AND KINETIC STUDY OF
RHODIUM(I) AND IRIDIUM(I) TRIAZOLE
COMPLEXES.**

A thesis submitted to meet the requirements for the degree of

Magister Scientiae

in the

**Department of Chemistry
Faculty of Science**

at the

University of the Orange Free State

by

Alfred Johannes Muller

Supervisor

Prof. S.S. Basson

Co-Supervisor

Prof. W. Purcell

November 2000

Acknowledgements

My utmost gratitude to God Almighty who gave me the strength and courage with which this project was executed.

I would also like to thank to following people:

My supervisor, Prof. S.S. Basson and co-supervisor, Prof. W. Purcell for their great ideas and the keen interest they showed towards this project. Their valuable time devoted in helping out in difficult circumstances in the course of this study is very highly appreciated. I am grateful for what I have learnt through this experience.

My warm gratitude to many members of the Chemistry Department, such as Prof. A. Roodt, fellow postgraduate students, especially people like Dr. Fanie Otto, Mr. Hendrik Engelbrecht for their friendship and contribution to the NMR studies.

I thank my mother and entire family for their valuable encouragement, understanding, generous and tireless support throughout the study. Words will never be sufficient to express my gratitude in this regard.

Joanine for her love, patience and motivation through the course of this study.

A. Muller.

*I've never been afraid of failing,
only in failing to try and try again.*

Gary Player

Contents

List of Tables.

List of Figures.

Abbreviations.

CHAPTER 1 – General overview.

1.	Introduction.	1
2.	Research review.	5
3.	Aim of this study.	10

CHAPTER 2 – Oxidative addition reactions.

1.	Introduction.	12
2.	General overview.	12
3.	The mechanism of oxidative addition.	18
3.1	One-electron oxidative addition mechanism.	20
3.2	Two-electron oxidative addition mechanism.	24
	a) The one-step concerted mechanism.	24
	b) The two-step S_N2 mechanism.	29
	c) The ionic mechanism.	34

CONTENTS

4.	Factors influencing oxidative addition.	35
	a) The metal.	36
	b) The bonded ligands.	38
	Electronic effects.	38
	Steric effects.	43
	c) The bidentate ligand.	46
	d) The added molecule.	50
	e) The effect of a solvent.	52
	The effect of a solvent on the rate of oxidative addition reactions.	52
	The influence of solvents on the stereochemistry of oxidative addition.	55
	The influence of solvent in the mechanism of oxidative addition.	56
	The influence of solvent on the product composition of oxidative addition.	57
	f) The catalytic effect of halogen ions on the rate of oxidative addition.	59
	g) The influence of neighbouring groups on the rate of oxidative addition.	60

CHAPTER 3 - Synthesis and Characterisation of the ligands and complexes.

1.	Introduction.	62
----	---------------	----

CONTENTS

2.	Synthesis of the ligands hbpt and bpt-NH ₂ .	62
	a) Synthesis of 3,6-di(pyridin-2-yl)-1,2-dihydro-1,2,4,5-tetrazine (bptz).	65
	b) Synthesis of 4-Amino-3,5-bis(pyridin-2-yl)-1,2,4-triazole (bpt-NH ₂).	65
	c) Synthesis of 3,5-bis(pyridin-2-yl)-1,2,4-triazole (hbpt).	66
3.	Synthesis of the starting metal complexes.	71
	a) Synthesis of bis-[η^4 -cyclo octa-1,5-diene- μ -chloroiridium(I)].	71
	b) Synthesis of bis-[η^4 -cyclo octa-1,5-diene- μ -chlororhodium(I)].	76
4.	Synthesis of [M(bpt-NH)(cod)] and [M(bpt)(cod)].	80
	a) Synthesis of [Ir(bpt)(cod)].	80
	b) Synthesis of [Ir(bpt-NH)(cod)].	82
	c) Synthesis of [Rh(bpt)(cod)].	83
	d) Synthesis of [Rh(bpt-NH)(cod)].	84
5.	Synthesis of [M(bpt-NH)(cod)(CH ₃)(I)] and [M(bpt)(cod)(CH ₃)(I)].	94
	a) Synthesis of [Ir(bpt)(cod)(CH ₃)(I)].	94
	b) Synthesis of [Ir(bpt-NH)(cod)(CH ₃)(I)].	95
	c) Synthesis of [Rh(bpt)(cod)(CH ₃)(I)].	95
	d) Synthesis of [Rh(bpt-NH)(cod)(CH ₃)(I)].	96
6.	Discussion.	106

CONTENTS

CHAPTER 4 - The oxidative addition kinetics of CH₃I with [M(LL')(cod)].

1.	Introduction.	108
2.	Theoretical Principles.	108
	a) Basic concepts.	109
	b) Activation enthalpy and entropy.	111
3.	Experimental.	113
4.	Kinetic Results.	115
	a) Kinetic investigation of the oxidative addition between CH ₃ I and [Ir(bpt)(cod)].	116
	b) Kinetic investigation of the oxidative addition between CH ₃ I and [Ir(bpt-NH)(cod)].	118
	c) Kinetic investigation of the oxidative addition between CH ₃ I and [Rh(bpt)(cod)].	120
	d) Kinetic investigation of the oxidative addition between CH ₃ I and [Rh(bpt-NH)(cod)].	121
5.	Discussion.	124
	a) The influence of the solvent.	124
	b) The influence of the bidentate ligands and the metal atom.	125
	c) The implication of the activation parameters.	127

CONTENTS

ADDENDUM A – Supplementary kinetic aspects.	129
ADDENDUM B – Purification of Solvents.	135
SUMMARY.	137
OPSOMMING.	139

List of Tables

Table 1 : A short summary of the substitution reactions investigated in this laboratory on rhodium(I) and iridium(I) complexes.	6
Table 2 : A summary of the oxidative addition reactions done on complexes of the type $[\text{Rh}(\text{LL}')(\text{CO})(\text{PPh}_3)]$, $[\text{Rh}(\text{LL}')(\text{PX}_3)]$ and $[\text{Ir}(\text{LL}')(\text{cod})]$ in this laboratory.	7
Table 3 : A list of molecules which can be used in oxidative addition reactions.	15
Table 4 : Experimental data for the oxidative addition of CH_3I to $[\text{Rh}(\text{acac})(\text{CO})(\text{PX}_3)]$.	42
Table 5 : Comparison of the effect of electronic and steric parameters on the rate of oxidative addition induced by different phosphine ligands.	46
Table 6 : Summary of the different substituents on different β -diketones and their pK_a values.	48
Table 7 : Experimental results for the oxidative addition of CH_3I with different $[\text{Rh}(\beta\text{-diketone})(\text{CO})(\text{PPh}_3)]$ complexes in acetone at 25°C .	48
Table 8 : Influence of different donor atoms on the rate of oxidative addition between $[\text{Ir}(\text{LL}')(\text{cod})]$ and CH_3I .	49
Table 9 : The different classes of oxidative addition reagents X-Y.	50
Table 10 : The influence of solvent on the rate of oxidative addition in the reaction between $[\text{Rh}(\text{tfaa})(\text{CO})(\text{PPh}_3)]$ and CH_3I .	53
Table 11 : The influence of solvent on the rate of oxidative addition in the reaction between $[\text{Rh}(\text{cupf})(\text{CO})(\text{PPh}_3)]$ and CH_3I .	55
Table 12 : Summary of the ligands used in this study.	63
Table 13 : Summary of the crystal data of the two structures of $[\text{Ir}(\text{Cl})(\text{cod})]_2$.	72

LIST OF TABLES

Table 14 : Summary of the crystal data of [Rh(Cl)(cod)] ₂ .	77
Table 15 : Summary of the ratio between nitrogen (in the bidentate ligand) and the metal used in the studied complexes.	107
Table 16 : Summary of the kinetic data for the oxidative addition between CH ₃ I and [M(bpt)(cod)] (M = Rh, Ir) in different solvents and temperatures.	124
Table 17 : Summary of the kinetic data for the oxidative addition between CH ₃ I and [Ir(LL')(cod)] with different solvents and ring sizes.	127
Table 18 : Kinetic results for the oxidative addition between CH ₃ I and [Ir(bpt)(cod)] in acetone at different temperatures.	127
Table 19 : Kinetic results for the oxidative addition between CH ₃ I and [Ir(bpt-NH)(cod)] in benzene at different temperatures.	128
Table 20 : Kinetic results for the oxidative addition between CH ₃ I and [Ir(bpt-NH)(cod)] in DCM at different temperatures.	128
Table 21 : Kinetic results for the oxidative addition between CH ₃ I and [Rh(bpt)(cod)] in acetone at different temperatures.	129
Table 22 : Kinetic results for the oxidative addition between CH ₃ I and [Rh(bpt-NH)(cod)] in benzene at different temperatures.	129
Table 23 : Kinetic results for the oxidative addition between CH ₃ I and [Rh(bpt-NH)(cod)] in DCM at different temperatures.	130

List of figures

Figure 1 : Comparison between rhodium and cobalt catalysts used for the synthesis of acetic acid.	3
Figure 2 : A simplified schematic representation of the <i>Cativa</i> catalytic cycle.	4
Figure 3 : Structures of the ligands used in this study with their names and abbreviations.	11
Figure 4 : General representation of two-electron oxidative addition.	14
Figure 5 : Typical oxidative addition reactions to Vaska's complex.	16
Figure 6 : Intramolecular oxidative addition.	17
Figure 7 : Reaction scheme for the oxidative addition reaction of S-(-)- α -phenylbromide and Ph_3PdCO .	19
Figure 8 : Oxidative addition reaction of an acyl halide with PdL_4 ($\text{L} = \text{PPh}_3$).	20
Figure 9 : Proposed radical mechanism between <i>cis</i> - $[\text{Mo}(\text{CO})_2(\text{dmpe})_2]$ and Ph_3CCl .	21
Figure 10 : Competing reaction mechanisms for the oxidative addition reaction of $[\text{Pt}(\text{PEt}_3)_3]$ and an alkyl halide.	23
Figure 11 : Oxidative addition of H_2 to Vaska's complex resulting in a <i>cis</i> product.	25
Figure 12 : A tungsten complex containing a coordinated hydrogen molecule proving that H_2 bonds <i>cis</i> because of its bonding character.	25
Figure 13 : Oxidative addition of $[\text{Rh}(\text{dtc})\text{L}_2]$ and I_2 .	26
Figure 14 : The two-way electron flow in a concerted mechanism.	27
Figure 15 : The three-center (a) and linear (b) transition state used to represent oxidative addition reactions in general.	28

LIST OF FIGURES

Figure 16 : The addition of a polar molecule like CH ₃ I to a square- planar complex.	29
Figure 17 : Representation of the mechanism of S _N 2 two-step oxidative addition and the differences in the polarity of the transition state.	30
Figure 18 : The oxidative addition of an alkyl halide to a variation of Vaska's complex.	32
Figure 19 : The oxidative addition of an alkyl halide to a macrocyclic rhodium(I) complex.	33
Figure 20 : Examples of two variants of the ionic mechanism.	35
Figure 21 : Ability of d ⁸ metal ions of group VIII to undergo oxidative addition and to be five-coordinated.	36
Figure 22 : Electron flow in the reaction between a metal and CO.	39
Figure 23 : Conditions where π-bonding is possible depending on the oxidation state of the metal and the electronegativity of the phosphorous ligands.	41
Figure 24 : Representation for the calculation of the cone angles in symmetrical phosphines.	43
Figure 25 : Representation for the calculation of the cone angles in non-symmetrical phosphines.	44
Figure 26 : General structure of a β-diketone.	46
Figure 27 : Keto-enol tautomerism of β-diketones.	47
Figure 28 : The reaction scheme of the oxidative addition of CH ₃ I and [Rh(cupf)(CO)(PX ₃)].	54
Figure 29 : The reaction of [IrCl(CO)(PPh ₃) ₂] and HX (X = Cl, Br) gives different isomers in different solvents.	56
Figure 30 : Proposed reaction scheme for the oxidative addition reactions of [Ir(LL')(cod)] (LL' = Sacac, tfaa) with CH ₃ I.	57
Figure 31 : The reaction of <i>trans</i> -[IrCl(CO)(PPh ₃) ₂] with acyl azides.	58
Figure 32 : The iodine catalysed iodomethane addition to [Rh(I)(CO)L ₂].	59

LIST OF FIGURES

Figure 33 : The bromide catalysed oxidative addition of iodomethane to [Ir(acac)(cod)].	60
Figure 34 : Electron donation of the oxygen of the methoxy group increases the nucleophilicity on the metal.	61
Figure 35 : Synthesis of the ligands bpt-NH ₂ and hbpt.	64
Figure 36 : NMR spectrum of the ligand bpt-NH ₂ .	67
Figure 37 : IR spectrum of the ligand bpt-NH ₂ .	68
Figure 38 : NMR spectrum of the ligand hbpt.	69
Figure 39 : IR spectrum of the ligand hbpt.	70
Figure 40 : Structure of [Ir(Cl)(cod)] ₂ .	72
Figure 41 : NMR spectrum of the complex [Ir(Cl)(cod)] ₂ .	74
Figure 42 : IR spectrum of the complex [Ir(Cl)(cod)] ₂ .	75
Figure 43 : Structure of [Rh(Cl)(cod)] ₂ .	76
Figure 44 : NMR spectrum of the complex [Rh(Cl)(cod)] ₂ .	78
Figure 45 : IR spectrum of the complex [Rh(Cl)(cod)] ₂ .	79
Figure 46 : Synthetic route of the complexes [M(bpt-NH)(cod)] and [M(bpt)(cod)].	81
Figure 47 : NMR spectrum of the complex [Ir(bpt)(cod)].	86
Figure 48 : IR spectrum of the complex [Ir(bpt)(cod)].	87
Figure 49 : NMR spectrum of the complex [Ir(bpt-NH)(cod)].	88
Figure 50 : IR spectrum of the complex [Ir(bpt-NH)(cod)].	89
Figure 51 : NMR spectrum of the complex [Rh(bpt)(cod)].	90
Figure 52 : IR spectrum of the complex [Rh(bpt)(cod)].	91
Figure 53 : NMR spectrum of the complex [Rh(bpt-NH)(cod)].	92
Figure 54 : IR spectrum of the complex [Rh(bpt-NH)(cod)].	93
Figure 55 : NMR spectrum of the complex [Ir(bpt)(cod)(Me)(I)].	98
Figure 56 : IR spectrum of the complex [Ir(bpt)(cod)(Me)(I)].	99

LIST OF FIGURES

Figure 57 : NMR spectrum of the complex [Ir(bpt-NH)(cod)(Me)(I)].	100
Figure 58 : IR spectrum of the complex [Ir(bpt-NH)(cod)(Me)(I)].	101
Figure 59 : NMR spectrum of the complex [Rh(bpt)(cod)(Me)(I)].	102
Figure 60 : IR spectrum of the complex [Rh(bpt)(cod)(Me)(I)].	103
Figure 61 : NMR spectrum of the complex [Rh(bpt-NH)(cod)(Me)(I)].	104
Figure 62 : IR spectrum of the complex [Rh(bpt-NH)(cod)(Me)(I)].	105
Figure 63 : Spectrums of the decomposition of Rh(bpt-NH)(cod) in DCM and the reaction with CH ₃ I.	114
Figure 64 : Plot of k_{obs} against [MeI] for the oxidative addition between CH ₃ I and [Ir(bpt)(cod)] in acetone.	117
Figure 65 : Plot of k_{obs} against [MeI] for the oxidative addition between CH ₃ I and [Ir(bpt-NH)(cod)] in benzene.	118
Figure 66 : Plot of k_{obs} against [MeI] for the oxidative addition between CH ₃ I and [Ir(bpt-NH)(cod)] in DCM.	119
Figure 67 : Plot of k_{obs} against [MeI] for the oxidative addition between CH ₃ I and [Rh(bpt)(cod)] in acetone.	120
Figure 68 : Plot of k_{obs} against [MeI] for the oxidative addition between CH ₃ I and [Rh(bpt-NH)(cod)] in benzene.	122
Figure 69 : Plot of k_{obs} against [MeI] for the oxidative addition between CH ₃ I and [Rh(bpt-NH)(cod)] in DCM.	123
Figure 70 : Possible rearrangement of the bonding sites of bpt-NH ₂ to a metal atom.	124

Abbreviations

acac	acetylacetonato anion
act	acetone
AnMetha	N-Methyl-p-methoxyphenylthiohydroxamato anion
ba	benzoylacetylacetonato anion
bz	benzene
bipy	2,2'-bipyridyl
CO	carbon monoxide
cod	<i>cis,cis</i> -cycloocta-1,5-diene
cupf	cupferrate anion
CH ₃ I	iodomethane
d	doublet
DCM	dichloromethane
dbm	dibenzoylmethane
dtc	dimethyldithiocarbamato anion
DiPAMP	1,2-bis(phenyl-o-methoxy-phenyl-phosphino) anion
DMSO	dimethylsulphoxide
ϵ	dielectric constant
hfaa	hexafluoroacetylacetonato anion
IR	infrared
k_{obs}	observed first rate order constant
LL'	bidentate ligand

ABBREVIATIONS

m	multiplet
Me	methyl
MeOH	methanol
macsm	methyl (2-methylammino-1-cyclopentadiene-l-dithiocarboxylate) anion
NMR	nuclear magnetic resonance
phen	1,10-phenanthroline
phoss	<i>cis</i> -1,2-bis(diphenylphosphino)ethylene anion
P(OPh) ₃	triphenylphosphite
pK _a	p - function of acid dissociation constant
s	singulet
Sacac	thioacetylacetonato anion
t	triplet
tfaa	trifluoroacetylacetonato anion
tfba	trifluorobenzoylacetonato anion
tfdmaa	1,1,1 -trifluoro-5,5 -dimethylpentanedione
tftmaa	1,1,1-trifluoro-5,5,5-trimethylpentanedionate anion
VIS	visible
UV	ultraviolet
λ	wavelength
X	halide

Chapter 1

General overview

1. Introduction.

Rhodium and iridium were discovered independently in the same year and share many resemblances in their chemistry¹⁻⁹. Both metals exhibit extensive chemistry, principally in the +3 and +1 oxidation states with significant iridium chemistry in the +4 state. In contrast to cobalt, few compounds of +2 oxidation state are known for rhodium and iridium.

The scientist W.H. Wollaston discovered rhodium in 1803. He dissolved platinum metal concentrates in aqua regia and found that on removal of the platinum and palladium a red solution remained from which he obtained the salt $\text{Na}_3[\text{RhCl}_6]$. Upon reduction with hydrogen the metal was obtained. The rose-red colour (Greek: *rhodon*) of many rhodium salts gave the element its name.

In the same year, Smithson Tennant studied the black aqua regia insoluble portion of platinum ores. He found that, after fusion with

¹ Hartley, F.R., *The Chemistry of the Platinum Group Metals*, Elsevier, Amsterdam, 407 (1991)

² Griffith, W.P., *The Chemistry of the Rarer Platinum Metals*, Wiley-Interscience, New York (1967)

³ Livingstone, S.E., *Comprehensive Inorganic Chemistry*, Pergamon, Oxford, 3, 1233 (1973)

⁴ Jardine, F.H.; Sheridan, P.S., *Comprehensive Coordination Chemistry*, Pergamon, Oxford, 5, 901 (1987)

⁵ Hughes, R.P., *Comprehensive Organometallic Chemistry I*, Pergamon, Oxford, 5, 277 (1982)

⁶ Serpone, N.; Jamieson, M.A., *Comprehensive Coordination Chemistry*, Pergamon, Oxford, 5, 1097 (1987)

⁷ Leigh, G.J.; Richards, R.L., *Comprehensive Organometallic Chemistry*, Pergamon, Oxford, 5, 241 (1982)

⁸ Atwood, J.D., *Comprehensive Organometallic Chemistry II*, Pergamon, Oxford, 8, 303 (1995)

⁹ Dickson, R.S., *Organometallic Chemistry of Rhodium and Iridium*, Academic Press (1983)

soda and extraction with water, the black residue gave a blue solution in hydrochloric acid that when heated turned red. The red crystals obtained yielded the metal upon further heating. Tennant gave iridium its name from the Greek word *iris* (rainbow) since iridium compounds have a variety of colours.

It was only until much later that both metals had any significant usefulness. The main use of rhodium is in conjunction with platinum as an oxidation catalyst for automobile exhaust emissions. Many applications of iridium rely on its inertness, e.g. high temperature crucibles, electrode coatings and thermocouples. It also has applications in the defence, nuclear and aerospace industries. The inert alloy with osmium is traditionally used in pen nibs.

The interest of this study lies in these metals' uses as organometallic complexes. Probably the best-known industrial application of organometallic chemistry is that of the catalytic carbonilation of methanol by rhodium or iridium. Compared to the now historical BASF-process, in which a cobalt catalyst was used, the rhodium catalyst has proved to be far superior to its cobalt counterpart. (Figure 1). The rhodium catalyst operates at lower concentrations, less drastic reaction conditions (lower temperature and pressure) and a higher selectivity towards the desired product is obtained. Recent figures¹⁰ indicate that about 5.5 million tons (60%) of the world acetic acid is produced using this process.

¹⁰ Howard, M.J.; Jones, M.D.; Roberts, M.S.; Taylor, S.A.; *Catal. Today*, 18, 3250 (1993)

increases by 30% compared to that of the rhodium catalyst. These factors lead to the newly implemented *Cativa* process (Figure 2).¹³⁻¹⁵ The similarities between the two processes enable the *Cativa* process to be introduced into existing Monsanto plants with only minor conversions. A plant implementing the *Cativa* process is running successfully in Texas.

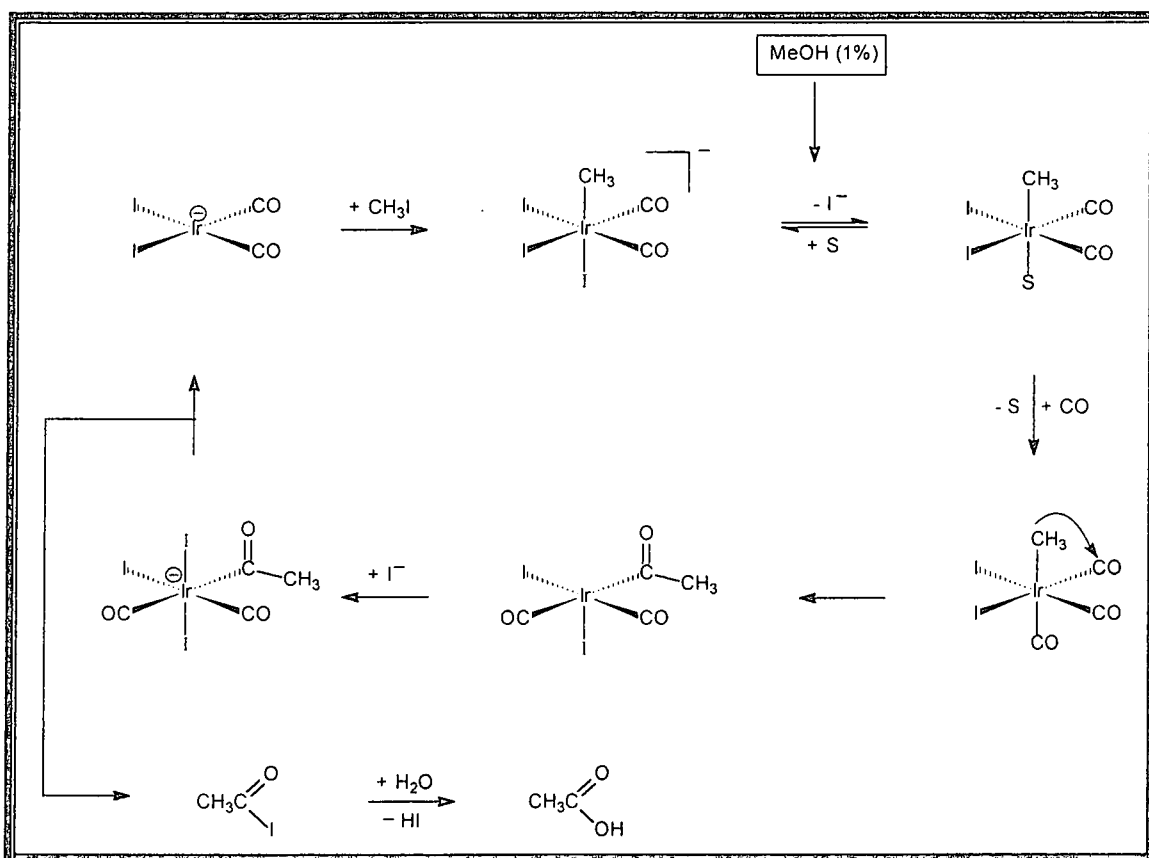


Figure 2 : A simplified schematic representation of the *Cativa* catalytic cycle.

In general, chemical reactions catalysed by transition metal complexes consist of a sequence of elementary key reactions which include^{16,17}:

¹⁴ Ellis, P.R., *Platinum Metals Rev.*, 41, 8 (1997)

¹⁵ Maitlis, P.M.; Haynes, A.; Sunley, G.J.; Howard, M.J., *J. Chem. Soc. Dalton Trans.*, 2187 (1996)

¹⁶ Koga, W.; Morokuma, K., *Chem. Rev.*, 91, 823 (1991)

¹⁷ Schriver, D.F.; Atkins, P.W.; Langford, C.H., *Inorganic Chemistry*, 2nd Ed., Oxford University, Oxford (1994)

- i) Olefin insertion.
- ii) Carbonyl insertion.
- iii) β -hydrogen elimination.
- iv) Nucleophilic addition to coordinated ligands.
- v) Oxidative addition.
- vi) Reductive elimination.
- vii) *Cis* migration.

Organometallic complexes, used as catalysts, should have the ability to partake in these reactions and should be able to exert kinetic control¹⁸. Rhodium and iridium prove to have these characteristics. The high selectivity of these complexes offset the cost of the metals involved.

2. Research review.

Substitution and oxidative addition reactions of square planar rhodium(I) and iridium(I) complexes have been studied intensively by our research group. During these studies, different bidentate ligands were used with donor atoms varying from O-O-, O-S- to S-N-donor combinations to investigate their effect on the kinetic rate of substitution and oxidative addition. The mechanisms of these reactions were also investigated. It was found that the rhodium complexes are in general more reactive and thus better suited for a wider variety of catalytic reactions. Some examples^{19,20} of these are the hydrogenation of olefins with Wilkinson's catalyst, $[\text{RhCl}(\text{PPh}_3)_3]$, asymmetric hydrogenation of pro-chiral alkenes with

¹⁸ Dickson, R.S., *Homogeneous Catalysis with compounds of Rhodium and Iridium*, D. Reidel Publishing Company, Dordrecht (1985)

¹⁹ Cotton, F.A.; Wilkinson, G., *Advanced Inorganic Chemistry*, 5th Ed., John Wiley & Sons, New York (1980)

²⁰ Halpern, J., *Inorg. Chem. Acta.*, 50, 11 (1980)

[Rh(DiPAMP)₂] and hydroformulation of alkenes with a variety of rhodium(I) complexes.

Although we have not studied substitution reactions in this work, it is worth mentioning since it plays a significant role in a number of catalytic cycles. A short summary on the substitution reactions done by our group on rhodium(I) and iridium(I) complexes are given in Table 1.

Table 1 : A short summary of the substitution reactions investigated in this laboratory on rhodium(I) and iridium(I) complexes.

Complex	β -diketone*	Incoming ligand	Displaced ligand	Reference
[Rh(β -diketone)(cod)]	acac,tfaa	phen	β -diketone	21
[Rh(β -diketone)(CO) ₂]	ba,dbm,tfaa, tfba,hfaa	cod	CO	22
[Rh(β -diketone)(cod)]	acac,ba,dbm, tfaa,tfba,hfaa	phen	β -diketone	23
[Rh(β -diketone)(cod)]	acac,ba,dbm, tfaa,tfba,hfaa	P(OPh) ₃	cod	24
[Rh(acac)(cod)]		phen bipy	acac	25
[Ir(β -diketone)(cod)]	acac,ba,dbm, tfaa,tfba,hfaa	Derivatives of phen and bipy		26

*See list of abbreviations for the names of the β -diketone and the incoming ligands.

Reactions of oxidative addition have also been studied intensively. This research can be divided into complexes of the type [Rh(LL')(CO)(PPh₃)], [Rh(LL')(PX₃)₂] and [Ir(LL')(cod)]. These are summarised in Table 2.

²¹ Leipoldt, J.G.; Steynberg, B.C.; Van Eldik, R., *Inorg. Chem.*, **26**, 3068 (1987)

²² Leipoldt, J.G.; Basson, S.S.; Schlebush, J.J.J.; Grobler, B.C., *Inorg. Chim. Acta*, **62**, 113 (1982)

²³ Leipoldt, J.G.; Grobler, B.C.; *Trans. Met. Chem.*, **11**, 110 (1986)

²⁴ Leipoldt, J.G.; Lamprecht, G.J.; Steynberg, E.C., *J. Organomet. Chem.*, **397**, 239 (1990)

²⁵ Leipoldt, J.G.; Lamprecht, G.J.; Steynberg, E.C., *J. Organomet. Chem.*, **402**, 259 (1991)

²⁶ Leipoldt, J.G.; Basson, S.S.; Van Zyl, G.J.; Steyn, G.J.J., *J. Organomet. Chem.*, **418**, 241 (1991)

GENERAL OVERVIEW

Table 2 : A summary of the oxidative addition reactions done on complexes of the type $[\text{Rh}(\text{LL}')(\text{CO})(\text{PPh}_3)]$, $[\text{Rh}(\text{LL}')(\text{PX}_3)]$ and $[\text{Ir}(\text{LL}')(\text{cod})]$ in our laboratories.

Complex	Addend molecule	LL'	Reference
$[\text{Rh}(\text{LL}')(\text{CO})(\text{PPh}_3)]$	CH_3I	acac, tfaa, hfaa, tfdmaa	27
$[\text{Rh}(\text{acac})(\text{CO})(\text{PX}_3)]$	CH_3I		28
$[\text{Rh}(\text{cupf})(\text{CO})(\text{PX}_3)]$	CH_3I		29
$[\text{Rh}(\text{LL}')(\text{P}(\text{OPh})_3)_2]$	I_2	acac, ba, dba, tfaa, tfba, hfaa	30
$[\text{Rh}(\text{LL}')(\text{P}(\text{OPh})_3)_2]$	CH_3I	acac, ba, dbm, tfaa, tfba, hfaa	31
$[\text{Rh}(\text{macsm})(\text{CO})(\text{PPh}_3)]$	CH_3I		32
$[\text{Rh}(\text{LL}')(\text{P}(\text{OPh})_3)_2]$	$\text{Hg}(\text{CN})_2$	acac, ba, dbm, tfaa, tfba, hfaa	33
$[\text{Rh}(\text{sacac})(\text{CO})(\text{PX}_3)]$	CH_3I		34
$[\text{Rh}(\text{LL}')(\text{CO})(\text{PX}_3)]$	CH_3I	hpt, AnMetha	35
$[\text{Rh}(\text{LL}')(\text{CO})(\text{PX}_3)]$	CH_3I	hpt, AnMetha, AnHtha, CIMetha	36
$[\text{Ir}(\beta\text{-diketone})(\text{cod})]$	CH_3I	acac, tfaa, hfaa	37
$[\text{Ir}(\beta\text{-diketone})(\text{cod})]$	$\text{Hg}(\text{CN})_2$	asas, ba, dbm, tfaa, tfba	38
$[\text{Ir}(\text{LL}')(\text{cod})]$	CH_3I	macsm, sacac, tfaa, cupf	39
$[\text{Ir}(\text{LL}')(\text{cod})]$	CH_3I	hpt, AnMetha	40

*See list of abbreviations for the names of LL'.

From these studies a few deductions can be made:

- i) The substitution of these complexes appears to proceed via a simple and straightforward associative mechanism.

²⁷ Basson, S.S.; Leipoldt, J.G.; Nel, J.T., *Inorg. Chim. Acta*, **84**, 167 (1984)

²⁸ Basson, S.S.; Leipoldt, J.G.; Roodt, A.; Venter, J.A.; Van der Walt, T.J., *Inorg. Chim. Acta*, **119**, 35 (1986)

²⁹ Basson, S.S.; Leipoldt, J.G.; Roodt, A.; Venter, J.A., *Inorg. Chim. Acta*, **128**, 31 (1987)

³⁰ Van Zyl, G.J.; Lamprecht, G.J.; Leipoldt, J.G., *Inorg. Chim. Acta*, **129**, 35 (1987)

³¹ Van Zyl, G.J.; Lamprecht, G.J.; Leipoldt, J.G., *Inorg. Chim. Acta*, **143**, 233 (1988)

³² Steyn, G.J.J.; Roodt, A.; Leipoldt, J.G., *Inorg. Chem.*, **31**, 3477 (1992)

³³ Van Zyl, G.J.; Lamprecht, G.J.; Leipoldt, J.G., *Trans. Met. Chem.*, **15**, 170 (1990)

³⁴ Leipoldt, J.G.; Basson, S.S.; Botha, L.J., *Inorg. Chim. Acta*, **168**, 215 (1990)

³⁵ Smit, D.M.C., *M.Sc.-Thesis*, U.O.V.S. (1992)

³⁶ Preston, H., *Ph.D.-Thesis*, U.O.V.S. (1993)

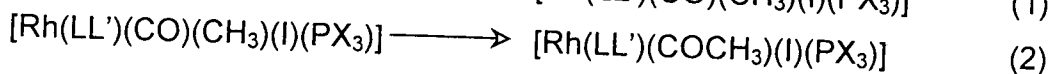
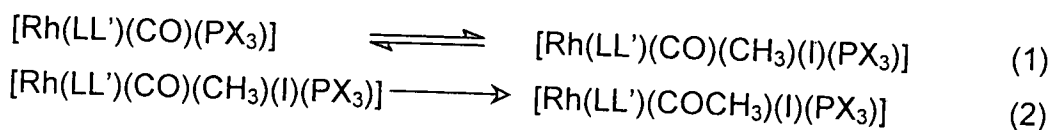
³⁷ Basson S.S.; Leipoldt, J.G.; Purcell, W.; Schoeman, J.B., *Inorg. Chem.*, **173**, 155 (1990)

³⁸ Steyn, G.J.J.; Basson, S.S.; Leipoldt, J.G.; Van Zyl, G.J., *J. Organomet. Chem.*, **418**, 113 (1991)

³⁹ Terblans, Y.M., *M.Sc.-Thesis*, U.O.V.S. (1993)

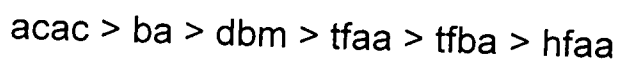
⁴⁰ Theron, M., *M.Sc.-Thesis*, U.O.V.S. (1994)

- ii) The first step of oxidative addition with CH_3I usually involves the formation of a rhodium(III) alkyl complex, $[\text{Rh}(\text{LL}')(\text{CO})(\text{PX}_3)(\text{CH}_3)\text{I}]$ followed by the formation of the rhodium(III) acyl complex as shown in the following reactions:



The acyl formation (reaction (2)) is one of the key steps in the *Monsanto* and *Cativa* processes.

- iii) Electron withdrawing groups on the bidentate ligands (as in the case of $[\text{Rh}(\text{hfaa})(\text{CO})(\text{PPh}_3)]$) have an effect on the rate of oxidative addition and that of acyl formation. The reason for this is that electron density on the rhodium(I) centre is withdrawn by substituents resulting in a weaker Lewis basicity of the rhodium(I) centre and thus slower rates²⁷. We thus see a decrease in the reactivity as the bidentate ligand becomes more electron withdrawing for the following series:^{27,31,33}



- iv) The phosphines used in the metal complexes have an effect on the rate of oxidative addition due to the differences in σ -donating capabilities and steric hindrance, which can be expressed as a Tolman cone angle⁴¹. It was found that a

⁴¹ Tolman, C.A., *Chem. Soc. Rev.*, 77, 313 (1977)

phosphine with a high σ -donating capability and a small cone angle resulted in a higher rate of oxidative addition and acyl formation. Tolman cone angles are further discussed in **Chapter 2**.

- v) Different donor atoms not only have an influence on the rate of oxidative addition but also the composition of the final product. As an example a rhodium(III) acyl complex was found primarily in the case of $[\text{Rh}(\text{macsm})(\text{CO})(\text{PPh}_3)]$ (S-N-donating)³² and a rhodium(III) alkyl complex was found in the case of the $[\text{Rh}(\text{cupf})(\text{CO})(\text{PPh}_3)]$ (O-O-donating)²⁹. Some of these oxidative addition reactions also show a solvent dependency which will be discussed later on.
- vi) Iridium complexes without CO ligands frequently show oxidative addition equilibrium with the alkylated iridium(III) product, similar to the behaviour of the rhodium(I) complexes. Similarly to that of the rhodium complexes, it was found that the electron withdrawing groups on the bidentate ligand decrease the rate of oxidative addition in the following order:³⁷
- $\text{acac} > \text{tfaa} > \text{hfaa}$
- vii) It was also found that the addition of bromide ions lead to the formation of a five-coordinated intermediate which increased the rate of oxidative addition³⁷.

3. Aim of this study.

From the preceding discussion it is clear that a lot of research has already been done on the oxidative addition of square planar rhodium(I) and iridium(I) complexes. It was found that the donor atoms of the bidentate ligands and the solvent used have a significant influence on the rate of oxidative addition, the mechanism of the reaction and the final composition of the product.

Although acyl formation from the alkyl complexes has a very important place in the catalytic industry, it is however troublesome from a kinetic point of view. It sometimes happens that the reaction rate of oxidative addition and that of acyl formation are of the same magnitude. The reaction rates of these cannot be studied independently since the resulting reaction is too complex. In addition, there may also exist two consecutive competing equilibria, one consisting of formation of the alkyl derivation and its corresponding reverse reaction and the other a migratory CO insertion towards the acyl complex with its reverse reaction. With all these factors to compensate for it is almost impossible to accurately determine which other factors such as donor atom variations, solvent and ring size, etc. influence the rate of oxidative addition. This problem can be solved by the use of other ligands in place of CO and PX_3 . Acyl formation would then be impossible since there is no CO ligand present. It was thus decided to prepare complexes without the aforementioned ligands and instead to *cis,cis*-cycloocta-1,5-diene (cod). Great success had been

obtained with this ligand in previous studies. In addition, the $[\text{Ir}(\text{LL}')(\text{cod})]$ reacts slower than its $[\text{Ir}(\text{LL}')(\text{CO})(\text{PX}_3)]$ counterpart and has a greater stability. In previous studies, analogous $[\text{Rh}(\text{LL}')(\text{cod})]$ complexes remained inert in solution with CH_3I over a period of 48 hours.

In this study we aim to address the following:

- To synthesize both rhodium(I) and iridium(I) complexes of the form $[\text{M}(\text{LL}')(\text{cod})]$ ($\text{M} = \text{Rh}, \text{Ir}$ and $\text{LL}' = \text{N-N}'\text{-bidentate}$ ligands. These are shown in **Figure 3**).
- To characterise the starting materials as well as the products by means of NMR techniques, IR spectroscopy and element analyses.
- To study the reaction rate of oxidative addition of these complexes with CH_3I . This can then be compared to the O-O-, O-S-, and S-N-bidentate ligand complexes studied in our laboratories.

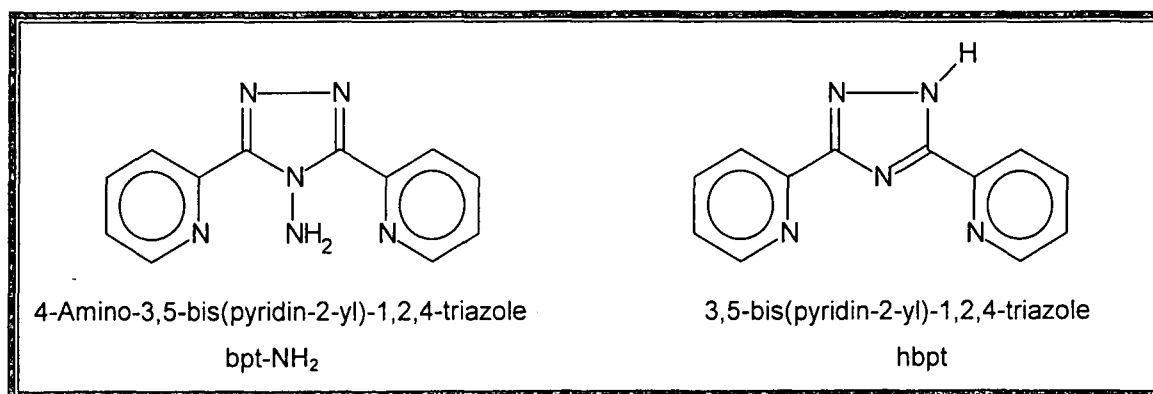


Figure 3 : Structures of the ligands used in this study with their names and abbreviations.

Chapter 2

Oxidative addition reactions

1. Introduction.

The chemical behaviour of square planar rhodium(I) and iridium(I) complexes are very important in homogeneous catalysis. These complexes are coordinative unsaturated and can partake in a series of elementary reactions that are key steps in the catalytic synthesis of organic products^{19,20}. To understand the process of homogeneous catalysis better, it is important to have extensive knowledge of each of these elementary key reactions. In this chapter, we take a closer look at the theoretical aspects of oxidative addition, one of these elementary reactions.

2. General overview.

The term oxidative addition originated in the 1960's among researchers such as Vaska⁴² and Collman⁴³. Collman stated that one of the most important factors for oxidative addition to occur is that the complex should be coordinative unsaturated.

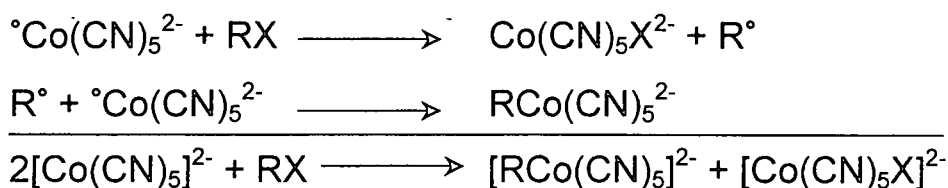
Oxidative addition was later defined as the reaction between a coordinative unsaturated d^8 or d^{10} transition metal complex L_nM

⁴² Vaska, L., *Acc. Chem. Res.*, 1, 335 (1968)

⁴³ Collman, J.P., *Acc. Chem. Res.*, 1, 136 (1968)

($n = 4$ or 5) and group X-Y where the complex acts as both Lewis base and acid. There is also an increase in the oxidation number and coordination sphere⁴⁴⁻⁴⁷. Both one and two electron oxidative addition reactions can occur and the metals' oxidation number also increases⁴⁸.

The free-radical reaction of $[\text{Co}(\text{CN})_5]^{2-}$ is an example of an one electron oxidative addition from a d^7 to a d^6 species.⁴⁸



The two-electron oxidative addition can be represented generally as in Figure 4. The terms saturated and unsaturated used in Figure 4 indicate the state of the coordination sphere of the metal. Vacant sites on the metal are necessary for the coordination of X and Y. This can be described as the unsaturated state. If coordination sites are not available, vacant sites must be created by thermal or photochemical dissociation as in the case of the trigonal bipyramidal d^8 complex in Figure 4.

⁴⁴ Collman, J.P.; Hegedus, L.S., *Principles and Application of Organotransition Metal Chemistry*, University Science Books, Mill Valley, California (1980)

⁴⁵ Cotton, F.A.; Wilkinson, G., *Advanced Inorganic Chemistry*, 4th Ed., John Wiley & Sons, New York (1980)

⁴⁶ Cotton, F.A.; Wilkinson, G., *Basic Inorganic Chemistry*, Wiley International Ed., New York (1976)

⁴⁷ Purcell, K.F.; Kotz, J.C., *Inorganic Chemistry*, Holt-Saunders International Ed., Philadelphia (1977)

⁴⁸ Douglas, B.; McDaniel, D.H.; Alexander, J.J., *Concepts and Models of Inorganic Chemistry*, 2nd Ed., John Wiley & Sons, New York (1983)

OXIDATIVE ADDITION REACTIONS

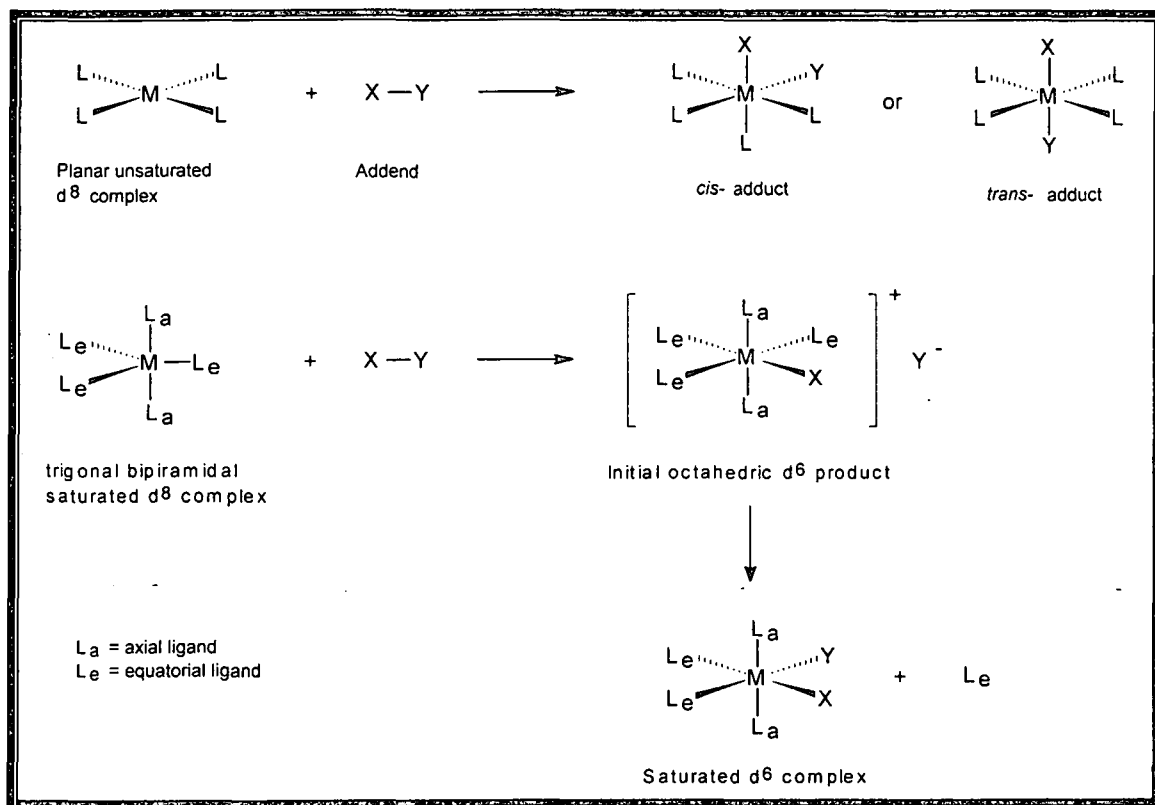


Figure 4 : General representation of two-electron oxidative addition.

It is important to note that the reaction between the added molecule $X-Y$ and the metal complex may lead to total bond breaking of the added molecule or only partial breaking. If partial breaking of the molecule $X-Y$ occurs, only the *cis* product is possible. If it breaks completely we can expect a number of *cis* and/or *trans* isomers depending on which of the isomers are thermodynamically stable under the reaction conditions. Factors that have an important influence on the geometry of the final products are:

- i) the solvent in which the reaction was carried out;
- ii) properties of the ligand bonded to the metal;
- iii) temperature and pressure of the reaction.

Table 3 shows a list of different molecules that can be used for oxidative addition.

Table 3 : A list of molecules which can be used in oxidative addition reactions⁴⁵.

Molecules with single bonding character (atoms separate)		Molecules with multiple bonding character (atoms remain attached)
X-X	H ₂ , Cl ₂ , Br ₂ , I ₂ , (SCN) ₂ , RSSR	O ₂ SO ₂ CF ₂ =CF ₂ (CN) ₂ C=C(CN) ₂ RC≡CR'
C-C	Ph ₃ C-CPh ₃ , (CN) ₂ , C ₆ H ₅ CN, MeC(CN) ₃ , cyclopropanes	RNCS RNCO RN=C=NR'
H-X	HCl, HBr, HI, HClO ₄ , C ₆ F ₅ OH, C ₆ F ₅ SH, PH ₃ , H ₂ S, H ₂ O, CH ₃ OH, NH ₃ , C ₆ F ₅ NH ₂ , C ₄ H ₄ NH, HC≡CR, C ₅ H ₆ , CH ₃ CN, HCN, HCO ₂ R, C ₆ H ₆ , C ₆ F ₅ H, HSiR ₃ , HSiCl ₃ , H- B ₁₀ C ₂ HPMe ₂ , H-B ₅ H ₈ , CH ₄ , RCHO	RCON ₃ CS ₂ (CF ₃) ₂ CO (CF ₃) ₂ CS CF ₃ CN R ₂ C=C=O
C-X	CH ₃ I, C ₆ H ₅ I, CH ₂ Cl ₂ , CCl ₄ , CH ₃ COCl, C ₆ H ₅ CH ₂ COCl, C ₆ H ₅ COCl, CF ₃ COCl, RCN, RCO ₂ R', ROR', R ₂ S	
M-X	Ph ₃ PAuCl, HgCl ₂ , MeHgCl, R ₃ SnCl, RGeCl ₃ , H ₈ B ₅ Br, Ph ₂ BX	
Ionic	PhN ₂ ⁺ BF ₄ ⁻ , Ph ₃ C ⁺ BF ₄ ⁻	

Probably the best example to illustrate oxidative addition is that of the complex *trans*-[IrCl(CO)(PPh₃)₂], better known as Vaska's complex. Figure 5 indicates oxidative addition reactions involving Vaska's complex with a number of different molecules, resulting in *cis* and *trans* additions as well as examples of partial bond breaking.

OXIDATIVE ADDITION REACTIONS

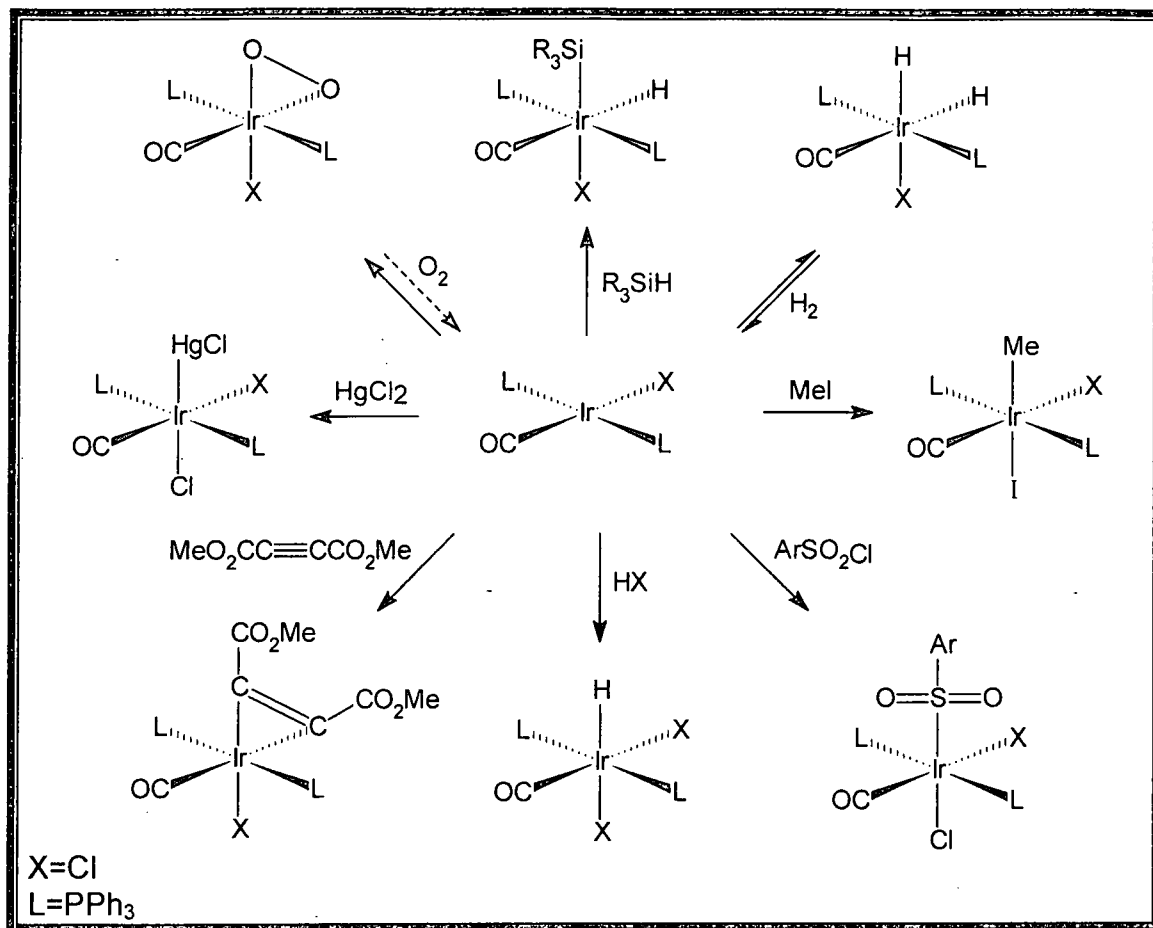


Figure 5 : Typical oxidative addition reactions to Vaska's complex⁴⁴.

Some of the reactions in **Figure 5** show equilibrium with the oxidative addition product. These equilibria are generally determined by the following factors:

- i) the solvent in which the reaction was carried out;
- ii) the properties of the added molecule XY and that of the formed M-X and M-Y bonds;
- iii) the properties of the metal and the coordinated ligands.

Experimentally it was found that ligands, which increase electron density on the metal, improve the ability of the metal to be oxidised and thus favour the equilibrium towards the oxidative addition product⁴⁵.

An interesting case⁴⁵ is that of intramolecular oxidative addition where a bonded ligand can oxidise the metal. (Figure 6) This is also known as *ortho*-metallation, in which the *ortho* C-H bond of the phenyl group on a coordinated aromatic phosphine or phosphite bonds to the metal to yield an aryl-hydrido complex.

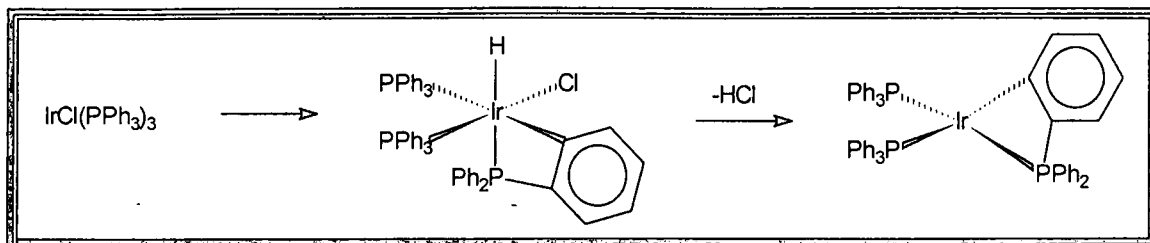


Figure 6 : Intramolecular oxidative addition.

The reverse reaction of oxidative addition is known as reductive elimination, where the oxidation and coordination numbers of the metal decrease by the same number of electrons involved.

The processes of oxidative addition and reductive elimination are important steps during various catalytic processes. With oxidative addition bond breaking of the substrate, e.g. CH_3I , occurs and with reductive elimination a specific bond is created, e.g. C-C, C-X, C-H or C-O. Combining these with other elementary processes a number of useful synthetic methods have been developed for organic substrates.

It is important to note that these two terms merely describe the reaction and have no mechanistic implication. The mechanisms involved can be complex and may be influenced by a number of different factors discussed later.

3. The mechanism of oxidative addition.

Although it is still widely speculated what the intimate mechanism of oxidative addition is, two general types can be defined, that of one- and two-electron oxidative addition^{44,55}. These two types can be differentiated from one another due to the fact that the intermediate of the one-electron mechanism is paramagnetic and the two-electron mechanism involves a paired electron process^{49,55}.

Information can be found on the mechanism of oxidative addition by studying the stereochemistry of the starting material and that of the product. From this, possible postulations of intermediate products can be made. Unfortunately this can be complicated by the fact that ligand exchange and isomerisation can occur before isolation of the final product.⁵⁰ There are indications that the solvent used during oxidative addition reactions also has an effect on the stereochemistry of the product. This can be seen from the reaction between CH_3X ($\text{X} = \text{Cl}, \text{I}$) with $[\text{IrCl}(\text{CO})\text{L}_2]^{51}$ ($\text{L} = \text{PPhMe}_2$ or PPh_2Me). If methanol is used both *cis* and *trans* products are found, but in the case of benzene with $[\text{IrBr}(\text{CO})(\text{PPhMe}_2)_2]$ only the *trans* product can be found.

Another way of obtaining more information on the mechanism is by investigating the regiochemistry of the newly bonded carbon atom to the metal. By determining the configuration on the carbon atom

⁴⁹ Cross, R.J., *Chem. Soc. Rev.*, **14**, 197 (1985)

⁵⁰ Dickson, R.S., *Organometallic Chemistry of Rhodium and Iridium*, Academic Press Inc., London Ltd. (1983)

⁵¹ Deeming, A.J.; Shaw, B.L., *J. Chem. Soc. A.*, 1128 (1969)

before and after oxidative addition, a possible transition state can be postulated to describe the mechanism.

Lau⁵² *et al* studied this aspect of oxidative addition with the reaction scheme as shown in Figure 7. S-(-)- α -phenylbromide adds oxidatively to Ph_3PdCO with an inversion of the configuration. After this, insertion (with retention of the configuration) occurs.

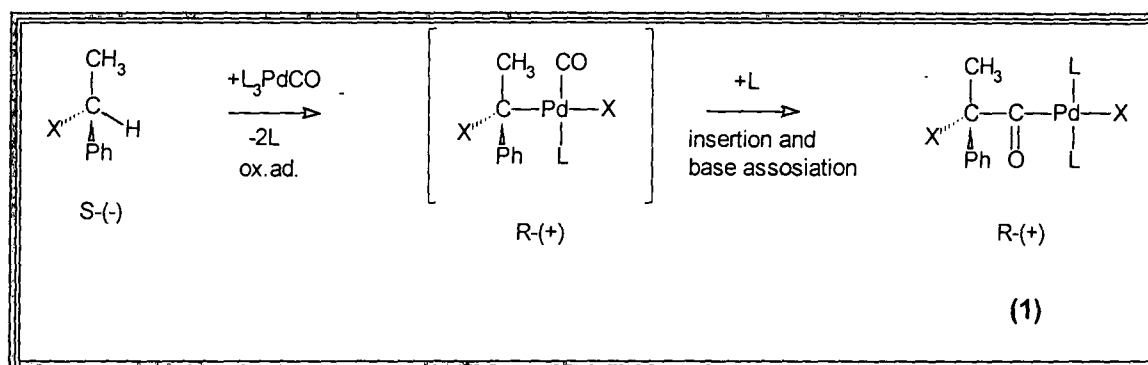


Figure 7 : Reaction scheme for the oxidative addition reaction of S-(-)- α -phenylbromide and Ph_3PdCO .

Complex (1) in Figure 7 can also be obtained by oxidative addition of an acyl halide (with known configuration) to $\text{Pd}(\text{PPh}_3)_4$ (Figure 8). This proves that the oxidative addition of S-(-)- α -phenylbromide occurs with inversion of the configuration since the reaction in Figure 8 only proceeds with retention of the configuration of the acyl halide.

⁵² Lau, K.S.Y.; Fries, R.W.; Stille, J.K., *J. Amer. Chem. Soc.*, 96, 4983 (1974)

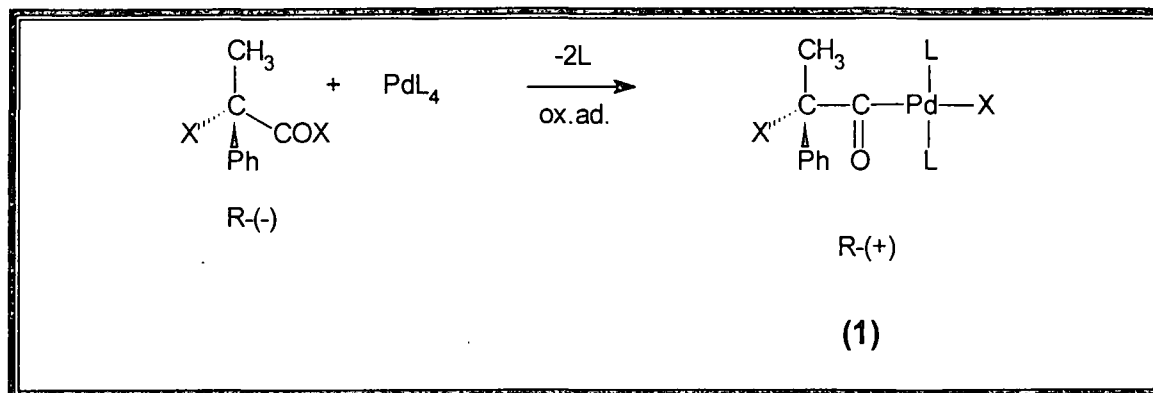


Figure 8 : Oxidative addition reaction of an acyl halide with PdL₄ (L = PPh₃).

Cases where racemisation occur have also been reported^{52,53,54}.

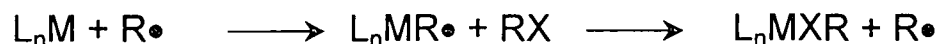
The one-electron mechanism can be described as a free radical mechanism while the two-electron mechanism is dependent on the polarity of the proposed transition state and can be divided into the following subcategories:

- i) concerted one step,
- ii) S_N2 two-step⁴⁹,
- iii) ionic mechanism⁴⁵.

3.1 One-electron oxidative addition mechanism.

The free radical mechanism is an one-electron process and can be generally written in the following two ways⁵⁵:

Radical chain reaction (propagating follow up)

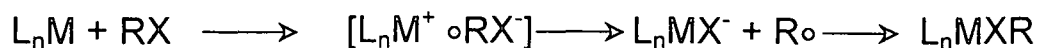


⁵³ Lau, K.S.Y.; Fries, R.W.; Stille, J.K., *J. Amer. Chem. Soc.*, **96**, 5956 (1974)

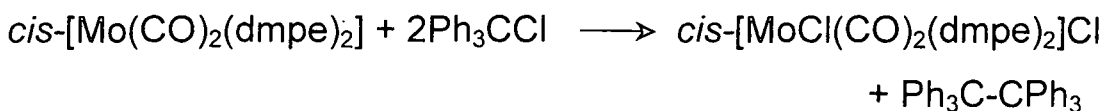
⁵⁴ Lappert, M.F.; Lednor, P.W., *Adv. Organomet. Chem.*, **14**, 345 (1976)

⁵⁵ Kochi, J.K., *Organometallic Mechanism and Catalysis*, Academic Press, London (1978)

Radical non-chain reaction (electron transfer)



The earliest proof for a free radical mechanism was done by Connor and co-workers⁵⁶ in the reaction:



They used an ESR-spectrophotometer (ESR = Electron Spin Resonance) and discovered signals which could be assigned to *trans*-[Mo(CO)(dmpe)₂]⁺ and the radical Ph₃C \cdot . The proposed reaction mechanism is shown in **Figure 9**.

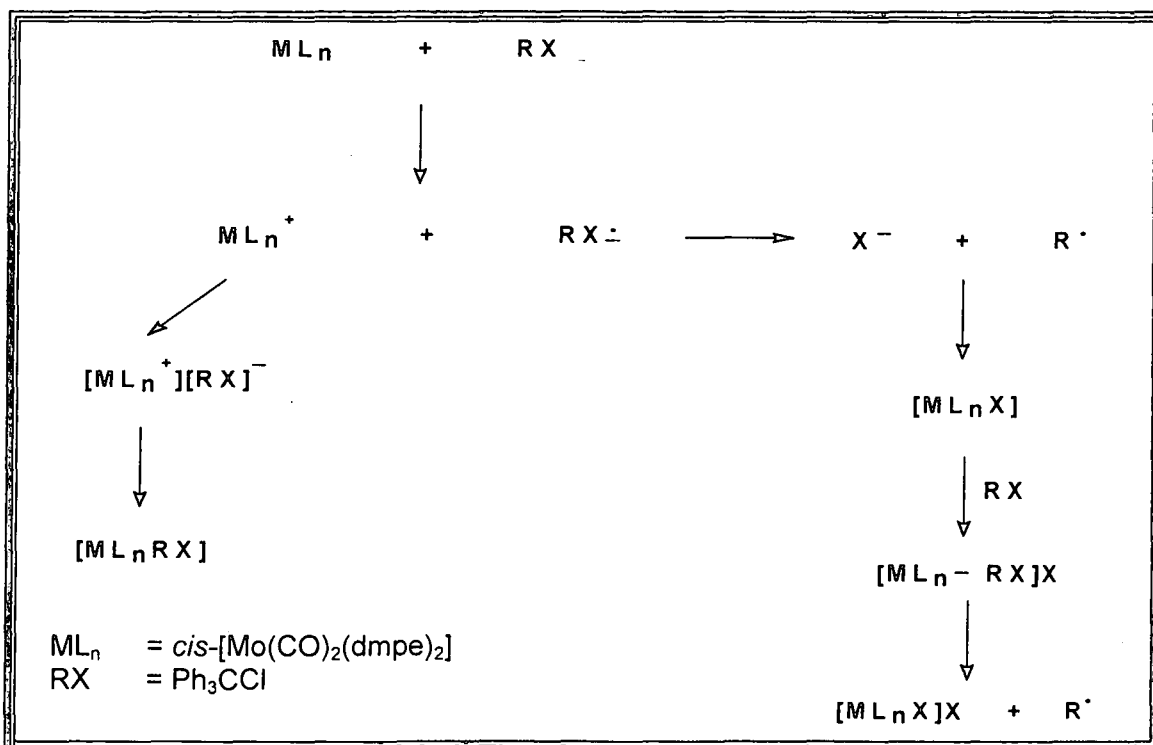


Figure 9 : Proposed radical mechanism between *cis*-[Mo(CO)₂(dmpe)₂] and Ph₃CCl.

⁵⁶ Connor, J.A.; Riley, P.I., *J. Chem. Soc., Chem. Commun.*, 634 (1976)

Further proof for the existence of the free radical mechanism was found in the reaction between $[\text{IrCl}(\text{CO})(\text{PMe}_3)_2]$ and $\text{PhCHFCH}_2\text{Br}$ ⁵⁷. This reaction is retarded by the addition of radical scavengers like hydroquinone, galvinoxyl and duroquinone and is enhanced by radical sources like O_2 and benzoylperoxide. Also when $\text{MeCHBrCO}_2\text{Et}$ was added to the above metal complex a loss of chirality (stereochemistry) was detected on the newly added carbon atom⁵⁸. This is a known characteristic of free radical reactions.

The most important discovery for the free radical mechanism is that of the observation of the CIDNP-effect (CIDNP = Chemically Induced Dynamic Nuclear Polarization) in proton NMR. This effect can only be observed if free radicals are present in the reaction⁵⁹. The reaction between $[\text{Pt}(\text{PEt}_3)_3]$ and isopropyl iodide done by Kramer and Osborne⁵⁸ is a good example where free radicals were detected by the CIDNP-effect.

Free radical mechanisms may also compete with other mechanisms in oxidative addition.^{30,56,58,60,61} This can be illustrated with the competition between a free radical mechanism and a $\text{S}_{\text{N}}2$ -type mechanism (nucleophilic attack) for the oxidative addition reaction of $[\text{Pt}(\text{PEt}_3)_3]$ and an alkyl halide in **Figure 10**.

⁵⁷ Kramer, A.V.; Labinger, J.A.; Bradley, J.S.; Osborn, J.A., *J. Am. Chem. Soc.*, **96**, 7145 (1974)

⁵⁸ Kramer, A.V.; Osborn, J.A., *J. Am. Chem. Soc.*, **96**, 7832 (1974)

⁵⁹ Lowry, T.H.; Richardson, K.S., *Mechanism and Theory in Organic Chemistry*, Harper and Row, New York (1976)

⁶⁰ Purcell, K.F.; Kotz, J.C., *Inorganic Chemistry*, W.B. Saunders Co, Hong Kong (1977)

⁶¹ Pearson, R.G.; Frigidore, D.E., *J. Am. Chem. Soc.*, **93**, 6339 (1971)

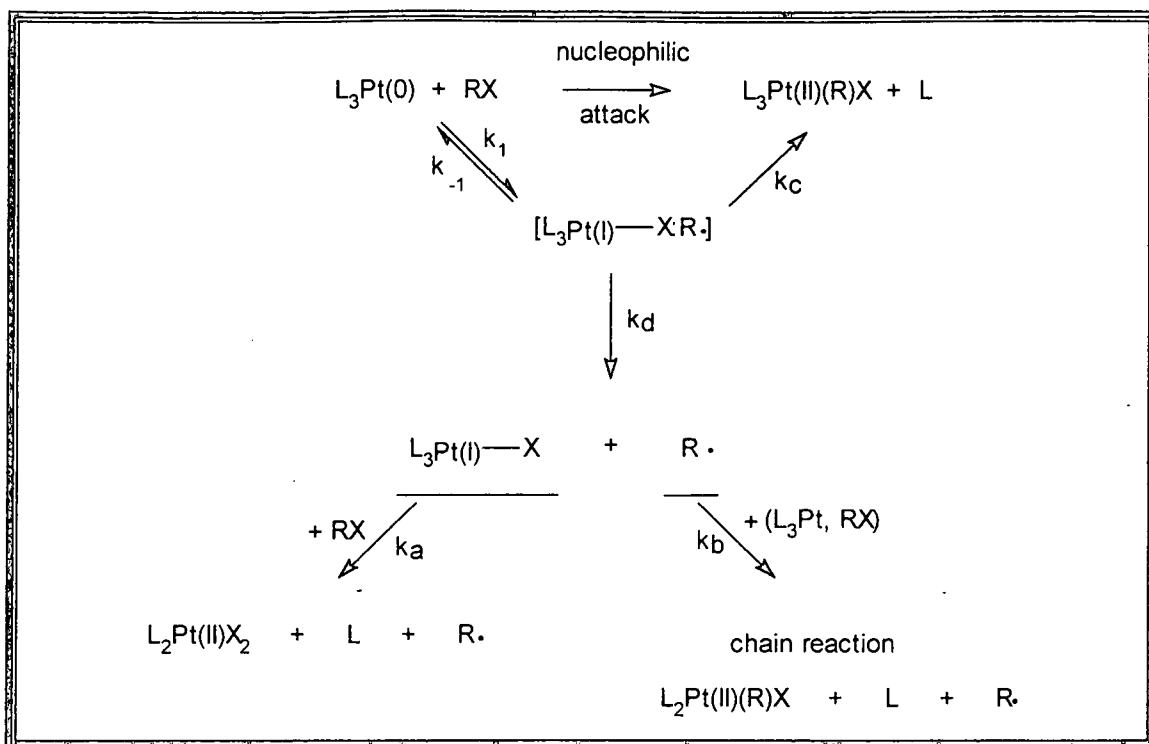


Figure 10 : Competing reaction mechanisms for the oxidative addition reaction of $[Pt(PEt_3)_3]$ and an alkyl halide.

Except for the nucleophilic attack on the metal complex, there is also an additional k_1 -path which involves removal of a halide from the metal complex to form the radical pair, $[L_3Pt(I)-X:R\cdot]$. This k_1 -path occurs simultaneously with the nucleophilic attack. The radical produced may decompose to yield the product of the nucleophilic attack (k_c -path). Alternatively it may decompose to form $[L_3Pt(I)X]$ and $R\cdot$ (k_d -path). Further reactions are dependent on the reactivity of the alkyl halide. For isopropyl bromide with the stronger C-Br bond the chain mechanism (k_b -path) is dominant, while with isopropyl iodide there is competition between the k_b and k_a -paths because of the weaker C-I bond.

As seen, the choice for a specific route is dependent on a number of factors⁶² :

⁶² Kramer, A.V, Osborne, J.A., *J. Am. Chem. Soc.*, **96**, 7364 (1972)

- i) The nature of the carbon-halogen bond.
- ii) The nucleophilicity of the metal complex.
- iii) Steric effects.
- iv) Ligand exchange processes.
- v) The ability of the metal to undergo one-electron processes.

The right balance of these factors will determine which route in the oxidative addition reaction would be dominant. Most of the simple organic bromides and iodides react with Ir(I), Pd(0), Pt(0) with a one electron mechanism while CH_3I , $\text{C}_6\text{H}_5\text{Cl}$ and $\text{CH}_2=\text{CH}-\text{CH}_2\text{Cl}$ generally follow other mechanistic routes. No radical mechanism has been observed for Rh(I)⁴⁵.

3.2 Two-electron oxidative addition mechanism.

a) The one step concerted mechanism.

Concerted oxidative addition on $16e^-$ square planar d^8 species lead to products where, at least initially, the entering groups of the added molecule are *cis* to one another. The products formed were $18e^-$ octahedral species. Examples of these are the H_2 addition to Vaska's complex⁶³ (**Figure 11**):

⁶³ Cross, R.J., *Chem. Soc. Rev.*, 14, 197, 1985

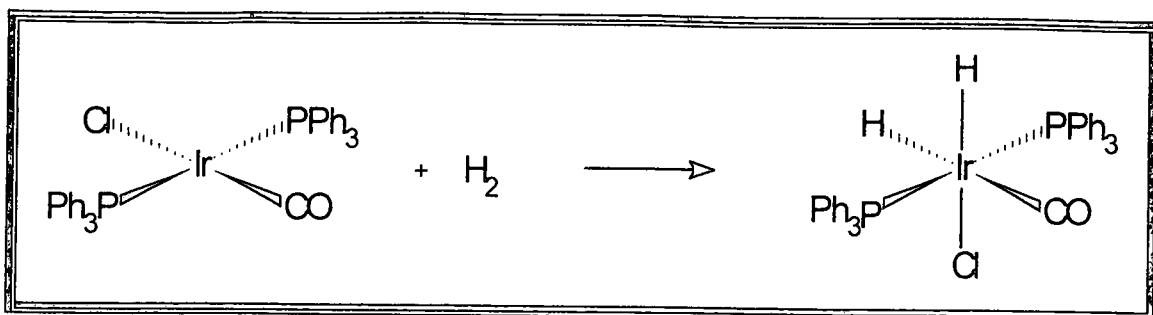


Figure 11 : Oxidative addition of H_2 to Vaska's complex resulting in a *cis* product.

and a tungsten complex characterised by Kubas⁶⁴ (Figure 12).

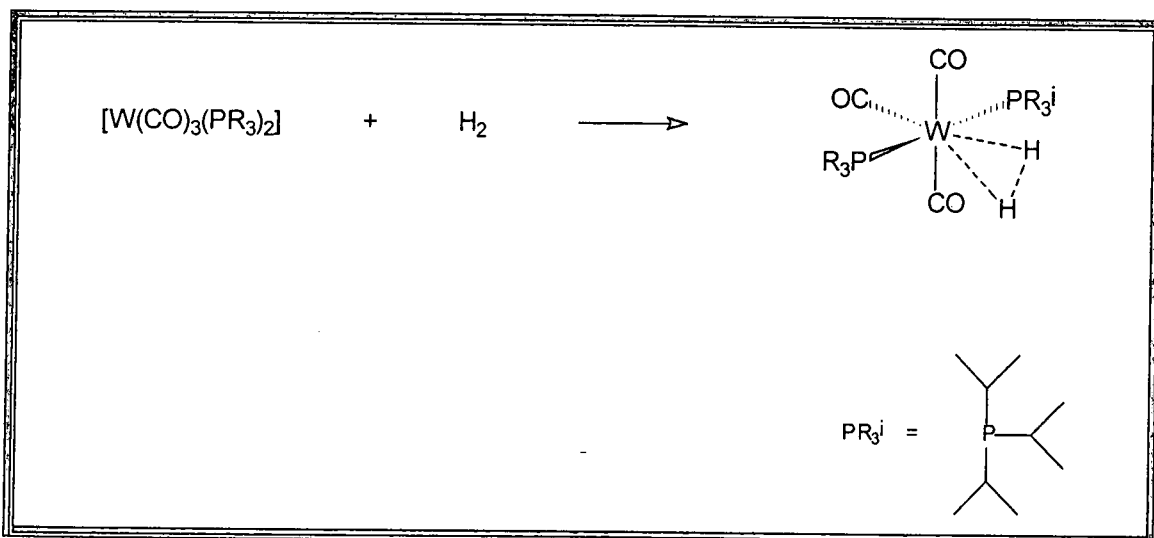


Figure 12 : A tungsten complex containing a coordinated hydrogen molecule proving that H_2 bonds *cis* because of its bonding character.

In rare cases the *cis* isomer is formed first, but subsequent rearrangement yields the *trans* isomer as found in the work done by Kuwae and Kawakami⁶⁵ (Figure 13).

⁶⁴ Kubas, G.J.; Ryan, R.R.; Swanson, B.I.; Vergamini, P.J.; Wasserman, H.J., *J. Am. Chem. Soc.*, **106**, 451 (1984)

⁶⁵ Kuwae, R.; Kawakami, K., *Bull. Chem. Soc. Jpn.*, **52**, 437 (1979)

OXIDATIVE ADDITION REACTIONS

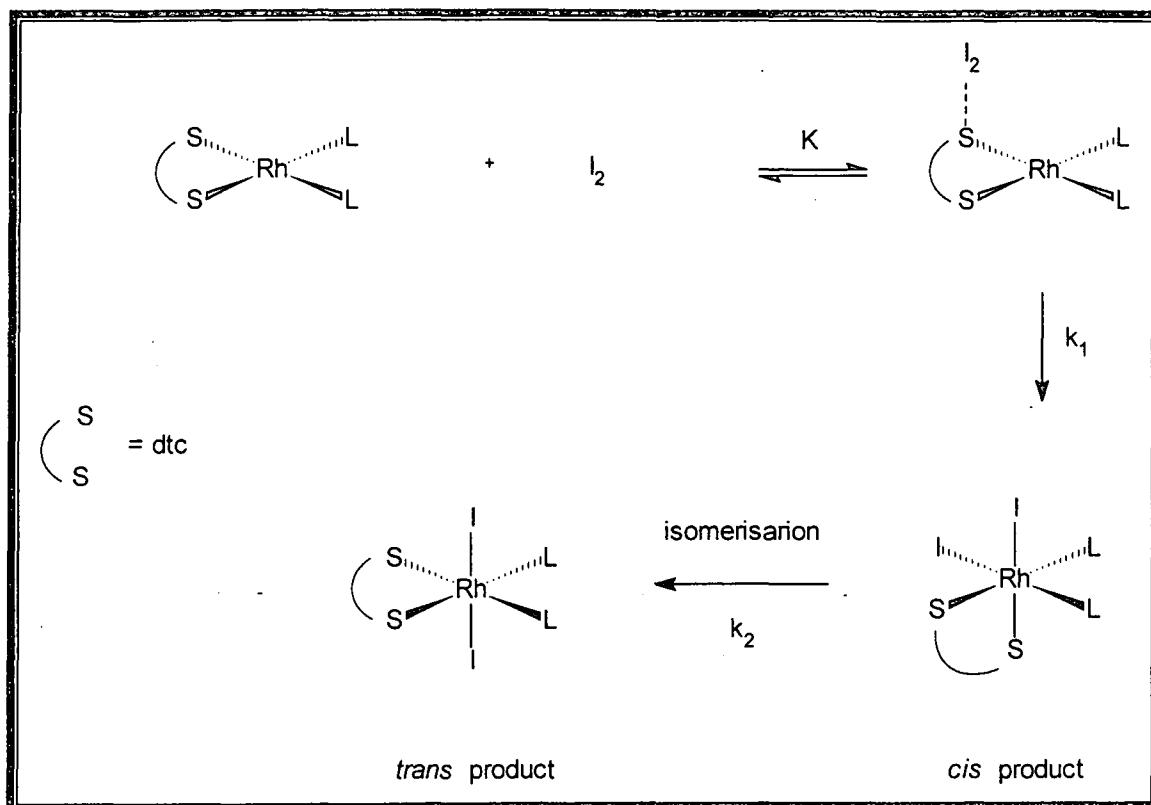


Figure 13 : Oxidative addition of $[\text{Rh}(\text{dtc})\text{L}_2]$ and I_2 .

The concerted *trans* addition of the entering group is a symmetry-forbidden process while *cis* addition is acceptable⁶⁶. *Cis* addition proceed with a cyclic, three-center transition state and can be described as the overlapping of a filled metal d_{xy} or d_{xz} orbital with an empty σ^* -orbital of the added molecule⁶⁸⁻⁶⁹. There is also overlapping of a filled σ -orbital of the added molecule with an empty metal acceptor orbital (p_z or d_z^2).

Work done by Saillard and Hoffman⁷⁰ on molecular orbital theory indicate that electrons flow in both directions in reactions that proceed with a concerted mechanism. There is electron flow from the metal to the added molecule and also from the σ -bond of the

⁶⁶ Braterman, P.S.; Cross, R.J., *Chem. Soc. Rev.*, **2**, 271 (1973)

⁶⁷ Johnson, C.E.; Eisenberg, R., *J. Am. Chem. Soc.*, **107**, 3148 (1985)

⁶⁸ Pearson, R.G., *Symmetry Rules for Chemical Reactions*, Wiley-Interscience, New York, 316 (1976)

⁶⁹ Kunin, A.J.; Johnson, C.E.; Maguire, J.A.; Jones, W.D.; Eisenberg, R., *J. Am. Chem. Soc.*, **109**, 2963 (1981)

⁷⁰ Saillard, J.; Hoffmann, R., *J. Amer. Chem. Soc.*, **106**, 2006 (1984)

added molecule back to the metal. Both these interactions weaken the X-Y bond of the added molecule and the M-X and M-Y bonds increase in strength (Figure 14).

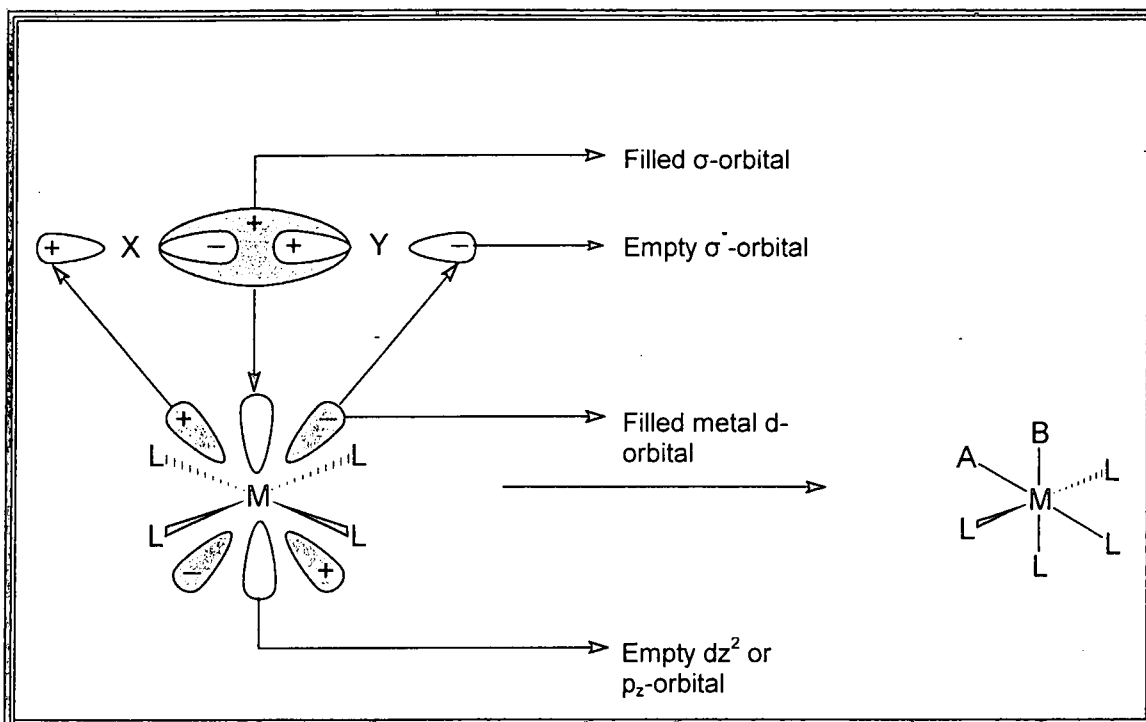


Figure 14 : The two-way electron flow in a concerted mechanism.

They concluded that nucleophilic attack of the added molecule on the metal at the early stages of the reaction is the most important step in the concerted addition. It also seems that this mechanistic route is favoured when the added molecules are H_2 , O_2 , Cl_2 or C_2H_4 and if the reaction is conducted in non-polar solvents^{44,46,47,49,50}.

It still remains a difficult task to determine the mechanism for a specific oxidative addition reaction. As an example the reaction between $[Rh(LL)(PR_3)(CO)]$ ($LL = acac, tfaa, cupf$ and $R = Ph$ or OPh) and CH_3I was believed to proceed along a S_N2 -ionic mechanistic route. After additional high pressure studies it was

discovered that the reaction actually proceeds along a concerted *cis* addition mechanistic route with a transition state as shown in **Figure 15(a)**.

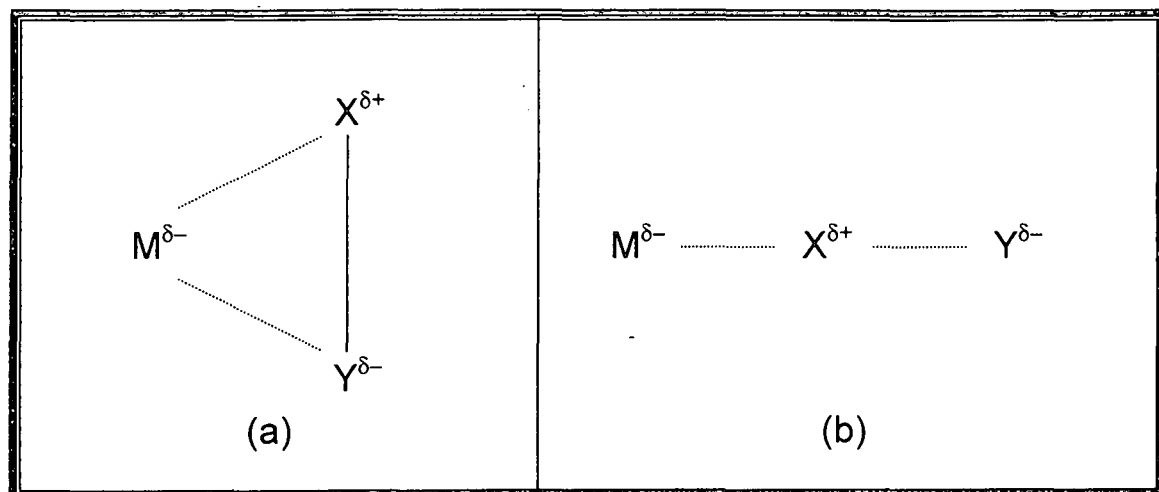


Figure 15 : The three-center (a) and linear (b) transition state used to represent oxidative addition reactions in general.

Thompson and Sears⁷¹ regarded it as useless to try and identify the transition state ((a) or (b) in **Figure 15**) for a number of reactions. They visualised a transition state between the two extremities shown in **Figure 15**, a three-center transition state (a) and a linear transition state (b).

Griffin⁷² *et al* used *ab initio* molecular orbital calculations for the addition of CH_3I to square planar complexes of rhodium and iridium and compared this to experimental kinetic data. They calculated values for both the three-center (one-step concerted mechanism) and linear transition (two-step $\text{S}_{\text{N}}2$ mechanism) states. The values for nucleophilic substitution (ΔE^\ddagger) showed a two fold increase in the reaction barrier in the three-center transition state, the same applied for the calculated kinetic rates. They found

⁷¹ Thompson, W.H.; Sears, C.T., *Inorg. Chem.*, **4**, 769 (1977)

⁷² Griffin, T.R.; Cook, D.B.; Hayes, A.; Pearson, J.M.; Monti, D.; Morris, G.E., *J. Am. Chem. Soc.*, **118**, 3029 (1995)

that the kinetic values of the linear transition state correlates best with the experimental values and concluded that the preferred mechanism for this reaction is the S_N2 mechanistic route.

We can thus see the correct choice of a mechanism for a reaction should be approached with caution.

b) The two-step S_N2 mechanism

The S_N2 mechanism is often found in the addition of methyl, allyl, acyl and benzyl halides to species such as Vaska's complex. Unlike the concerted mechanism, where nucleophilic attack of the added molecule on the metal occurs, the S_N2 mechanism involves nucleophilic attack by the metal on the α -carbon of the added molecule. Generally this can be represented as in Figure 16 where A represents the α -carbon of the added molecule.

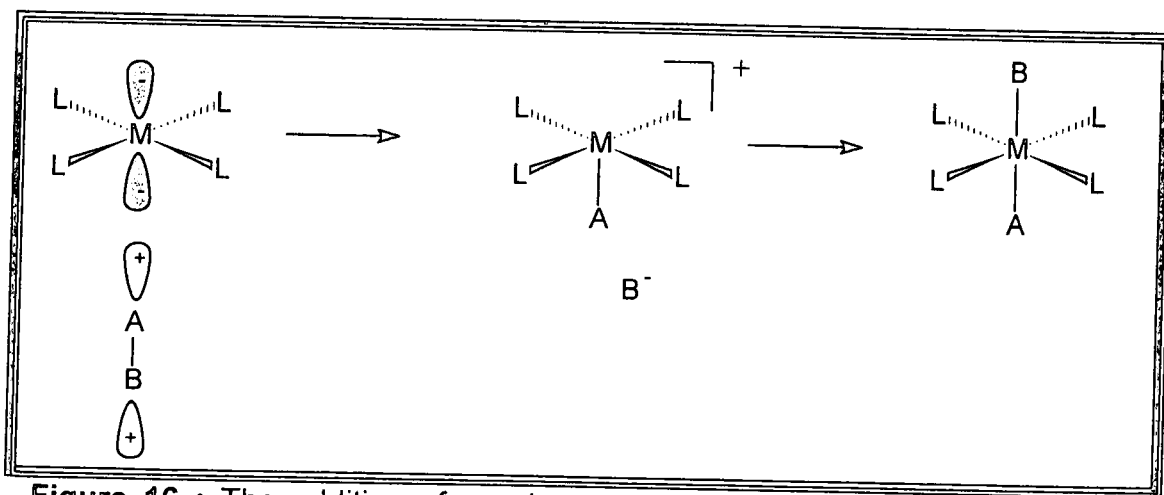


Figure 16 : The addition of a polar molecule like CH_3I to a square-planar complex.

The S_N2 mechanism, as in the case of the concerted type mechanism, is second order in nature, and can be accelerated by

OXIDATIVE ADDITION REACTIONS

the use of polar solvents. The S_N2 mechanism has large negative entropy values⁶⁰, which are dependent on solvent polarity. All this is consistent with a well-orientated, polar transition state, similar to what is seen for S_N2 reactions in organic chemistry. These observations lead to a proposed mechanism for oxidative addition where there is nucleophilic displacement of the halide by attack of the metal on the α -carbon in the initial step, followed by either a two-center or three-center transition state (Figure 17)^{55,60}.

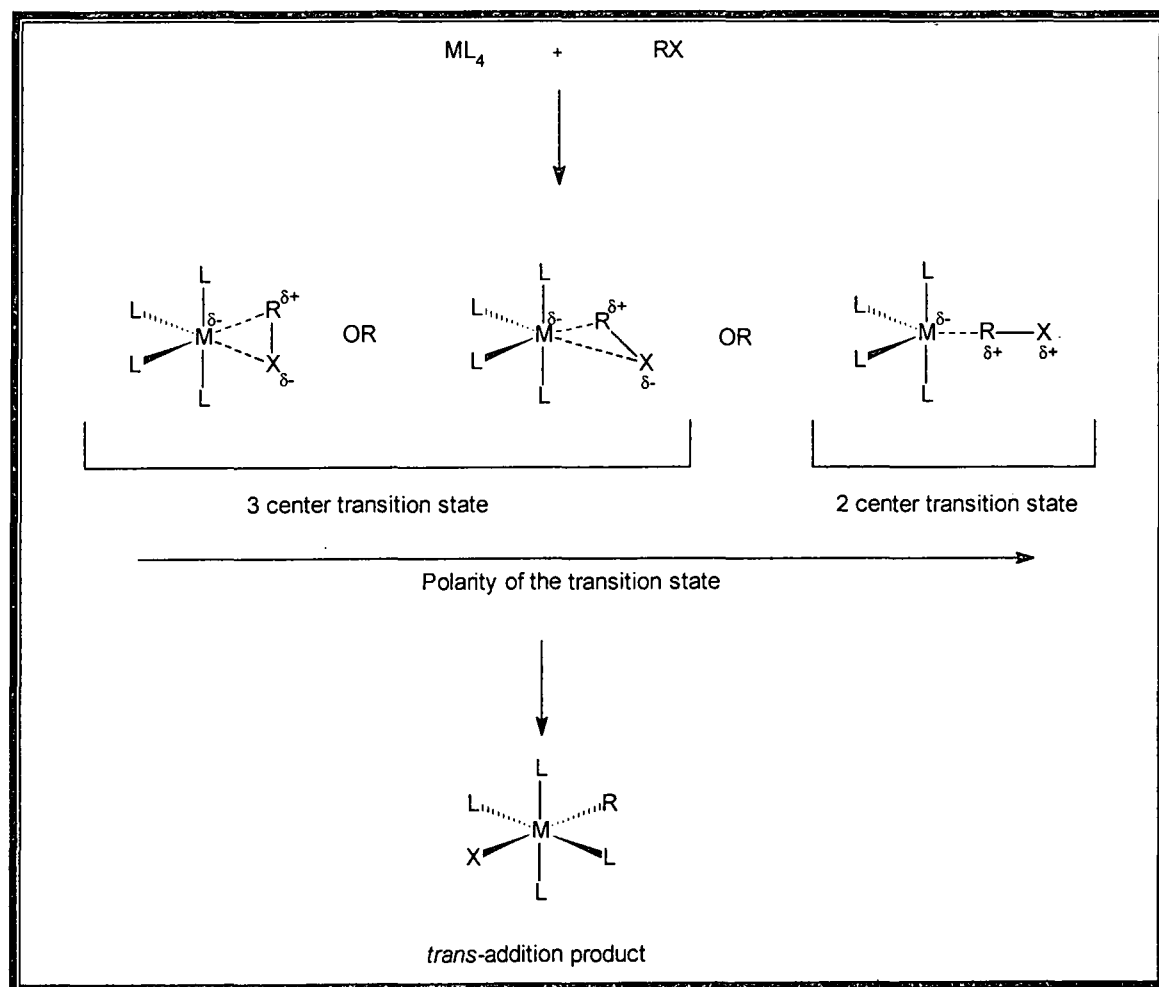


Figure 17 : Representation of the mechanism of S_N2 two-step oxidative addition and the differences in the polarity of the transition state.

Identification of the polar transition state would yield valuable proof for a S_N2 -type mechanism. Oliver and Graham⁷³ reported the first proof for the existence of a polar transition state with the reaction between $[\text{Rh}(\text{C}_5\text{H}_5)(\text{CO})\{\text{P}(\text{CH}_3)_2\text{C}_6\text{H}_5\}]$ and Br_2 . They used NaBPh_4 to isolate the cationic intermediate $[\text{Rh}(\text{C}_5\text{H}_5)(\text{CO})\{\text{P}(\text{CH}_3)_2\text{C}_6\text{H}_5\}\text{Br}]^+$. Similar results were found by Crespo⁷⁴ with the oxidative addition reaction between CH_3I and $[\text{Pt}(\text{Me})_2(\text{SMe})_2]$.

It is important to note that oxidative addition reactions proceeding along a S_N2 -type mechanism usually results in the *trans* product, unlike the one-step concerted mechanism where the *cis* configuration is dominant. It is however possible for the five-coordinated transition state in Figure 17 to isomerise to the *trans* product.

Stereochemistry might be a possibility to distinguish between the one-step concerted and the two-step S_N2 -type mechanism. The one-step concerted mechanism involves retention of the configuration, while inversion of the configuration is normally the case in the S_N2 -type mechanism. These changes in the stereochemistry of the final products can be assigned to the different interactions at the metal atom for the two mechanisms. Experimentally this proved not to be a viable method, since both inversion^{75,76,77} and retention⁷⁸ were reported for the oxidative addition reaction between the optically active $\text{CH}_3\text{CHBrCOOC}_2\text{H}_5$

⁷³ Oliver, A.J.; Graham, W.A.G., *Inorg. Chem.*, **9**, 243 (1970)

⁷⁴ Crespo, M.; Puddlephatt, R.J., *Organometallics*, **6**, 2548 (1987)

⁷⁵ Jensen, F.R.; Knickel, B., *J. Amer. Chem. Soc.*, **93**, 6339 (1971)

⁷⁶ Bradley, J.S.; Connor, D.E.; Dolphin, D.; Labinger, J.A.; Osborn, J.A., *J. Amer. Chem. Soc.*, **94**, 4043 (1972)

⁷⁷ Whitesides, G.M.; Boschetto, D.J., *J. Am. Chem. Soc.*, **93**, 1529 (1971)

⁷⁸ Connor, D.E.; Dolphin, D.; Labinger, J.A.; Osborn, J.A., *J. Amer. Chem. Soc.*, **95**, 7908 (1973)

and *trans*-[IrCl(CO)(PMePh₂)]. Final product geometries can thus not be used for identification between the two mechanisms, due to the fact of possible isomerisation of the transition state (**Figure 17**). Various examples where isomerisation was found have been reported^{79,80}.

Despite this there are still a number of examples where polar molecules bond *trans* to a metal complex. These can be used as proof of the mechanism⁸¹⁻⁸⁵.

The oxidative addition of an alkyl halide to a variation of Vaska's complex is a good example where the final product is *trans* as shown in **Figure 18**.

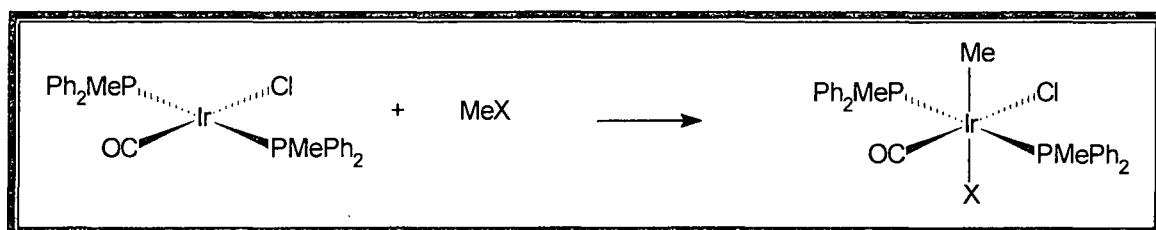


Figure 18 : The oxidative addition of an alkyl halide to a variation of Vaska's complex⁴⁹.

The work done by Collman and co-workers⁸¹ on a macrocyclic rhodium(I) complex is another fine example. As seen in **Figure 19** the chelate rings hinder isomerisation, resulting only in the *trans* product.

⁷⁹ Meakin, P.; Schunn, R.A.; Jesson, J.P., *J. Amer. Chem. Soc.*, **96**, 277 (1974)

⁸⁰ English, A.D.; Meakin, P.; Schunn, R.A.; Jesson, J.P., *J. Amer. Chem. Soc.*, **98**, 422 (1976)

⁸¹ Collman, J.P.; MacLaury, M.R., *J. Am. Chem. Soc.*, **96**, 3019 (1974)

⁸² Collman, J.P.; Sears Jr., C.T., *Inorg. Chem.*, **7**, 27 (1968)

⁸³ Collman, J.P.; Murphy, D.W.; Dolcetti, G., *J. Am. Chem. Soc.*, **95**, 2687 (1973)

⁸⁴ Patterson, J.L.; Nappier, I.T.E.; Meek, D.W., *J. Am. Chem. Soc.*, **95**, 8195 (1973)

⁸⁵ Morarskiy, A.; Stille, J.K., *J. Am. Chem. Soc.*, **103**, 4182 (1981)

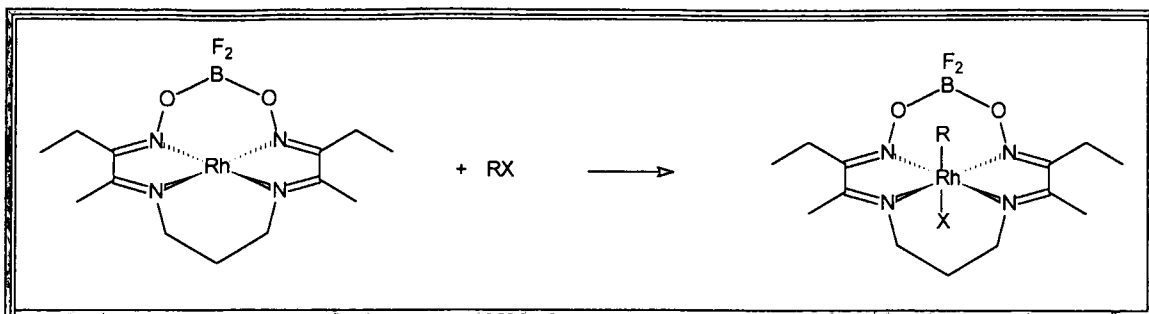


Figure 19 : The oxidative addition of an alkyl halide to a macrocyclic rhodium(I) complex.

From the results they concluded that the reaction proceeds *via* a cationic intermediate and predicted that the *trans* product found was a result of nucleophilic attack of the rhodium(I) complex on the carbon of the alkyl halide.

In general, polar solvents promote oxidative addition reactions that proceed *via* a two-step mechanism^{84,86-91}. The choice of solvent may however also influence the relation between the two pathways as is the case of the reaction between HX and Vaska's complex. When benzene⁹² or toluene⁹⁰ were used as solvents only *cis* addition was observed, while mixtures of *cis* and/or *trans* products was found in different benzene-methanol solutions. Both *cis* and *trans* isomers were found in solvents (CH₃CN, MeOH, H₂O and DMF) that solvates halide ions as well.

Nucleophiles like anions and some solvents, can act as ligands and therefore can coordinate with the metal complex thus making it more accessible for electrophilic attack. Such is the case with the

⁸⁶ Douek, I.C.; Wilkinson, G., *J. Chem. Soc. (A)*, 2604, (1969)

⁸⁷ Chock, P.B.; Halpern, J., *J. Amer. Chem. Soc.*, **88**, 3511 (1966)

⁸⁸ Ugo, R.; Pasini, A.; Fusi, A.; Cenini, S., *J. Amer. Chem. Soc.*, **94**, 7364 (1972)

⁸⁹ Stieger, H.; Kelm, H.Z., *J. Phys. Chem.*, 290 (1973)

⁹⁰ Jawad, J.K.; Puddephalt, R.J., *J. Organomet. Chem.*, **117**, 297 (1976)

⁹¹ Walper, K.; Kelm, H.Z., *Z. Phys. Chem. (Neue Folge)*, **113**, 207 (1978)

⁹² Blake, D.M.; Kubota, M., *Inorg. Chem.*, **9**, 989 (1970)

coordination of Br^- to the neutral complex $[\text{Ir}(\text{acac})(\text{cod})]$ to form a five-coordinated complex. The result of this was an increase in the rate of oxidative addition with CH_3I ⁹⁵. Both catalysed and uncatalysed pathways resulted in the same product.

Chelating ligands also have a positive effect on the rate of oxidative addition since this interaction increases the nucleophilicity on the metal.⁹³⁻⁹⁶ A good example of this is the use of the phosphine $\text{P}(\text{Me}_2)(o\text{-MeOC}_6\text{H}_4)$. When bonded to the metal, direct interaction between the *o*-oxygen and the metal occur, increasing the nucleophilicity of the metal and thus the rate of oxidative addition.

If all the factors are taken into consideration, the proof for a $\text{S}_{\text{N}}2$ mechanism can sometimes be clear, while in other cases it seem to fluxuate between the two- and three-center configurations. Thus, it is quite difficult to have absolute proof that a reaction proceeds along one specific pathway.

c) The ionic mechanism.

Hydrogen halides tend to react along an ionic mechanism in solution, where they are often largely dissociated. Two variants have been recognised of which examples are shown in **Figure 20**. In the more common one, the complex is sufficiently basic to protonate, after which the anion bonds to give the final product. The opposite case, in which the halide ion attacks first, followed by

⁹³ Constable, A.G.; Langrick, C.R.; Shabanzadeh, B.; Shaw, B.L., *Inorg. Chim. Acta*, **65**, L151 (1982)

⁹⁴ Heddon, D.; Roundhill, D.M.; Fultz, W.C.; Rheingold, A.J., *J. Am. Chem. Soc.*, **106**, 5014 (1986)

⁹⁵ Hickey, C.E.; Maitlis, P.M., *J. Chem. Soc., Chem. Commun.*, 1604 (1984)

⁹⁶ Miller, E.M.; Shaw, B.L., *J. Chem. Soc., Dalton Trans.*, 480 (1974)

protonation of the intermediate, is rare. The first route is favoured by basic ligands and a low oxidation state, the second by electron acceptor ligands and by a positive charge on the metal.

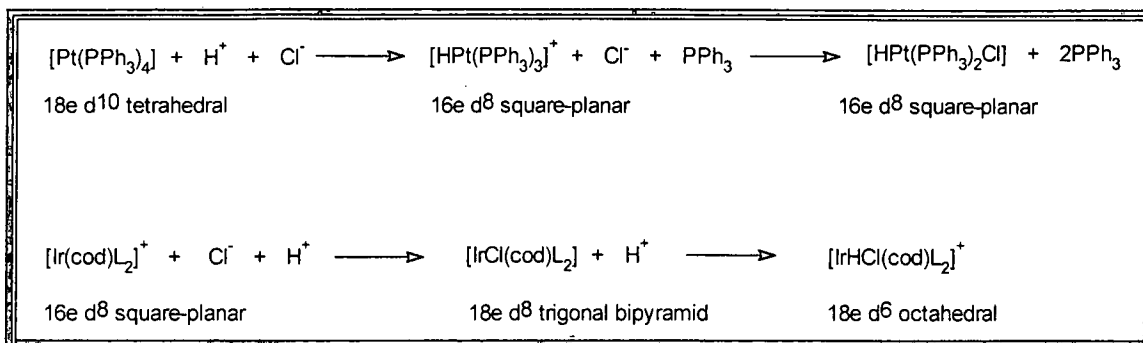


Figure 20 : Examples of the two variants of the ionic mechanism.

Polar solvents favour the pure ionic mechanism. Although a *trans* product is expected from this mechanism, a *cis* product can easily be formed with intermolecular exchange reactions during the intermediate steps of the reaction.

The solvent effect usually differentiates between the ionic and concerted mechanisms^{46,70} since the concerted mechanism generally occurs in non-polar solvents resulting in *cis* products.

4. Factors influencing oxidative addition.

From the previous discussion about mechanisms for oxidative addition it is clear that a number of factors play an important role in the preferred mechanism, the stereochemistry of the products and the reaction rate of oxidative addition. These factors are discussed in more detail in the following paragraphs.

a) The metal.

The metal atom in an organometallic complex is an important factor in the rate of oxidative addition. The ability of the metal to undergo oxidative addition is dependent on its ability to be oxidised as seen in **Figure 21** :

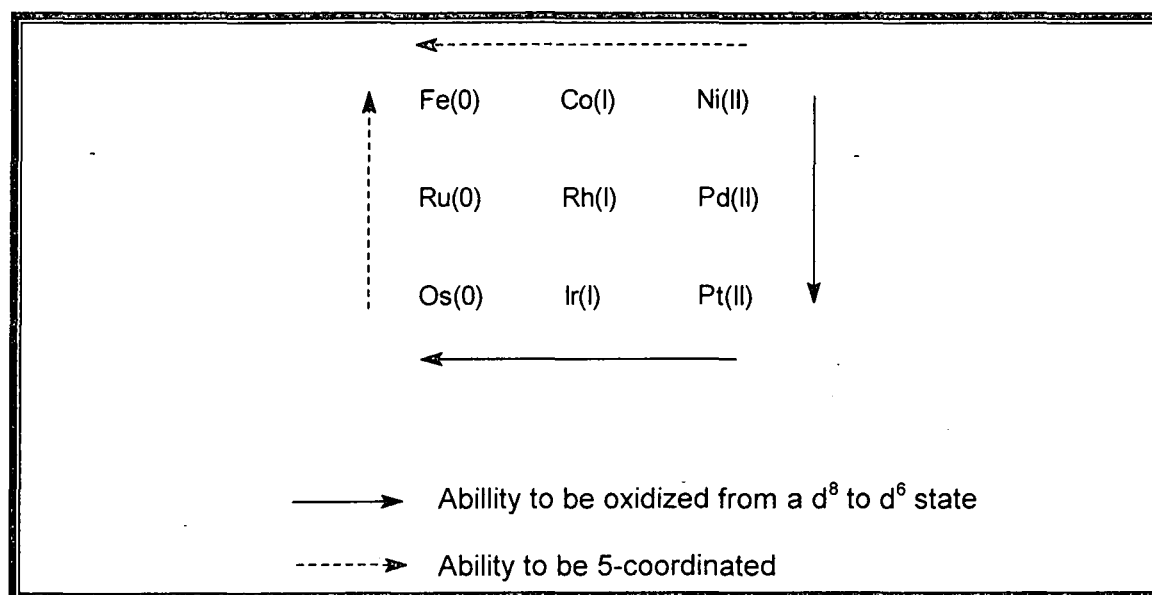


Figure 21 : Ability of d^8 metal ions of group VIII to undergo oxidative addition and to be five-coordinated.

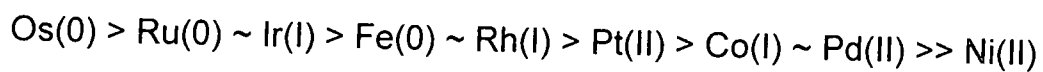
The general requirements for a metal to undergo oxidative addition are:

- i) The availability of non-bonding electron density on the metal.
- ii) The availability of two vacant coordination positions on the metal to form the two new bonds.
- iii) The ability to form a product with oxidation state two units higher than that of the starting product.

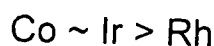
The nucleophilicity of organometallic complexes increases as one uses the larger 4d and 5d metal ions of group VIII. This tendency

can be observed in Vaska's complex, *trans*-[IrCl(CO)(PPh₃)₂], which reacts with the weak Lewis acid BF₃ to form a 1:1 complex.⁹⁷ The rhodium analogue requires stronger Lewis acids, e.g. BCl₃ and BBr₃ to react.⁹⁸ Thus it can be concluded that the iridium complex is more basic than the rhodium complex.

The increase in nucleophilicity of the metal complex also results in an increase of the rate of oxidative addition. An estimated reactivity series for oxidative addition can be presented as follows:⁹⁹



Generally this series can be used as an estimate when different metals are used for oxidative addition. There are however a few exceptions as reported by Vaska, Chen and Miller.¹⁰⁰ They found that oxidative addition to [M(phoss)₂][B(C₆H₅)₄] (M = Co, Rh, Ir) results in a change in the reactivity order:



Despite a few exceptions it seems that the larger 4d and 5d metal ions of group VIII are more basic and thus have a larger tendency to undergo oxidative addition.

⁹⁷ Scott, R.N.; Shiver, D.F.; Vaska, L., *J. Amer. Chem. Soc.*, **90**, 1079 (1968)

⁹⁸ Powell, P.; Nöth, H., *J. Soc. Chem. Commun.*, 637 (1966)

⁹⁹ Kubota, M.; Blake, D.M., *J. Amer. Chem. Soc.*, **93**, 1368 (1971)

¹⁰⁰ Vaska, L.; Chen, L.S.; Miller, W.N., *J. Amer. Chem. Soc.*, **93**, 6672 (1971)

b) The bonded ligands.◦ **Electronic effects.**

The σ - and π -bonding properties of ligands bonded to the metal can influence the rate of oxidative addition. Ligands with good σ -donating capabilities increase electron density on the metal and hence the rate of oxidative addition. The opposite effect is observed for π -acceptors that withdraw electron density from the metal.

The best example of a π -acceptor ligand is carbon monoxide. Although a weak σ -donor, it reacts with transition metals in low oxidation states (-1, 0, +1) to form stable complexes. Metals in a low oxidation state are electron rich and it can be expected of the d_{π} -electrons to become accessible because of the reduced effective nuclear charge Z^* . The interaction between the metal and the CO-ligand can be divided into two parts (**Figure 22**). Firstly, there is the overlap of the filled carbon σ -orbital with a σ -type orbital on the metal. This results in a high concentration of electrons on the metal, which it will attempt to reduce by pushing it back to the ligand. The second part involves the overlap of a filled d_{π} or hybrid dp_{π} -orbital of the metal with an empty p_{π} -orbital on CO.

The drift of metal electrons into the CO-orbitals, will tend to make CO as a whole negative, increasing the drift of electrons through the σ -bond to the metal. This drift of electrons to the metal in the σ -

bond tends to make the CO positive, enhancing the acceptor strength of its π -orbitals. This bonding mechanism is synergic, since the effects of σ -bond formation strengthen the π -bonding and *vice versa*.

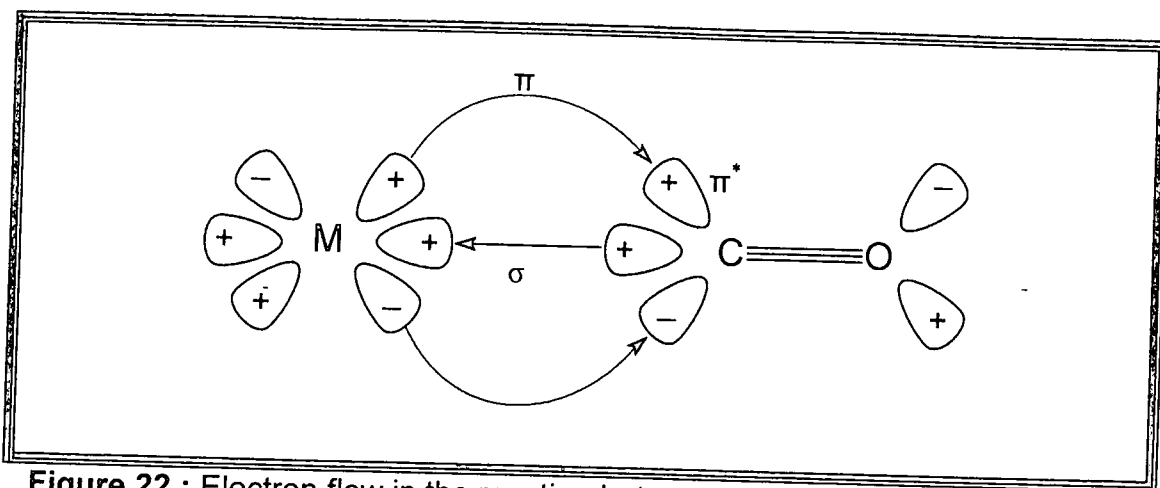


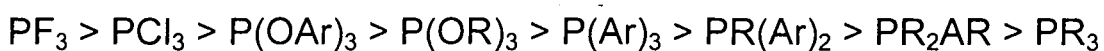
Figure 22 : Electron flow in the reaction between a metal and CO.

Ligands, which are capable of increasing nucleophilicity of the metal by their σ -donating capabilities, are the trivalent phosphorus compounds of the type PX_3 (also the AsX_3 , SX_2 and SeX_2 species) that is widely used in organometallic compounds. The lone pair of electrons in the phosphorus atom are responsible for the σ -donating capabilities of these types of ligands. There are however examples where some π -bonding between the ligand and the metal complex occurs. This usually happens when groups, e.g. OR, Cl or F, bonded to the phosphorus are electron withdrawing, resulting in a lower electron density on the metal and a lower nucleophilicity. Initial theories proposed that π -back bonding takes place to available empty 3d-orbitals. This was proved wrong by Marynick¹⁰¹ indicating with molecular orbital calculations that π -

¹⁰¹ Marynick, D.S., *J. Amer. Chem. Soc.*, 106, 4064 (1984)

back bonding is in actual fact from the d_{π} -orbitals of the metal to the σ^* -orbital of the metal-phosphorus bond.

The π -accepting capabilities were determined with the use of $[\text{LNi}(\text{CO})_3]$ -complexes for a large number of PX_3 , AsX_3 and SbX_3 ligands.^{102,103} According to the $\nu(\text{CO})$ values and ^{13}C NMR chemical shifts the π -accepting tendencies of phosphorus ligands can be placed in the following order:



Both the AsX_3 and SbX_3 correlate with the phosphorus ligand series.

All the properties of the metal phosphorus bond cannot be explained with the π -bonding model. Pidcock¹⁰⁴ proposed a model in which he indicated that two extreme possibilities in the bonding between the metal and the phosphorus ligand exist :

- i) Organophosphorus compounds only forms σ -bonds in cases where the metal has an oxidation state of +2 or higher.
- ii) Bonds with both σ - and π -components are formed between PF_3 , PCl_3 and $\text{P}(\text{OPh})_3$ ligands and metals in low oxidation states.

¹⁰² Bodner, G.M.; May, M.P.; McKinney, L.E., *Inorg. Chem.*, **19**, 1971 (1980)

¹⁰³ Bertik, T., et. al., *J. Organomet. Chem.*, **272**, 29 (1984)

¹⁰⁴ Pidcock, A., *Transition Metal Complexes of P, As, Sb and Bi ligands*, C.A. McAuliffe, Part 1, MacMillan, London (1973)

The influence of these variables is shown in **Figure 23**. Without electronegative groups bonded to the phosphorus ligands, the 3d-orbitals would be widely distributed and π -bonding would be impossible, as is the case with PBU_3 ¹⁰⁵. Similar results are found for PMe_3 ¹⁰⁶⁻¹⁰⁸.

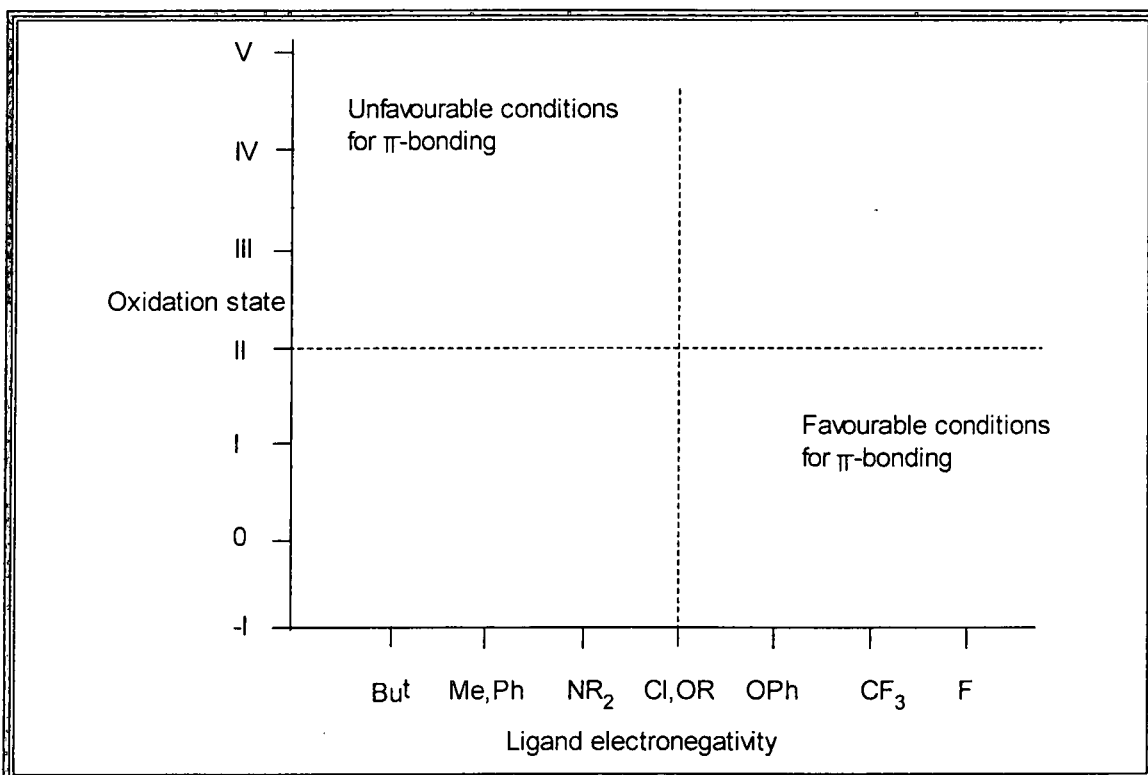


Figure 23 : Conditions where π -bonding is possible depending on the oxidation state of the metal and the electronegativity of the phosphorous ligands.

An excellent example of the electronic effect of a different phosphorus ligands is shown in the oxidative addition reaction of $[\text{Rh}(\text{acac})(\text{CO})(\text{PX}_3)]$ with CH_3I ($\text{PX} = \text{P}(\text{p-PhCl})_3, \text{PPh}_3, \text{P}(\text{p-PhOMe})_3$)²⁸. The $\nu(\text{CO})$ values in **Table 4** are those of the acyl product $[\text{Rh}(\text{acac})(\text{CH}_3)(\text{I})(\text{CO})(\text{PX}_3)]$ after oxidative addition.

¹⁰⁵ Emsley, J.; Hall, D., *The Chemistry of Phosphorous*, Harper & Row Publishers (1976)

¹⁰⁶ Huheey, J.E., *Inorganic Chemistry*, Harper & Row Publishers, New York (1972)

¹⁰⁷ Yarbrough, L.W.; Hall, M.B., *Inorg. Chem.*, **17**, 2269 (1978)

¹⁰⁸ Ball, E.E.; Ratner, M.M.; Sabin, J.R., *Chem. Scr.*, **12**, 128 (1977)

OXIDATIVE ADDITION REACTIONS

Table 4 : Experimental data for the oxidative addition of CH₃I to [Rh(acac)(CO)(PX₃)].

PX ₃	k ₁ x 10 ³ (M ⁻¹ s ⁻¹)	K(M ⁻¹)	ν(CO)cm ⁻¹
P(<i>p</i> -PhCl) ₃	3.46(9)	4.0(2)	2064
PPh ₃	23(3)	9(1)	2060
P(<i>p</i> -PhOMe) ₃	138(3)	16(2)	2056

The kinetic results shown in **Table 4** indicate an increase in the rate constants from P(*p*-PhCl)₃ to P(*p*-PhOMe)₃, which can be correlated to the phosphines σ-donating capabilities. This correlation can be seen from the ν(CO) values, which are an indication of the electronic influence of the different phosphines. A decrease in the ν(CO) value indicates a weakening of the carbon-oxygen bond due to the increase in bond strength of the metal-carbon bond. This results in better π-back donating capabilities for the more electron-rich phosphine.

The phosphines can be placed in the following order of donating capabilities derived from the ν(CO) values:



These differences in oxidative addition rates can only be assigned to electronic effects, since the same solvent was used and the steric parameters (described in the next paragraph) for the three phosphines are the same.

- Steric effects.

The accessibility of the metal ion for electrophilic attack is an important factor in the rate of oxidative addition reactions. The degree of accessibility is greatly influenced by the bulkiness of the bonded ligands, e.g. PX_3 . These steric properties of the ligand play an important role in some highly selective catalytic reactions like hydroformylation and asymmetric hydrogenation^{19,20}.

It was Tolman¹⁰⁹ who first quantified values for the steric and electronic parameters of phosphines and phosphites. The steric parameter θ for symmetrical ligands is defined as follows: It is the top angle of a cone constructed so that the distance between the top of the cone and the center of the phosphorus atom is 2.28\AA (average Ni-P bond distance) and the sides of the cone are tangent to the Van der Waals radii of the outermost atoms on the substituents (Figure 24).

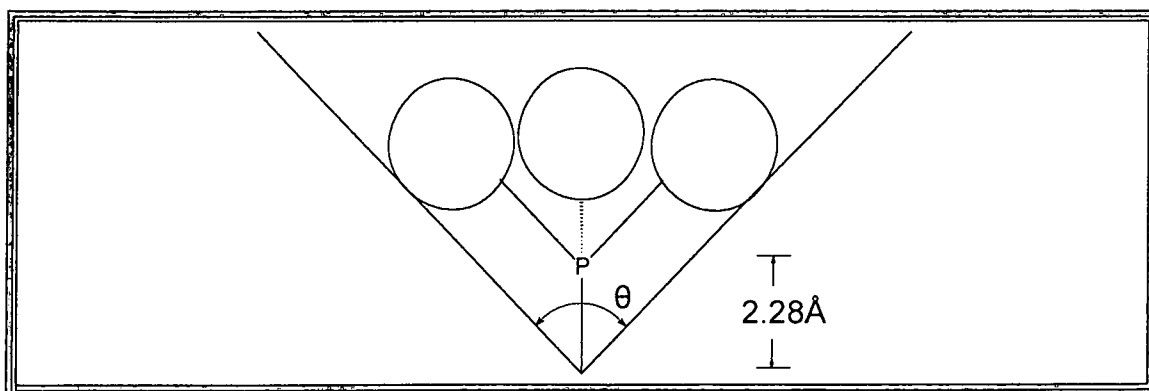


Figure 24 : Representation for the calculation of the cone angles in symmetrical phosphines.

¹⁰⁹ Tolman, C.A., *Chem. Rev.*, 77, 313 (1977)

OXIDATIVE ADDITION REACTIONS

In the case of non-symmetrical $PX_1X_2X_3$ ligands it is assumed that $\theta_i/2$ would be the same as $P(X_i)_3$ (**Figure 25**)

With use of the equation:

$$\theta = \left(\frac{2}{3} \right) \sum_{i=1}^3 \frac{\theta_i}{2}$$

the steric parameters of a non-symmetrical phosphine can be determined.

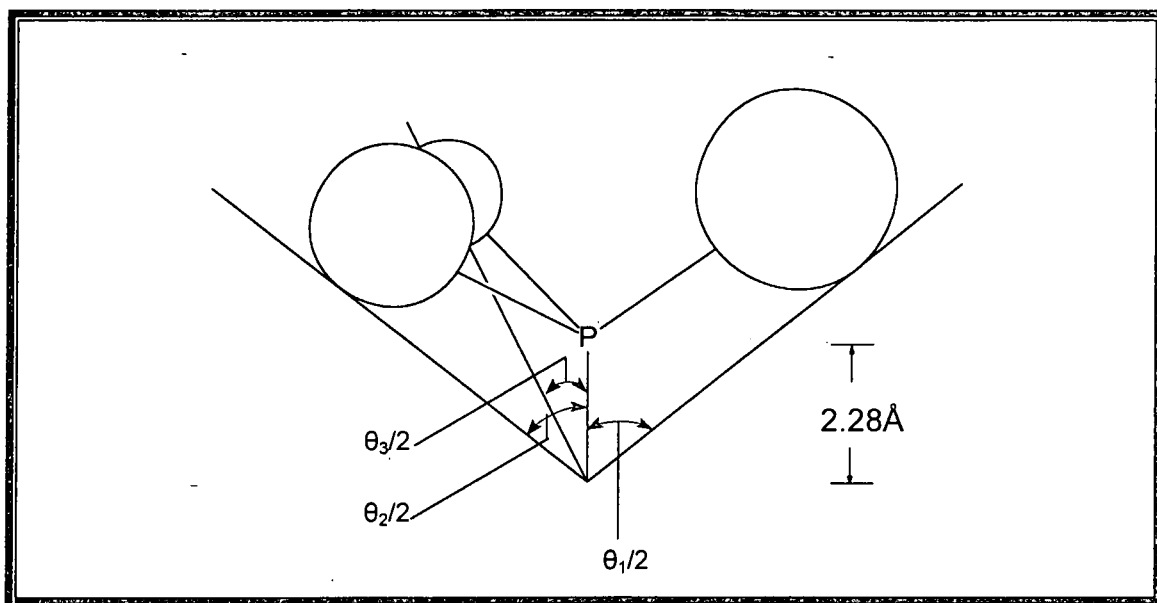


Figure 25 : Representation for the calculation of the cone angles in non-symmetrical phosphines.

The model of Tolman assumes that :

- i) The phosphines are tetrahedrally surrounded with substituents.
- ii) The angle between substituents in the unstrained model is $109,5^\circ$.
- iii) Free rotation is possible at all times around the bond axis.

Criticism¹¹⁰ against the model states that the Ni-P bond length varies from ligand to ligand and a fixed bond length is thus not realistic. It is also mentioned that the ligands are not cones. Despite this the model is still regarded as valid.

An increase in the steric properties of phosphines usually promotes the following:

- i) Complexes with lower coordination numbers.
- ii) Isomers with the least steric crowding.
- iii) An increase in the rate and equilibrium constants of the dissociation of bonded ligands.

An excellent example of the influence of the steric parameters were done by Hart-Davis and Graham¹¹¹ in the reaction between $[(\eta^5\text{-C}_5\text{H}_5)\text{Co}(\text{CO})\text{L}]$ and CH_3I where $\text{L} = \text{PPh}_3$, PMePh_2 and PMe_2Ph .

The kinetic results in **Table 5** show a clear increase in the relative rates of oxidative addition from PPh_3 to PMe_2Ph . Since the differences in the electronic parameters are negligible, it can be assumed that this influence remains constant. Thus, the increase in reaction rates can only be explained by the differences in steric bulkiness of the phosphine ligands.

¹¹⁰ McAuliffe, C.A.; Levasan, W., *Phosphine, Arsine and Stibine Complexes of Transition Elements*, Elsevier Scientific Publ. Comp., Amsterdam, 66 (1979)

¹¹¹ Hart-Davis, A.J.; Graham, W.A.G., *Inorg. Chem.*, 9, 2658 (1970)

OXIDATIVE ADDITION REACTIONS

Table 5 : Comparison of the effect of electronic and steric parameters on the rate of oxidative addition induced by different phosphine ligands.

Ligand	Electronic parameter (cm^{-1})	Tolman cone angle ($^{\circ}$)	Relative rates of oxidative addition
PPh_3	2068.4	145	1
$\text{PMe}(\text{Ph})_2$	2067.0	136	5.8
PMe_2Ph	2065.3	122	11.7

c) The bidentate ligand.

The influence of the bidentate ligand bonded to the metal also has an important role on the rate of oxidative addition. By changing the substituents bonded onto the bidentate ligand, electron density can be added or withdrawn from the metal, resulting in a change in the rate of oxidative addition.

The β -diketone bidentate ligands (**Figure 26**) were studied extensively by our research group and have shown a clear effect on the rate of oxidative addition.

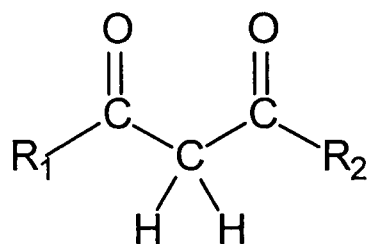


Figure 26 : General structure of a β -diketone.

It is important to notice that the reactivity of different β -diketones depend on their ability to undergo keto-enol tautomerism as shown in Figure 27.

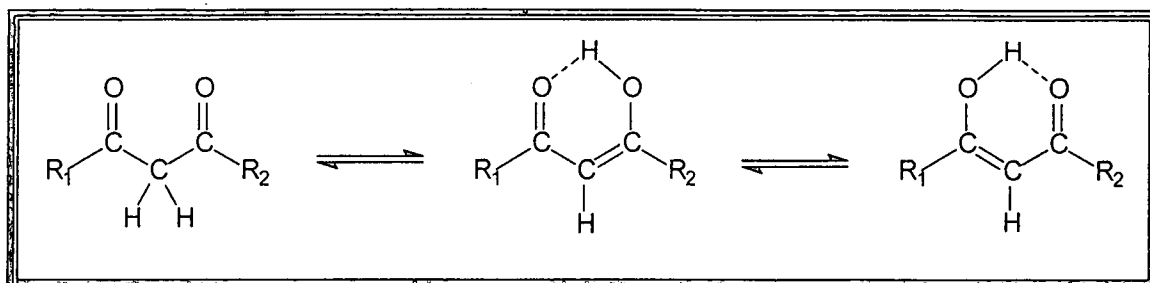


Figure 27 : Keto-enol tautomerism of β -diketones.

The enolic hydrogen atom of the β -diketone can, under favourable conditions, dissociate to produce the conjugate base anion that reacts with a metal cation to produce a six-membered chelate ring, resulting in the shift of the keto-enol equilibrium in favour of the enol form. The enol form is favoured in non-polar solvents, and the simultaneous conjugation and chelation through hydrogen bonding is responsible for the stability of the enol tautomers. Substitution of the R_1 and R_2 groups by highly electronegative atoms also enhances enolization of the β -diketones^{112,113} while the use of bulky groups often have a decreasing effect¹¹⁴⁻¹¹⁶.

Table 6 shows a summary of the different substituents on β -diketones. The table shows that the substitution of the R_1 and R_2 groups by electron withdrawing groups results in complexes with low pK_a values due to a decrease in enol formation.

¹¹² Park, J.D.; Brown, H.A.; Lachen, J.R., *J. Am. Chem. Soc.*, **75**, 4753 (1953)

¹¹³ Burdett, J.L.; Rogers, M.T., *J. Am. Chem. Soc.*, **86**, 2105 (1964)

¹¹⁴ Koshimura, H.; Saito, J.; Okubo, T., *Bull. Chem. Soc., Japan*, **46**, 632 (1923)

¹¹⁵ Uhlemann, E.; Suchan, W.W., *Z. Anorg. Alleg. Chem.*, **342**, 41 (1966)

¹¹⁶ Kloose, G.; Thomas, Ph.; Uhlemann, E.; Marki, J., *Tetrahedron*, **22**, 2695 (1966)

OXIDATIVE ADDITION REACTIONS

Table 6 : Summary of the different substituents of different β -diketones and their pK_a values.

β -diketone*	R ₁	R ₂	pK_a
dbm	Ph	CH ₃	9.35 ¹¹⁷
acac	CH ₃	CH ₃	8.95 ¹¹⁷
ba	Ph	CH ₃	8.55 ¹¹⁸
tfaa	CF ₃	CH ₃	6.30 ¹¹⁷
tfba	CF ₃	Ph	6.30 ¹¹⁷
hfaa	CF ₃	CF ₃	4.43 ¹¹⁸
tfdmaa	CH(CH ₃) ₂	CF ₃	-

*See list of abbreviations for the names of the β -diketones.

The reaction of CH₃I with [Rh(β -diketone)(CO)(PPh₃)] was investigated²⁷ by our group, using different substituents (R₁ and R₂) on the β -diketone, each influencing the rate of oxidative addition differently.

The results of the oxidative addition between [Rh(β -diketone)(CO)(PPh₃)] and CH₃I are given in **Table 7**.

Table 7 : Experimental results for the oxidative addition of CH₃I with different [Rh(β -diketone)(CO)(PPh₃)] complexes in acetone at 25°C.

β -diketone*	R ₁	R ₂	pK_a	$\nu(\text{CO})\text{cm}^{-1}$	Relative rates
acac	CH ₃	CH ₃	8.95	1988	50.7
tfaa	CF ₃	CH ₃	6.30	1996	12.2
tfdmaa	CH(CH ₃) ₂	CF ₃	-	1998	11.2
hfaa	CF ₃	CF ₃	4.43	2000	1.0

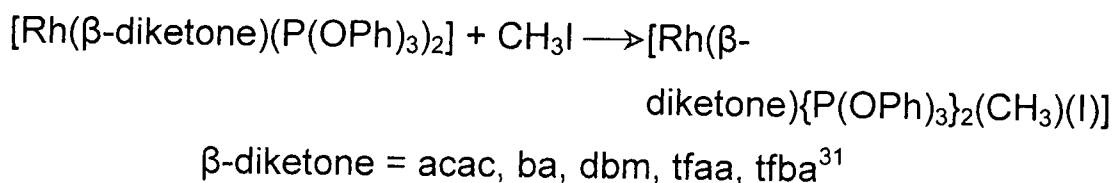
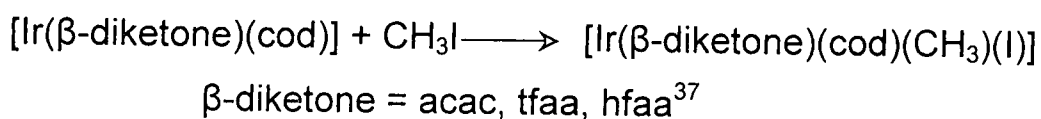
*See list of abbreviations for the names of the β -diketones.

Electronegative substituents on the β -diketone, e.g. CF₃, reduce the nucleophilicity of the metal. This makes the metal less reactive

¹¹⁷ Jiri Stary, *The Solvent Extraction of Metal Chelates*, Pergamon Press LTD Oxford, England (1964)

¹¹⁸ Sekine, T.; Hasegawa, Y.; Naohiko, I., *J. Inorg. Nucl. Chem.*, **35**, 3968 (1973)

towards oxidative addition as seen in the relative rates. The lower electron density on the metal results in a weaker π -back donation to the carbonyl ligand and can be seen in the increase of $\nu(\text{CO})$ (stronger CO-bonding). This also correlates with the pK_a values of the β -diketones (values of relative rates increase as pK_a increases). This effect is also noticed in the following reactions:



The rate of oxidative addition reactions are also dependent on the type of σ -donor atoms with which the bidentate ligand bonds. Terblans³⁹ investigated the influence of different O-O-, S-N- and O-S-bidentate ligands on the rate of oxidative addition between CH_3I and $[\text{Ir}(\text{LL}')(\text{cod})]$. The results are shown in Table 8.

Table 8 : Influence of different donor atoms on the rate of oxidative addition between $[\text{Ir}(\text{LL}')(\text{cod})]$ and CH_3I .

LL'*	Donor atoms	$k \times 10^3 (\text{M}^{-1} \text{s}^{-1})$
macsm	N-S	28.47(7)
sasas	O-S	5.2(2)
tfaa	O-O	4.4(2)
cupf	O-O	2.7(7)

*See list of abbreviations for the names of the LL' ligands.

The kinetic results in **Table 8** show a clear increase in the rate of oxidative addition from [Ir(cupf)(cod)] to [Ir(macsm)(cod)] indicating the effect of changing from O-O-donor ligands to N-S-donor ligands.

d) The added molecule.

The added molecule has an influence in the mechanism, the stereochemistry as well as the nature of the oxidative addition products. According to Collman and Hegedus⁴⁴ the added molecule can be classified, on the basis of stereochemistry and the type of oxidative addition products (*cis* or *trans*), into three groups. The classification of different added molecules is shown in **Table 9**.

Table 9 : The different classes of oxidative addition reagents X-Y.

Class A: Non-polar and low polarity reagents.
H ₂ , R ₃ SiH (R = alkyl, aryl), RH, ArH, R ₃ SnH, RSH, RSSR, RTeTeR, (SCN) ₂ , NC-CN, Ph-PPh ₂ , B-H, R ₃ Sn-SnR ₃
Class B: Electrophilic reagents.
HX, X ₂ , RCO ₂ H, RX, ArX, ArCN, CCl ₄ , CHCl ₃ , CH ₂ X ₂ , CH ₂ (OTs) ₂ , ROTs, RC(O)X, RSO ₂ X, ROSO ₂ X, RC(O)-OPh, HCHO, RCHO, H ₂ O ^m , ROH ^m , R ₃ C ₃ ⁺ , HgX ₂ , SnCl ₄ , GeCl ₄ , R ₃ SnCl, R ₃ PbCl, Ar ₂ SnCl ₂ , Ar ₂ PbCl ₂ , SnCl ₆ ²⁻
Class C: Reagents where X and Y retains a bond between them.
O ₂ , S ₂ , Se ₂ , cyclopropane en similar rings, epoxide, 1,3 dipoles

The non-polar addenda of class A react only with coordinative unsaturated complexes in a concerted three-center mechanism,

and only *cis* addition takes place (see **Figure 11**). If *trans* addition is found, isomerisation of the original *cis* product has occurred.

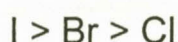
Added molecules of class B generally proceed along a polar, S_N2 two-step or a free radical mechanism. The products of these reactions can either be *cis* or *trans*, but in the case of alkyl halides it is generally found to be *trans*^{44,47}. The reactivity of alkyl halides in oxidative addition reactions are determined by:

- i) The length of the alkyl chain (also known as the steric volume of the substituents on the alkyl group).
- ii) The inductive effect of X (X = Cl, Br, I).
- iii) The polar character of the carbon atom attacked.
- iv) The dissociative energy of C-X.
- v) The donating properties of the halogen.

The reactivity of the alkyl substituent of alkyl halides can be ordered as follow in the series:⁸¹



The order of the halogen reactivity can be given in the series:^{86,83,119}



The possibility of a free radical mechanism increases as R changes in the series¹²⁰:

¹¹⁹ Stille, J.K.; Lau, K.S.Y., *Acc. Chem. Res.*, 10, 434 (1977)

OXIDATIVE ADDITION REACTIONS

Primary < secondary < tertiary < benzyl or allyl

The possibility of a free radical mechanism also increase as X changes:¹²⁰



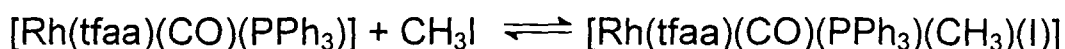
The unsaturated reagents in class C retain at least one bond in the added molecule. In this case only the *cis* product is possible. (See **Figure 5** reactions with O₂ and MeO₂CC≡CCO₂Me)

e) The effect of a solvent.

The solvent can influence the rate, stereochemistry, mechanism, and final product composition of an oxidative addition reaction. These will be discussed individually in the next paragraphs:

- The effect of a solvent on the rate of oxidative addition reactions.

The polarity (dielectric constant) of the solvent in which the reaction is carried out also influences the rate of the reaction^{27,92,81}. The reaction investigated by Basson and co-workers²⁷ is a good example of this:



The experimental rate law was derived as:

¹²⁰ Pearson, R.G.; Figidare, P.E. *J. Amer. Chem. Soc.*, 102 (5), 1541 (1980)

$$k_{\text{obs}} = \frac{k_2 K_1 [\text{CH}_3\text{I}]}{1 + K_1 [\text{CH}_3\text{I}]}$$

The solvent in which the reaction was carried out ranged from acetone to toluene. The use of a solvent with low polarity, e.g. toluene and chlorobenzene resulted in small K_1 values. The above rate law then simplifies to:

$$k_{\text{obs}} = k_2 K_1 [\text{CH}_3\text{I}]$$

The influence of solvent effectiveness towards oxidative addition is given in **Table 10** in terms of $k_2 K_1$ values.

Table 10 : The influence of solvent on the rate of oxidative addition in the reaction between $[\text{Rh}(\text{tfaa})(\text{CO})(\text{PPh}_3)]$ and CH_3I .

Solvent	ϵ	$K_1 k_2 \times 10^4 (\text{M}^{-1} \text{s}^{-1})$
acetone	20.7	17.2(7)
1,2-dichloroethane	10.36	11.3(5)
chlorobenzene	5.71	0.91(7)
toluene	2.44	0.32(4)

The $k_2 K_1$ values increases in the order of toluene to acetone (53.8 more than in toluene), which indicates that a highly polar solvent increases the rate of oxidative addition.

The same research group found similar results²⁹ with the oxidative addition reaction shown in **Figure 28**:

OXIDATIVE ADDITION REACTIONS

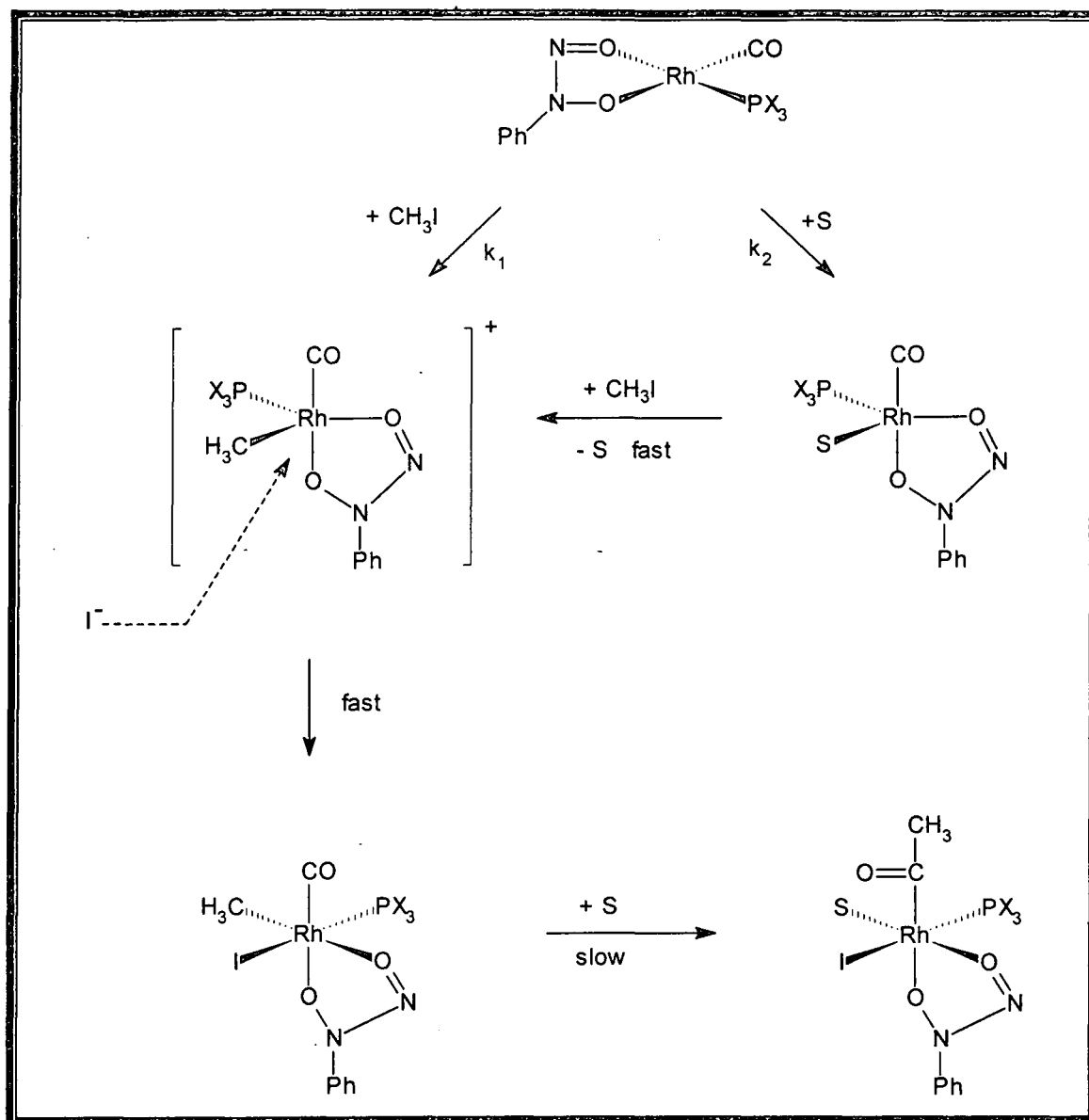


Figure 28 : The reaction scheme of the oxidative addition of CH_3I and $[\text{Rh}(\text{cupf})(\text{CO})(\text{PX}_3)]$.

Changes in the rates of the competing pathways were noticed as the polarity of the solvent change. These results are summarised in **Table 11**. The rate of oxidative addition (k_1 -path) changes with a factor 840 as the polarity of the solvents increase from benzene to DMSO and the mechanism also included a separate solvent catalysed route.

Table 11 : The influence of solvent on the rate of oxidative addition in the reaction between $[\text{Rh}(\text{cupf})(\text{CO})(\text{PPh}_3)]$ and CH_3I .

Solvent	ϵ	$10^3 k_1$ ($\text{M}^{-1}\text{s}^{-1}$)	$10^4 k_2$ (s^{-1})
benzene	2.3	0.0093(5)	0.006(3)
ethyl acetate	6.0	0.229(5)	0.14(3)
acetone	20.7	1.22(2)	3.1(1)
methanol	32.6	2.5(2)	0.2(1)
acetonitrile	38.0	4.2(2)	7.1(1)
DMSO	45.0	7.8(2)	28(1)

Highly polar solvents favour the solvent route (k_2 -path in **Figure 28**) since a factor 4667 increase was found in the k_2 -path, while only a factor of 840 was noticed for the k_1 -path.

Such results were also found by Ugo et al⁸⁸ with oxidative addition between *trans*- $[\text{IrCl}(\text{CO})(\text{PPh}_3)_2]$ and CH_3I and also by Pearson and Rajaram¹²¹.

All these results indicate that a polar solvent assists charge separation during the transition state and justifies the postulation of an ion pair as an intermediate¹¹¹.

◦ The influence of solvents on the stereochemistry of oxidative addition.

The stereochemistry of the oxidative addition products can also be influenced by the solvent used^{92,122}.

¹²¹ Pearson, R.G.; Rajaram, J., *Inorg. Chem.*, 13 (1), 246 (1974)

¹²² Henrici-Olive, G.; Olive, S., *J. Organometal. Chem.*, 35, 381 (1972)

The reaction of $[\text{IrCl}(\text{CO})(\text{PPh}_3)_2]$ and HX ($\text{X} = \text{Cl}, \text{Br}$) is an example of this⁹². If the reaction is done in methanol, acetonitrile, H_2O or DMF both *cis* and *trans* isomers can be found as shown in **Figure 29**.

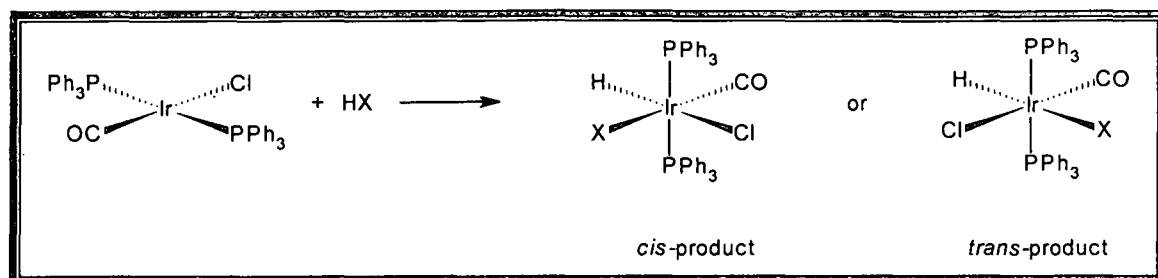


Figure 29 : The reaction of $[\text{IrCl}(\text{CO})(\text{PPh}_3)_2]$ and HX ($\text{X} = \text{Cl}, \text{Br}$) gives different isomers in different solvents.

Only the *cis* product can be found if benzene or chloroform is used.

- The influence of solvent in the mechanism of oxidative addition.

The solvent used can also influence the mechanism with which an oxidative addition reaction takes place. Solvents that act as ligands can coordinate to square planar complexes to form five coordinated complexes. These complexes then have a greater susceptibility to electrophilic attack, which means a faster rate of oxidative addition. An example of this is the reaction between $[\text{Ir}(\text{LL}')(\text{cod})]$ ($\text{LL}' = \text{Sacac}, \text{taa}$) and CH_3I in acetonitrile (**Figure 30**)³⁹.

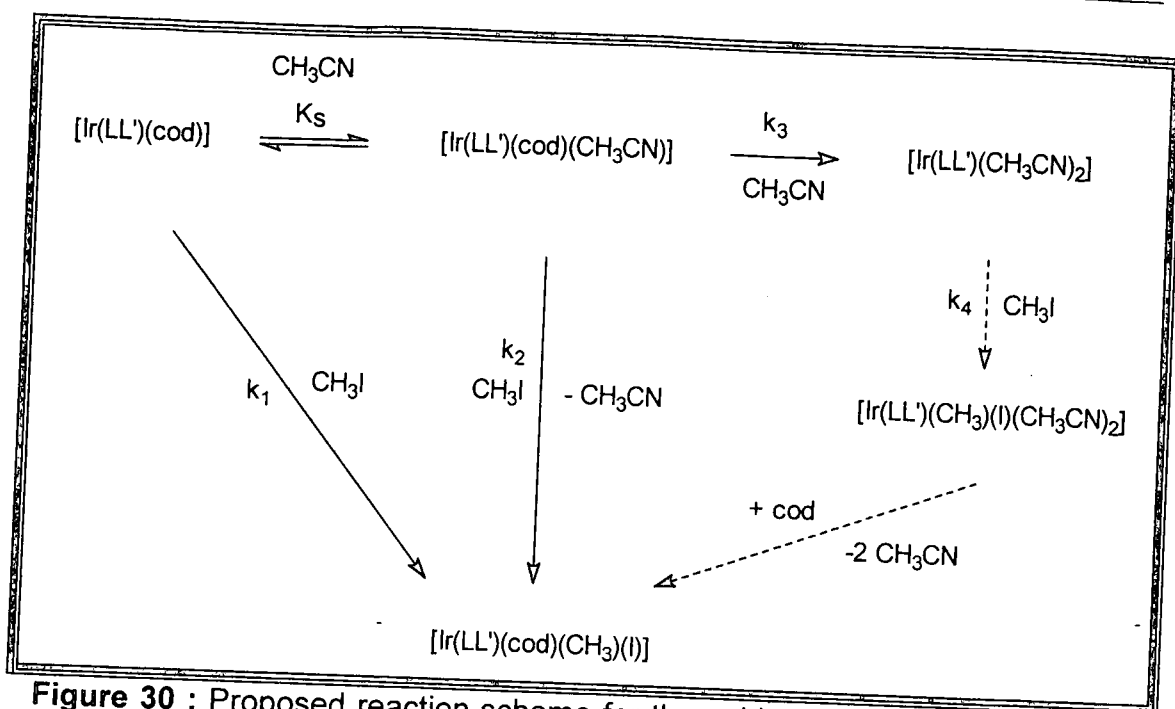


Figure 30 : Proposed reaction scheme for the oxidative addition reactions of [Ir(LL')(cod)] (LL' = Sacac, tfaa) with CH₃I.

If the reaction is carried out in chloroform, dichloromethane, acetone or chlorobenzene only the k_1 path is valid.

- The influence of solvent on the product composition of oxidative addition.

Lastly the solvent can also influence the composition of the products of an oxidation addition reaction. A good example of this is the reaction between *trans*-[IrCl(CO)(PPh₃)₂] and different azides done in different solvents (**Figure 31**)¹²³.

¹²³ Collman, J.P., Kubota, M., Vastine, F.D., Sun, J.Y., *J. Am. Chem. Soc.*, **90**, 5430 (1968)

OXIDATIVE ADDITION REACTIONS

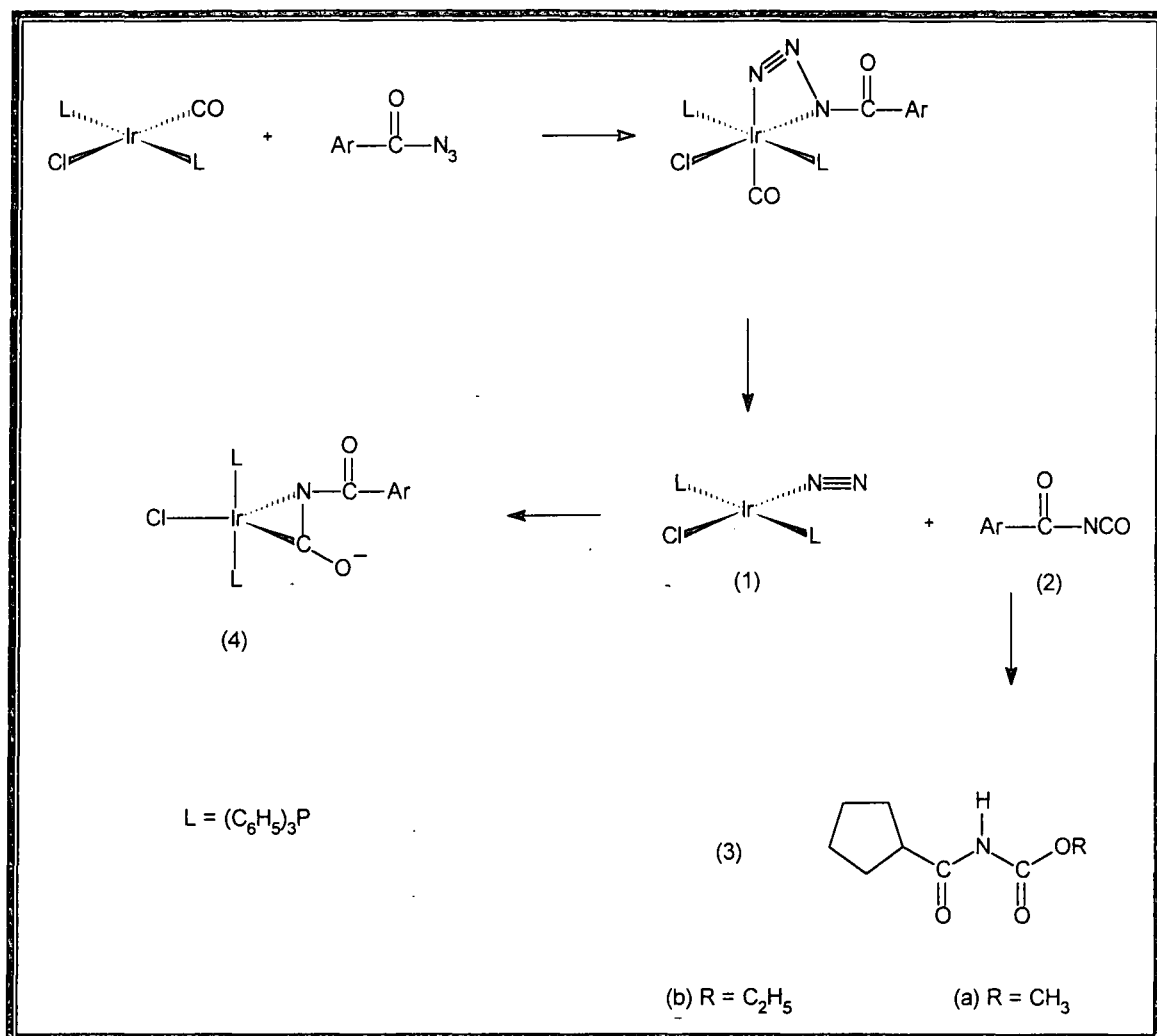


Figure 31 : The reaction of $trans-[IrCl(CO)(PPh_3)_2]$ with acyl azides.

If the solvent contains H_2O or alcohol the molecular nitrogen compound $[IrCl(PPh_3)(N_2)]$ is found (**Figure 31** product (1)). In dry, alcohol-free solvents the acyl isocyanide complex (**Figure 31** product (4)) was isolated. The explanation for this is that the nitrogen complex (**Figure 31** product (1)) was attacked by the acyl isocyanide intermediate (**Figure 31** product (2)) resulting in the substitution of the nitrogen that leads to the acyl isocyanide complex (**Figure 31** product (4)). If there is alcohol in the reaction mixture it reacts with the acyl isocyanide (**Figure 31** product (2)) to form the carbamate ester. Thus attack cannot occur on the molecular nitrogen complex.

f) The catalytic effect of halogen ions on the rate of oxidative addition.

Research also indicated that the addition of I^- and Br^- ions have a catalytic effect on the rate of oxidative addition. Foster¹²⁴ observed an iodine catalysed iodomethane addition to $[Rh(I)(CO)L_2]$ in cases where $L = AsPh_3, SbPh_3$ (not PPh_3) as indicated in **Figure 32** :

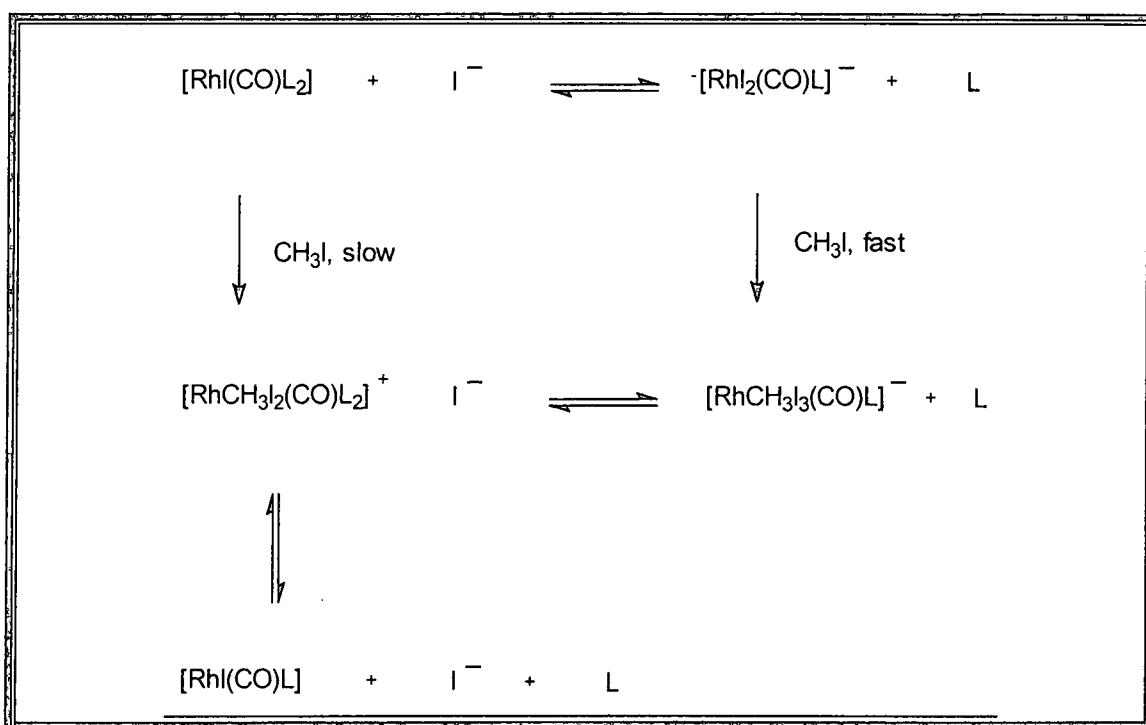


Figure 32 : The iodide catalysed iodomethane addition to $[Rh(I)(CO)L_2]$.

The ligand L is displaced by iodide to form an anionic complex that can react faster with CH_3I than the neutral complex.

Another type of iodide catalysis were reported by De Waal and co-workers^{125,126}. The iodide reacts with $[Ir(cod)(phen)]^+$ without displacing a ligand. The newly formed five-coordinated complex

¹²⁴ Forster, D., *J. Amer. Chem. Soc.* **97**, 951 (1975)

¹²⁵ De Waal, D.J.A.; Gerber, T.I.A.; Louw, W.J., *Inorg. Chem.*, **21**, 1259 (1982)

¹²⁶ Louw, W.J.; Gerber, T.I.A.; De Waal, D.J.A., *J. Chem. Soc. Chem. Commun.*, 760 (1980)

$[\text{Ir}(\text{cod})(\text{phen})\text{I}]$ reacts faster with CH_3I ¹²⁵ or O_2 ¹²⁶ than the square-planar complex $[\text{Ir}(\text{cod})(\text{phen})]$.

Similar results were found by Basson and co-workers³⁵ where Br^- was added to $[\text{Ir}(\text{cod})(\text{acac})]$ which accelerated the rate of oxidative addition by a factor ten more than the value found by De Waal and co-workers. The reaction also has more intricate pathways involving unusual coordination of CH_3I to a $\text{Ir}(\text{III})$ centre as shown in **Figure 33** (K_5 -path):

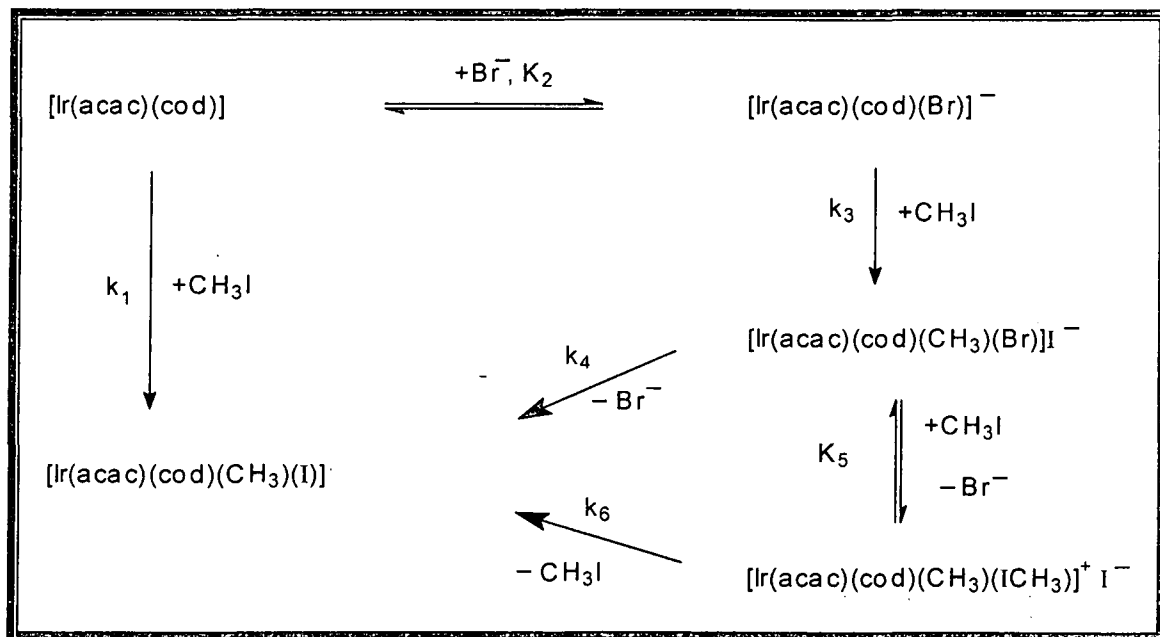
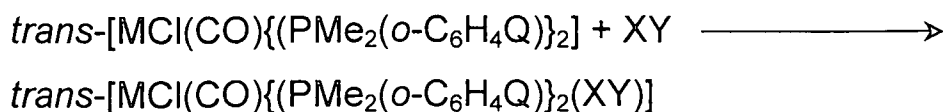


Figure 33 : The bromide catalysed oxidative addition of iodomethane to $[\text{Ir}(\text{acac})(\text{cod})]$.

g) The influence of neighbouring groups on the rate of oxidative addition.

Shaw and co-workers^{93,96} found the neighbouring groups also have an influence on the rate of oxidative addition reaction in the general reaction:



where M = Rh(I), Ir(I) and Pt(II)
 Q = H and OMe
 XY = HCl, MeCl, MeBr, MeI, CCl₄, Cl₂ and PhCOCl

In the case of Rh(I) and Pt(II) the rate of oxidative addition increases 100 – 250 times as Q changes from H to OMe⁹³. They explained this by proposing that the oxygen of the methoxy group does a nucleophilic attack on the metal creating a larger nucleophilicity on the metal (**Figure 34**).

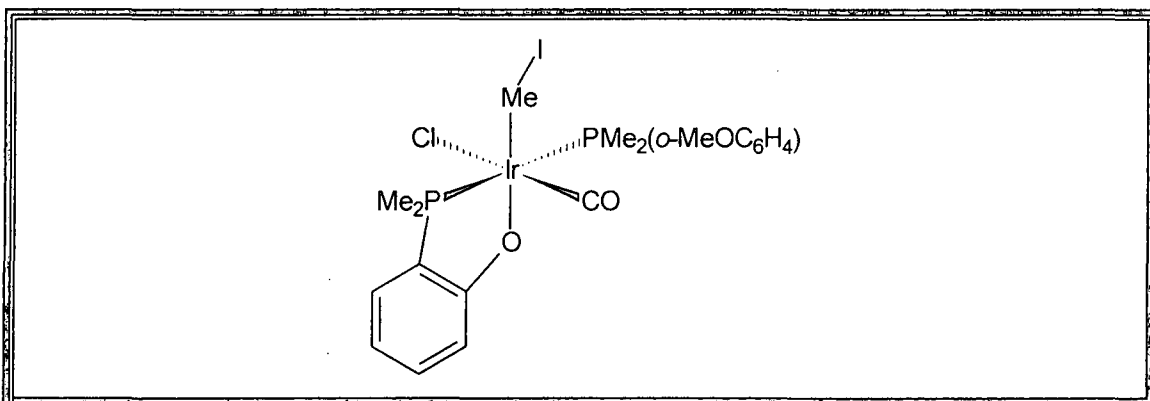


Figure 34 : Electron donation of the oxygen of the methoxy group increases the nucleophilicity on the metal.

There is however no activation effect by the *o*-methoxy groups in the addition of H₂ to *trans*-[IrCl(CO)L₂]. This can be explained by the low polarity of the transition state, or if the addition of H₂ to the metal is regarded as a nucleophilic attack.

Chapter 3

Synthesis and Characterisation of the ligands and complexes.

1. Introduction.

An aim of this study was to determine the effect of different donor atoms of the bidentate ligands on the rate of oxidative addition reactions. For this study bidentate ligands containing N-N- donor atoms were used for the synthesis of $[M(\text{bpt-NH})(\text{cod})]$ and $[M(\text{bpt})(\text{cod})]$ ($M = \text{Rh}$ and Ir), to study the oxidative addition reactions with CH_3I .

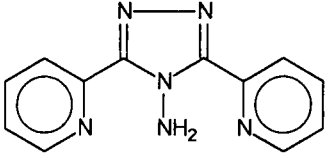
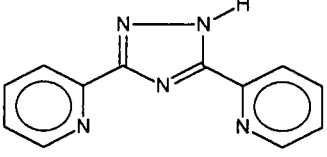
The synthesis and characterisation of these ligands and complexes used are discussed in this chapter.

Since the growth of single crystals proved to be impossible, the compounds were characterised by ^1H NMR spectroscopy on a Bruker 300MHz spectrometer, infrared spectroscopy on a Hitachi 270-50 spectrophotometer using KBr discs and elemental analysis (performed by Canadian Microanalytical Service, British Columbia).

2. Synthesis of the ligands hbpt and bpt-NH.

A summary of the ligands used for the synthesis of the complexes for the kinetic studies is given in Table 12.

Table 12 : Summary of the ligands used in this study.

Name	Abbreviation	Donor atoms	Structure
4-Amino-3,5-bis(pyridin-2-yl)-1,2,4-triazole	bpt-NH ₂	N-N'	
3,5-bis(pyridin-2-yl)-1,2,4-triazole	hbpt	N-N'	

Both ligands were prepared from a three-step synthesis as done by Geldard and Lions¹²⁷ with minor modifications to the experimental procedure. A schematic representation of this is given in Figure 35 and will be discussed in more detail.

¹²⁷ Geldard, J.F.; Lions, F., *J. Org. Chem.*, **30**, 318 (1965)

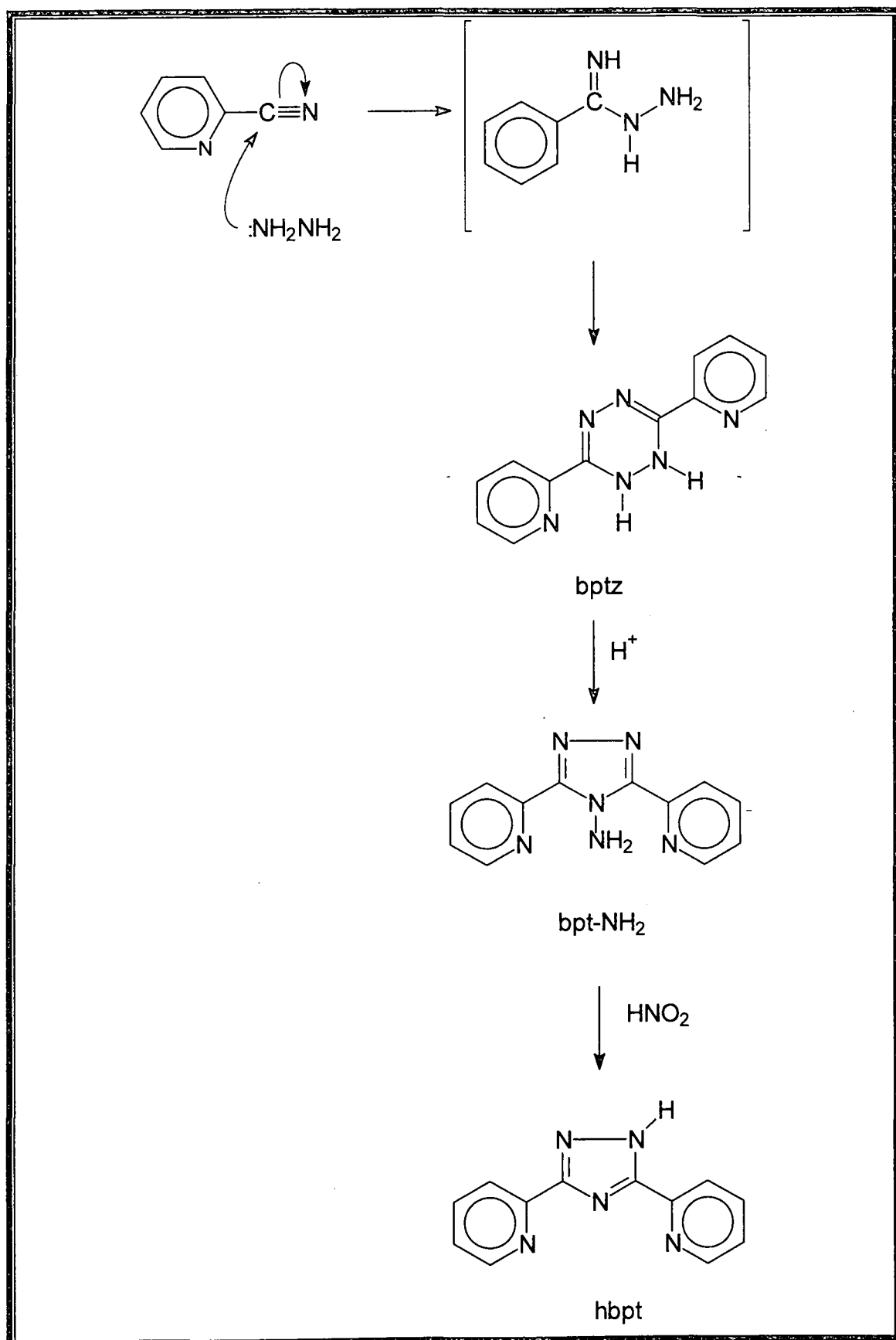


Figure 35 : Synthesis of the ligands bpt-NH₂ and hbpt.¹²⁷

a) Synthesis of 3,6-di(pyridin-2-yl)-1,2-dihydro-1,2,4,5-tetrazine (bptz).

A mixture of 2-cyanopyridine (20g) and an excess of hydrazine hydrate (20ml) were heated under reflux. The color of the mixture changed to red and the product precipitated after about 2 hours. The mixture was filtered and the solid were crystallized from pyridine as orange needles (Yield: 15.7g, 68.6%).

b) Synthesis of 4-Amino-3,5-bis(pyridin-2-yl)-1,2,4-triazole (bpt-NH₂).

3,6-di(pyridin-2-yl)-1,2-dihydro-1,2,4,5-tetrazine (5,7g) was added to diluted HCl (55cm³, 2M) and the brown mixture was refluxed until it became a transparent yellow (\approx 15 min). The mixture was cooled to room temperature and NH₄OH (3M) was added until complete product precipitation. The cream-white precipitate was filtered and crystallised from aqueous ethanol as colourless needles (Yield: 4.33g, 76%).

¹H NMR in CDCl₃ : Figure 36 : δ 8.68dt(2); 8.55s(2); 8.42dt(2); δ 7.91td(2); δ 7.4ddd(2)

IR_{KBr} : Figure 37 : $\nu(\text{NH}) = 3298 \text{ cm}^{-1}$

$\nu(\text{C}=\text{C}); \nu(\text{C}=\text{N}) = 1590, 1566, 1549, 1520 \text{ cm}^{-1}$

c) Synthesis of 3,5-bis(pyridin-2-yl)-1,2,4-triazole (hbpt).

4-Amino-3,5-bis(pyridin-2-yl)-1,2,4-triazole (2g) was added to diluted HNO_3 (20cm^3 , 5M) and gently boiled until dissolved. The solution was cooled to 0°C and an aqueous sodium nitrite solution (4g in 8cm^3) was added. The reaction mixture was left for 15 min in the fume hood and then boiled for another 5 min. After cooling, NH_4OH (3M) was added until complete product precipitation. The precipitate was filtered and crystallized from acetone or benzene (Yield : 0.8g, 42.7%).

^1H NMR in CDCl_3 : **Figure 38** : δ 8.78d(2); 8.36d(2); 7.86td(2); δ 7.38ddd(2); δ 2.1s(2)

IR_{KBr} : **Figure 39** : $\nu(\text{C}=\text{C})$; $\nu(\text{C}=\text{N}) = 1593, 1575, 1509 \text{ cm}^{-1}$

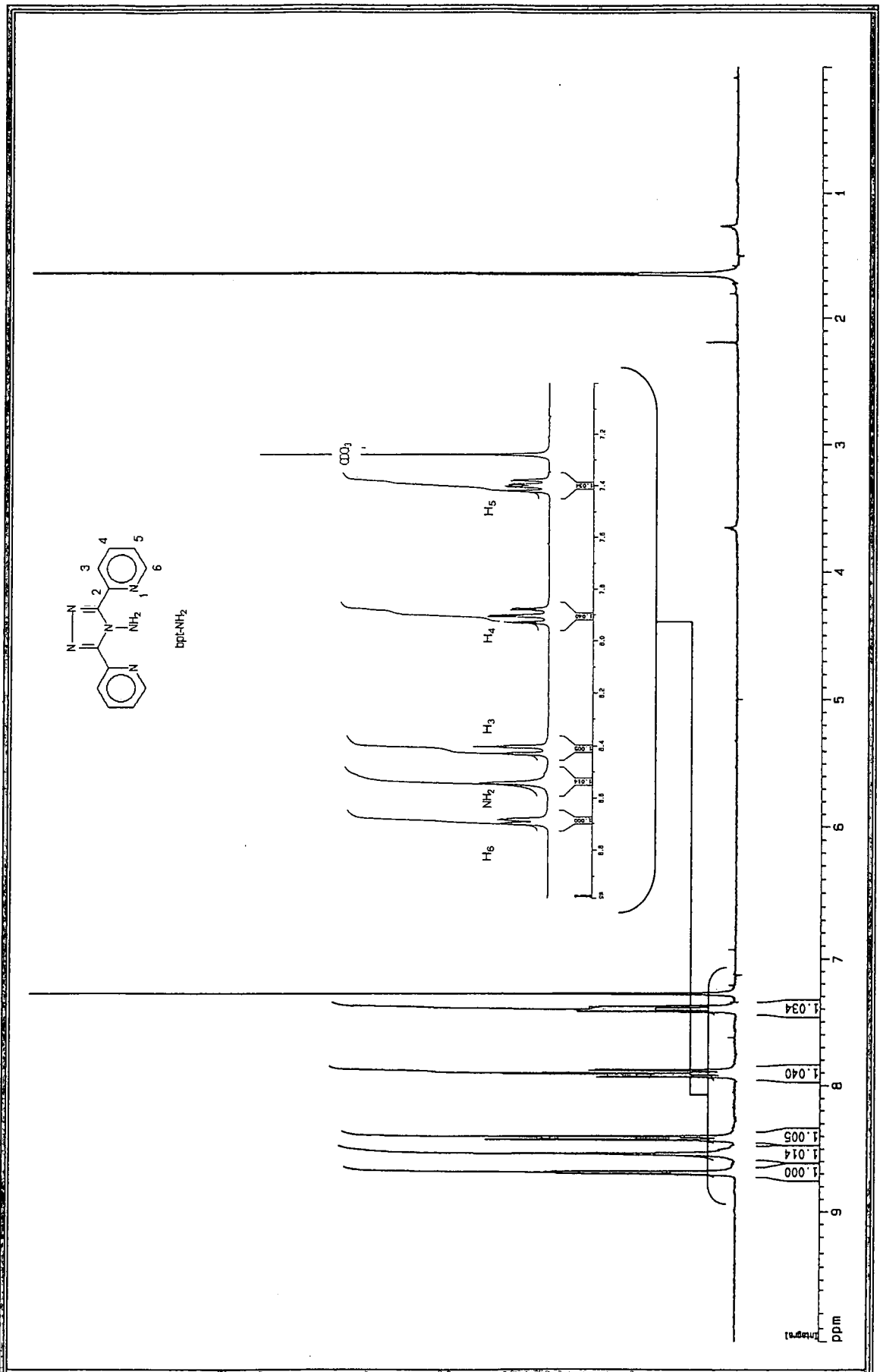


Figure 36 : NMR spectrum of the ligand *bpt-NH₂*.

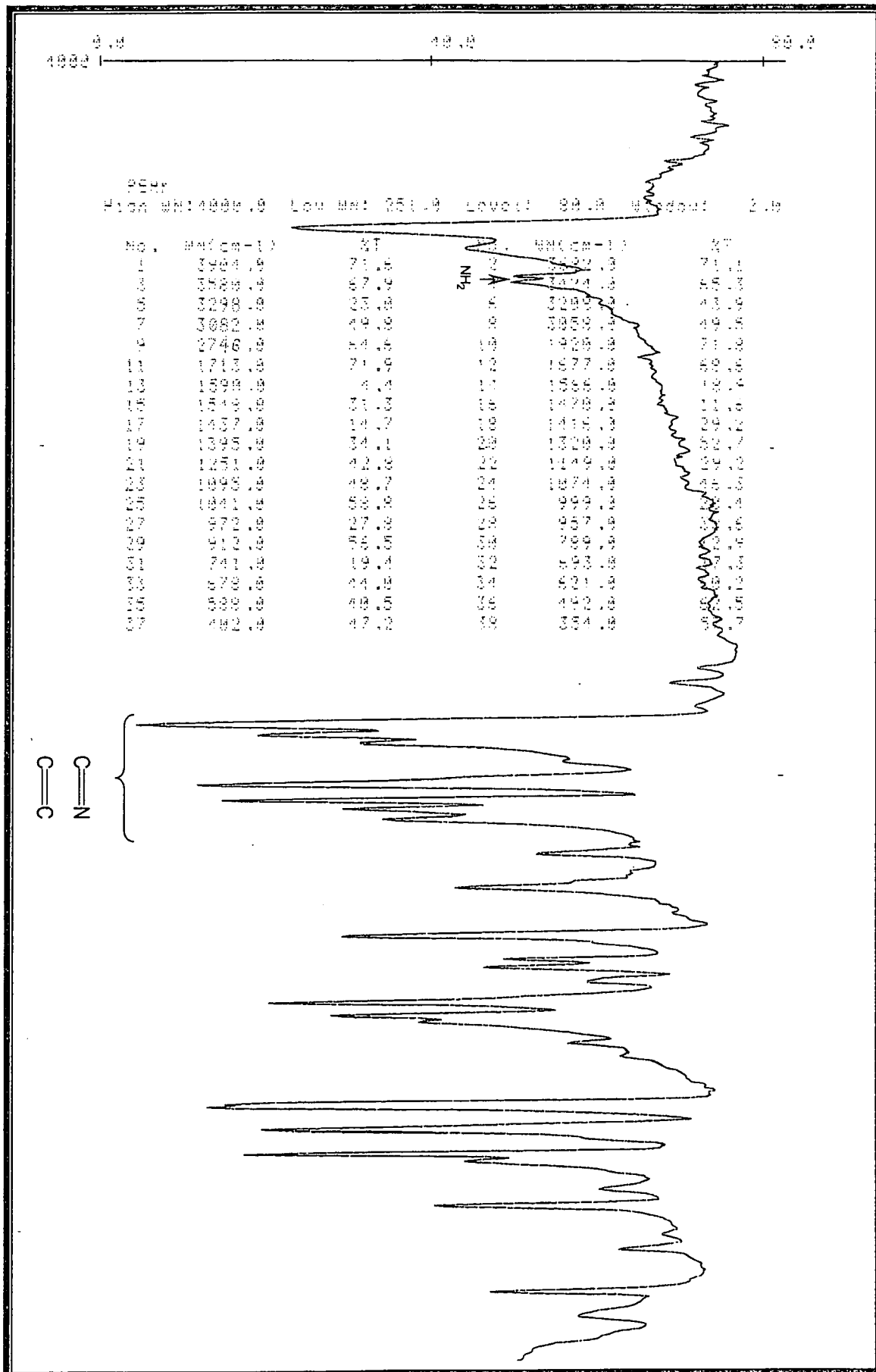


Figure 37 : IR spectrum of the ligand bpt-NH₂.

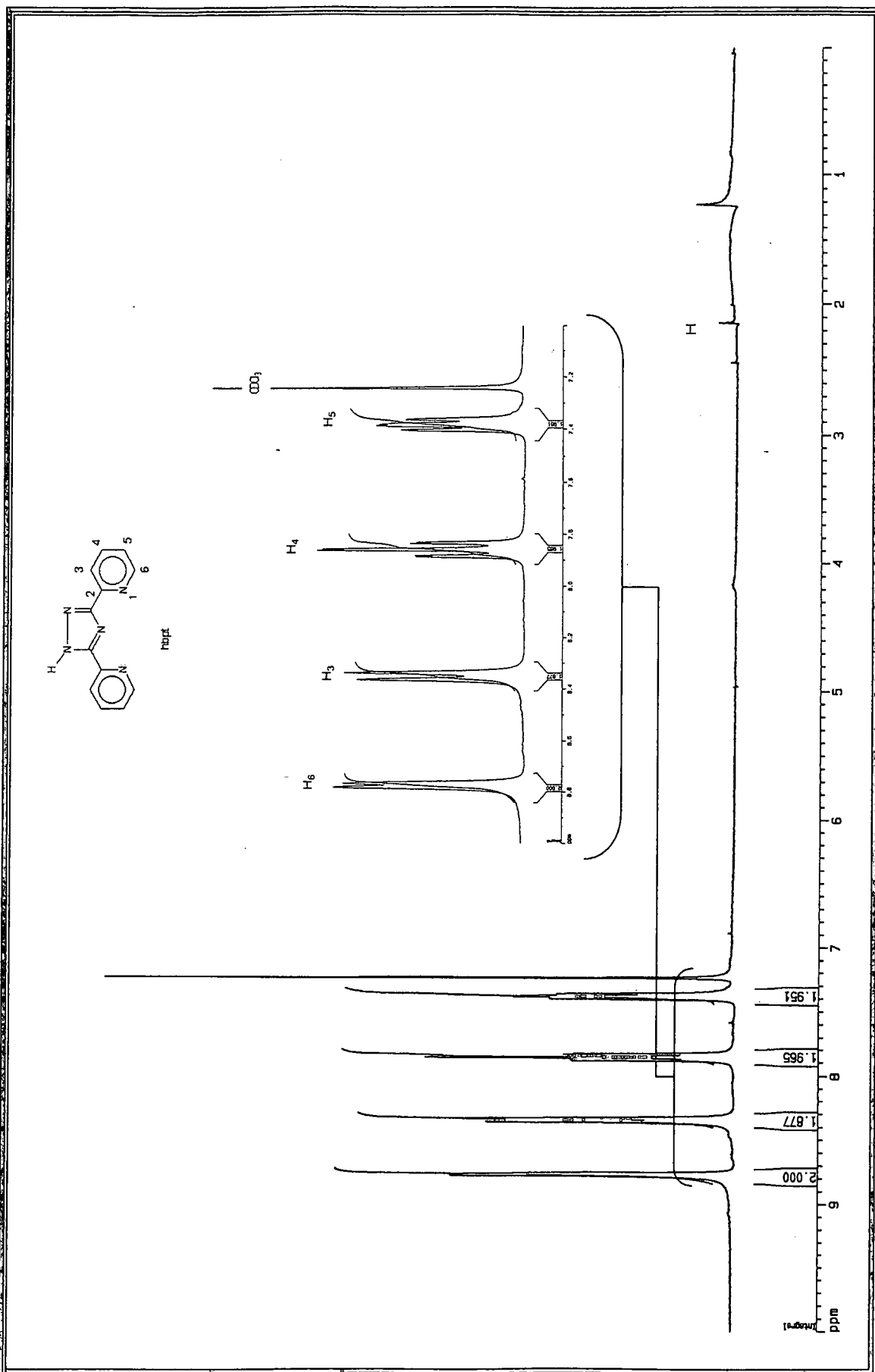


Figure 38 : NMR spectrum of the ligand hbpt.

SYNTHESIS AND CHARACTERISATION OF LIGANDS AND COMPLEXES

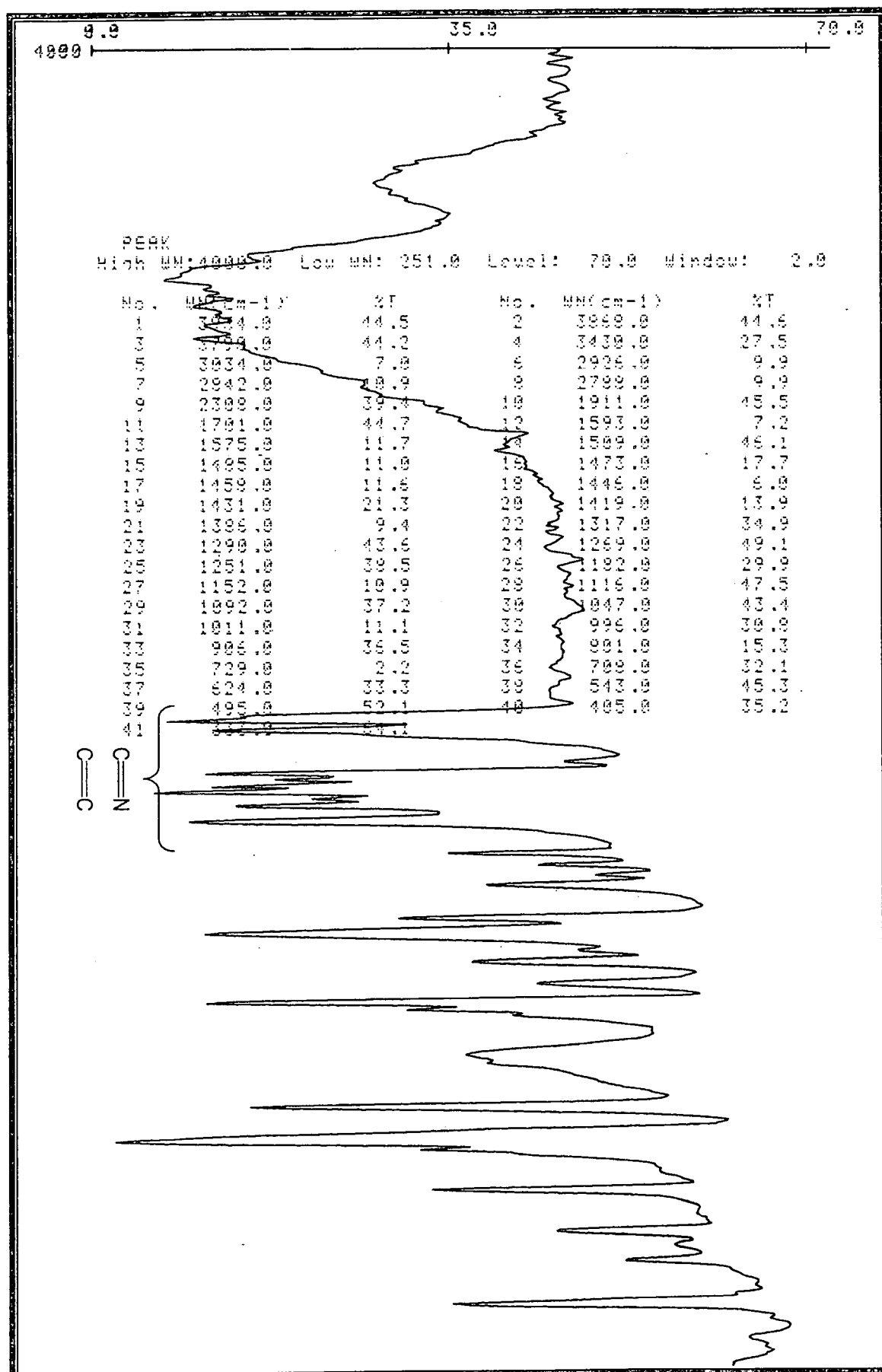


Figure 39 : IR spectrum of the ligand hbpt.

3. Synthesis of the starting metal complexes.

a) Synthesis of bis- $[\eta^4\text{-cycloocta-1,5-diene-}\mu\text{-chloroiridium(I)}]$.

The bis- $[\eta^4\text{-cycloocta-1,5-diene-}\mu\text{-chloroiridium(I)}]$ (abbreviated as $[\text{Ir}(\text{Cl})(\text{cod})]_2$) can be prepared by reaction of $\text{Na}_2[\text{IrCl}_6] \cdot 6\text{H}_2\text{O}$ or $\text{H}_2[\text{IrCl}_6] \cdot 6\text{H}_2\text{O}$ with cycloocta-1,5-diene^{128,129}. Other diene complexes can be prepared by reaction of $\text{Na}_2[\text{IrCl}_6] \cdot 6\text{H}_2\text{O}$ or $\text{H}_2[\text{IrCl}_6] \cdot 6\text{H}_2\text{O}$ with cycloocta-1,4-diene¹³⁰ or cycloocta-1,3-diene^{129,130} respectively.

The $[\text{Ir}(\text{Cl})(\text{cod})]_2$ dimer (Figure 40) crystallises in two crystal forms which is not isostructural¹³¹. The pure orange crystalline complex can be obtained when $\text{H}_2[\text{IrCl}_6]$ is first refluxed in a water-ethanol mixture (to reduce the iridium(IV) to an iridium(III) complex), followed by the addition of *cis,cis*-cycloocta-1,5-diene (cod). The dimer then crystallises in the monoclinic crystal system. If both $\text{H}_2[\text{IrCl}_6]$ and cod are reacted simultaneously in a water-ethanol mixture a red-brown crystalline complex is obtained¹³² which has an orthorhombic crystal habit. Both these structural types have been determined crystallographically and are summarised in Table 13.

¹²⁸ Hetkamp, S.; Stufkens, D.J.; Vrieze, K.J. *Organomet. Chem.*, **122**, 419 (1976)

¹²⁹ Winklaus, G.; Singer, H., *Z. Naturforsch. Teil. B*, **20**, 602 (1976)

¹³⁰ Tayim, H.A.; Mahmaoud, F.T., *J. Organomet. Chem.*, **92**, 107 (1975)

¹³¹ Panneter, G.; Bonnaire, R.; Fougeroux, P., *J. Less-Common Metals*, **21**, 103 (1970)

¹³² Pannetier, G.; Bonnaire, R.; Fougeroux, P., *J. Less-Common Metals*, **21**, 437 (1970)

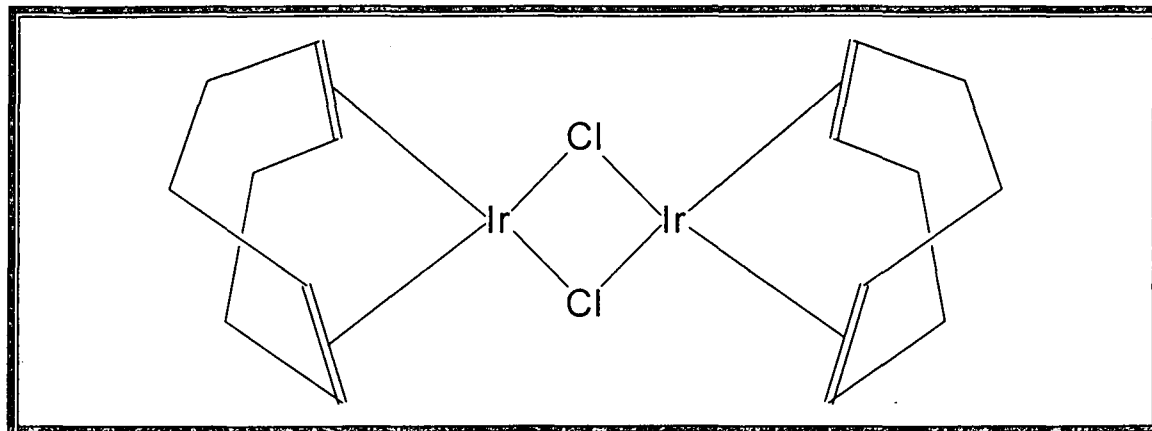


Figure 40: Structure of $[\text{Ir}(\text{Cl})(\text{cod})]_2$.

Table 13 : Summary of the crystal data of the two structures of $[\text{Ir}(\text{Cl})(\text{cod})]_2$.

Orange dimer ¹³³	Red brown dimer ¹³⁴
Monoclinic	Orthorhombic
$a=26.352(11) \text{ \AA}$	$a=15.247(4) \text{ \AA}$
$b=6.426(3) \text{ \AA}$	$b=16.369(4) \text{ \AA}$
$c=12.480(5) \text{ \AA}$	$c=13.697(4) \text{ \AA}$
$Z=4$	$Z=8$
$\beta=125.77(3)^\circ$	

A slightly different method¹³⁵ from these described above was used to obtain a higher yield.

A vigorous stream of nitrogen was bubbled through a mixture of ethanol and water (2:1, 180cm³) for 30 minutes. This removes oxygen that can lead to byproducts. $\text{H}_2\text{IrCl}_6 \cdot 6\text{H}_2\text{O}$ ($\approx 5\text{g}$, 0.01mol) and hydroquinone ($\approx 3.2\text{g}$, 0.03mol) was dissolved in this solution and refluxed for 1 hour under a nitrogen atmosphere. *Cis,cis*-cycloocta-1,5-diene ($\approx 5\text{cm}^3$, 0.04mol) was then added to the mixture and refluxed for an additional 4 hours under nitrogen. Distillation of 100cm³ of the solvent resulted in the formation of the

¹³³ Tabrizi, D.; Manoli, J.M.; Dereigne, A., *J. Less-Common Metals*, 21, 337 (1970)

¹³⁴ Pannetier, G.; Tabrizi, D., *J. Less-Common Metals*, 23, 110 (1971)

¹³⁵ Bezman, S.A.; Bird, P.H.; Fraser, A.R.; Osborn, J.A., *Inorg. Chem.*, 19, 3755 (1980)

orange product. The mixture was then cooled to room temperature and water (10cm³) was added to the solution. The precipitate was filtered and washed with cold methanol (3x10cm³) after which it was dried overnight in a vacuum desiccator over P₂O₅ (Yield: 2.76g, 80.96%).

¹H NMR in CDCl₃: **Figure 41** : δ 4.22(4); 2.26(4); 1.53(4)

IR_{KBr}: **Figure 42** : ν(C=C) = 1476, 1449 cm⁻¹

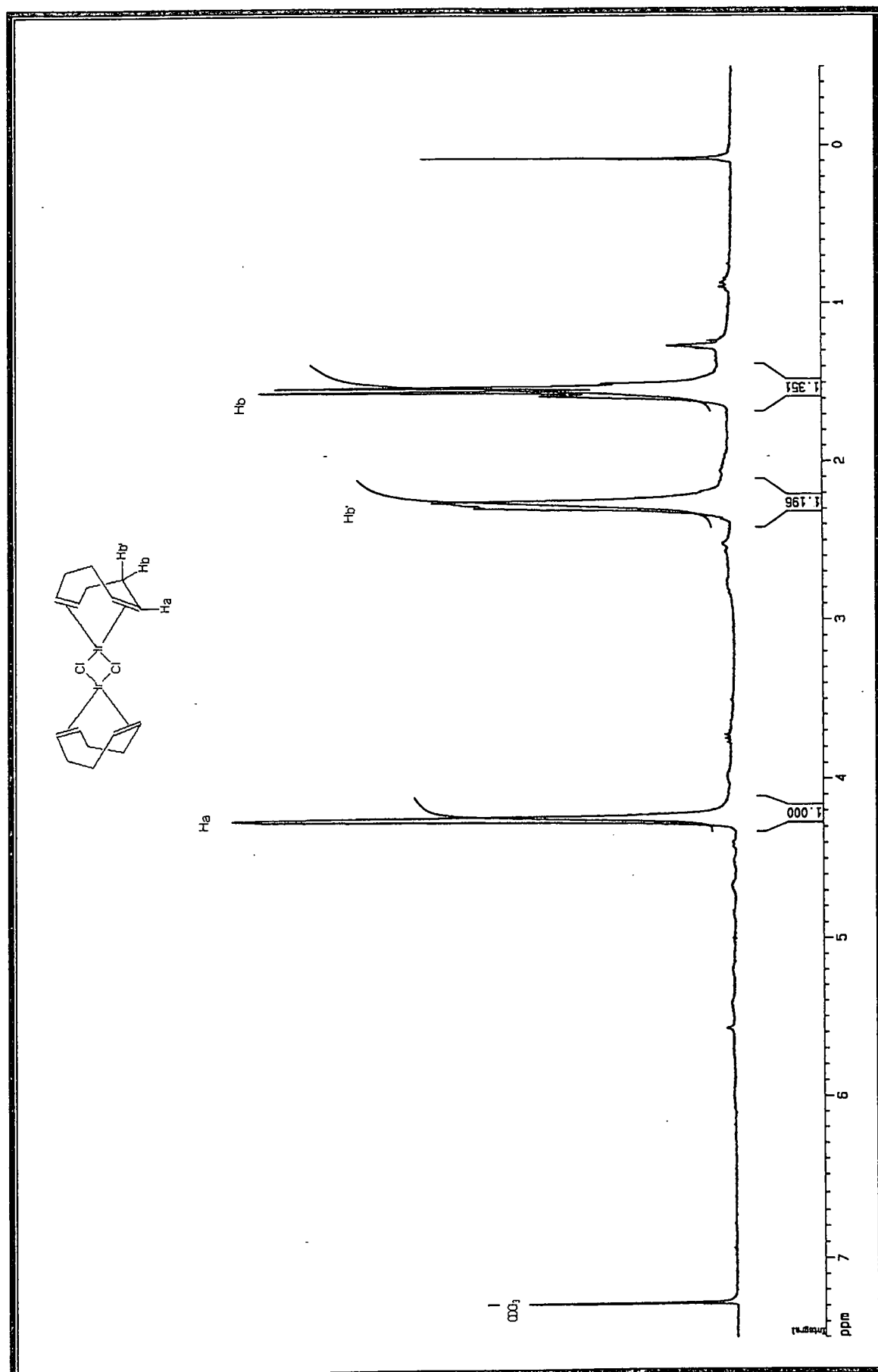


Figure 41 : NMR spectrum of the complex [Ir(Cl)(cod)]₂.

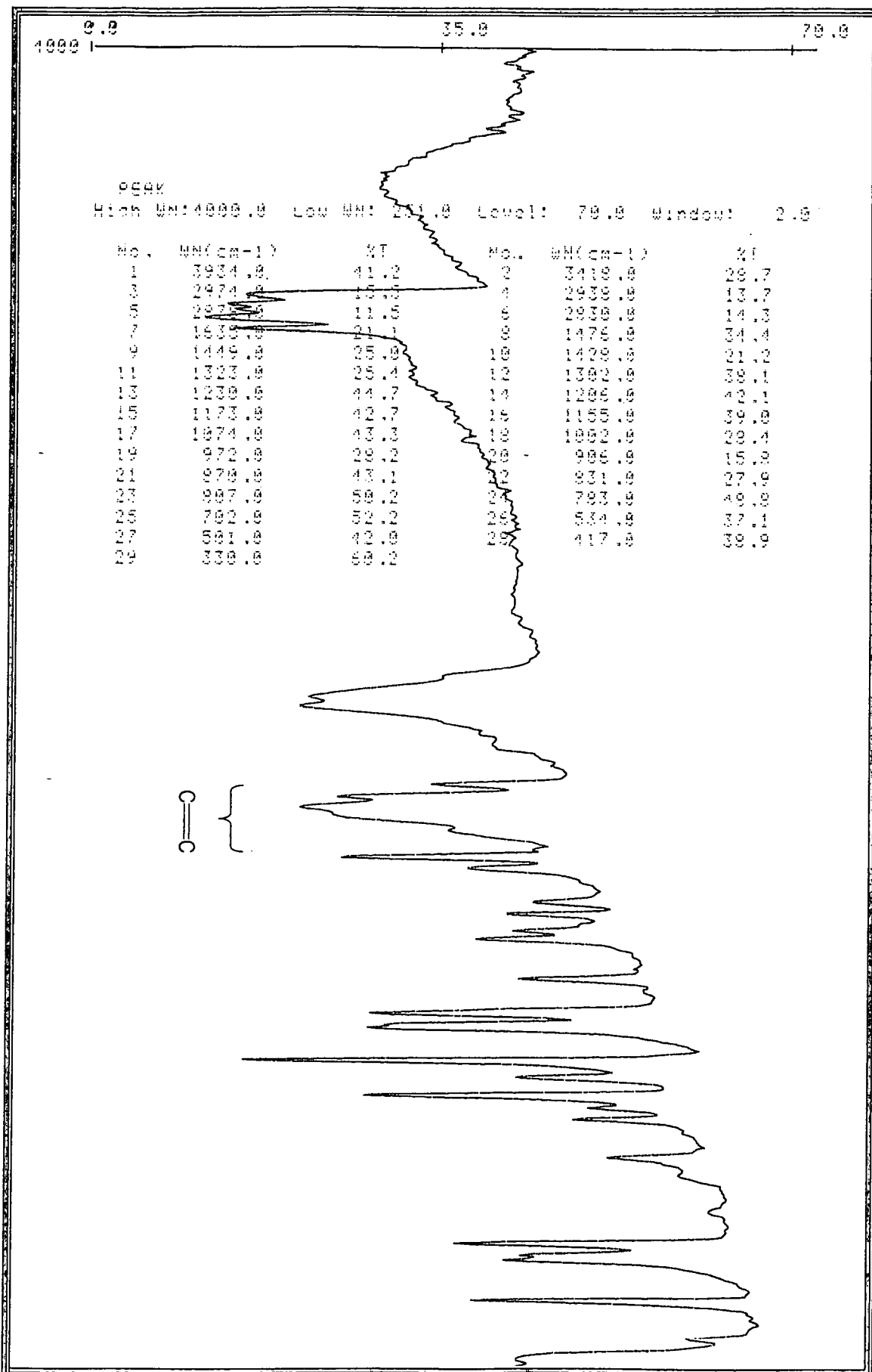


Figure 42: IR spectrum of the complex $[\text{Ir}(\text{Cl})(\text{cod})]_2$.

b) Synthesis of bis- $[\eta^4\text{-cycloocta-1,5-diene-}\mu\text{-dichlororhodium(I)}]$.

The bis- $[\eta^4\text{-cycloocta-1,5-diene-}\mu\text{-dichlororhodium(I)}]$ (abbreviated as $[\text{Rh}(\text{Cl})(\text{cod})]_2$) was previously prepared by reducing RhCl_3 in the presence of excess olefin in aqueous ethanol¹³⁶ in yields of 60% or more. More recently¹³⁷ this yield was increased to more than 90% by the addition of sodium carbonate.

The crystal structure of $[\text{Rh}(\text{Cl})(\text{cod})]_2$ was first determined by Ibers and Snyder¹³⁸ and later more accurately redetermined by De Ridder and Imhoff¹³⁹. The structure and crystallographic data are summarised in **Figure 43** and **Table 14**.

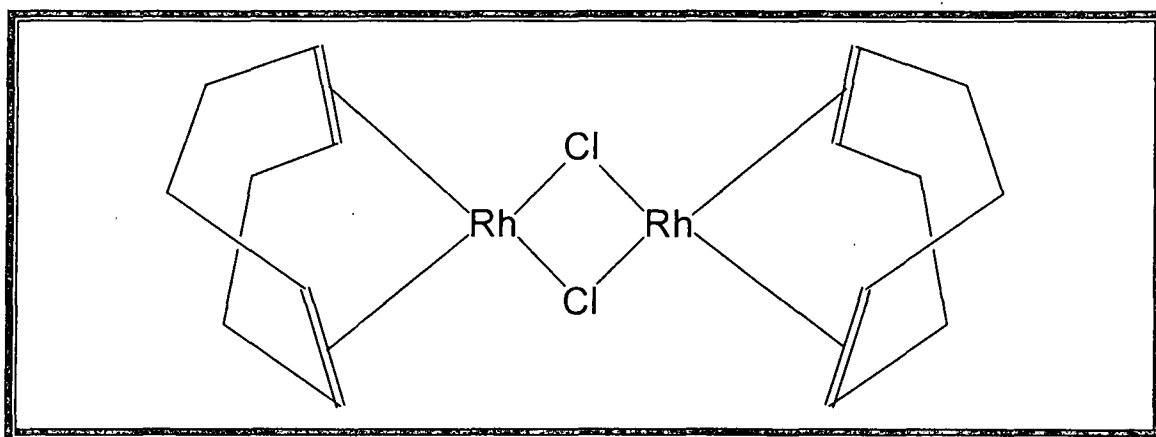


Figure 43: Structure of $[\text{Rh}(\text{Cl})(\text{cod})]_2$.

¹³⁶ Chatt, J; Venanzi, L.M., *J. Chem. Soc.*, 4735 (1957)

¹³⁷ Giordano, G.; Crabtree, R.H., *Inorganic Synthesis*, 28, 88 (1990)

¹³⁸ Ibers, J.A.; Snyder, R.G., *Acta Cryst.*, 15, 923 (1962)

¹³⁹ De Ridder, D.J.A.; Imhoff, P., *Acta Cryst.*, C50, 1569 (1994)

Table 14 : Summary of the crystal data of $[\text{Rh}(\text{Cl})(\text{cod})]_2$.

Monoclinic
$a=9.056(1) \text{ \AA}$
$b=25.475(6) \text{ \AA}$
$c=7.309(1) \text{ \AA}$
$Z=4$
$\beta=91.79(1)^\circ$

The improved method of Giordano and Crabtree¹³⁷ was used in the synthesis of this starting complex.

$\text{RhCl}_3 \cdot 3\text{H}_2\text{O}$ (1g, 0.0038mol) and Na_2CO_3 (1.1g, 0.00385mol) were added to a 100cm^3 round-bottomed flask and placed under a nitrogen atmosphere. A vigorous stream of nitrogen was bubbled through a mixture of ethanol and water (5:1, 10cm^3) for 30 minutes. The deoxygenated ethanol-water mixture and *cis,cis*-cycloocta-1,5-diene (3cm^3 , 0.025mol) was added to the round-bottomed flask charged with the RhCl_3 and Na_2CO_3 . This solution was refluxed for 18 hours under a nitrogen atmosphere. During this period the product precipitated as a yellow-orange solid. The mixture was then cooled to room temperature, filtered and washed with pentane (to remove excess cod) followed by methanol-water (1:5) until the washings no longer contained chloride. The precipitate was dried overnight in a vacuum desiccator over P_2O_5 . (Yield: 0.84g, 94%)

$^1\text{H NMR}$ in CDCl_3 : **Figure 44** : δ 4.2(4); 2.48(4); 1.72(4)

IR_{KBr} : **Figure 45** : $\nu(\text{C}=\text{C}) = 993\text{-}1326 \text{ cm}^{-1}$ (cod)

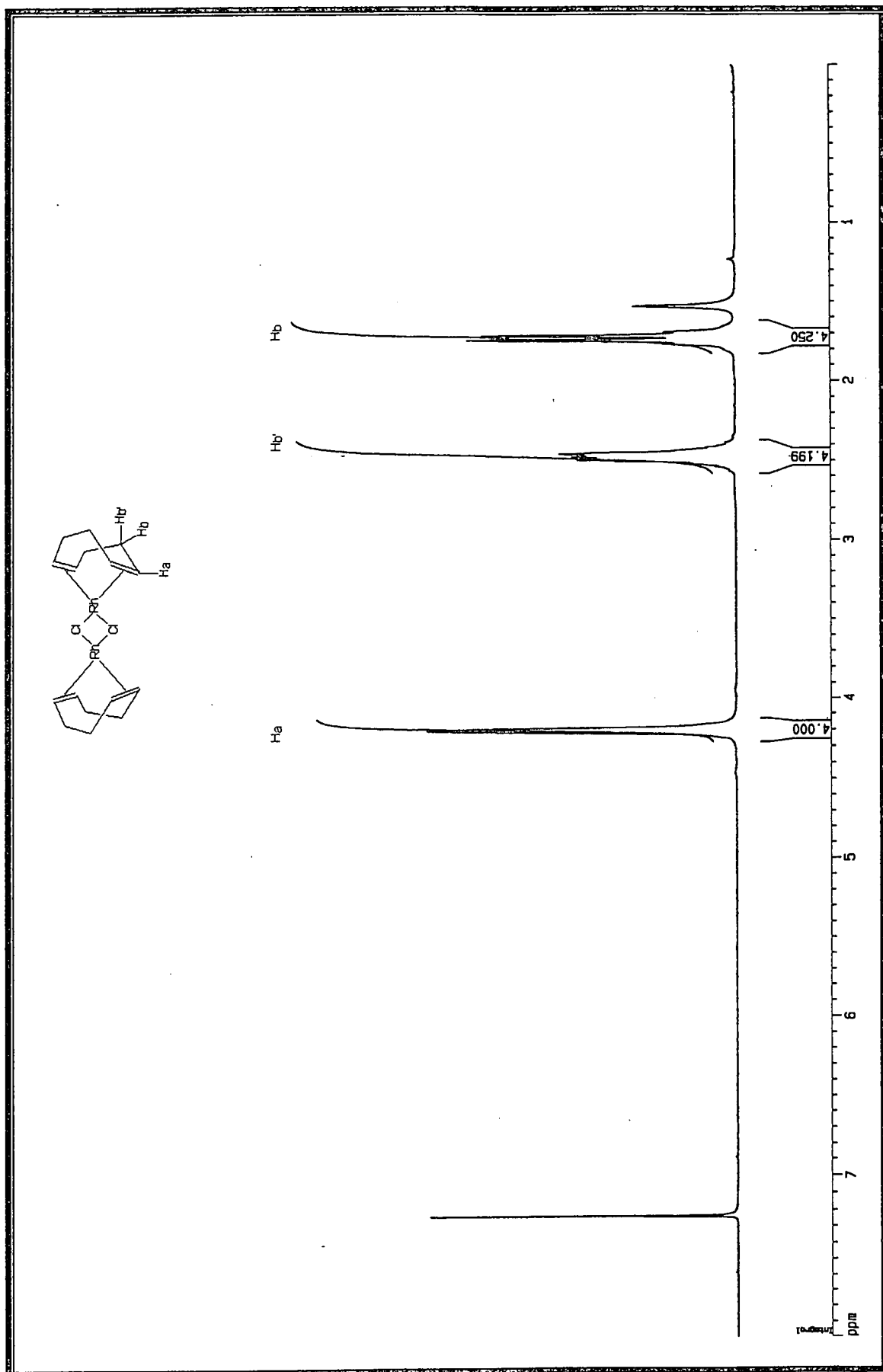


Figure 44 : NMR spectrum of the complex $[\text{Rh}(\text{Cl})(\text{cod})]_2$.

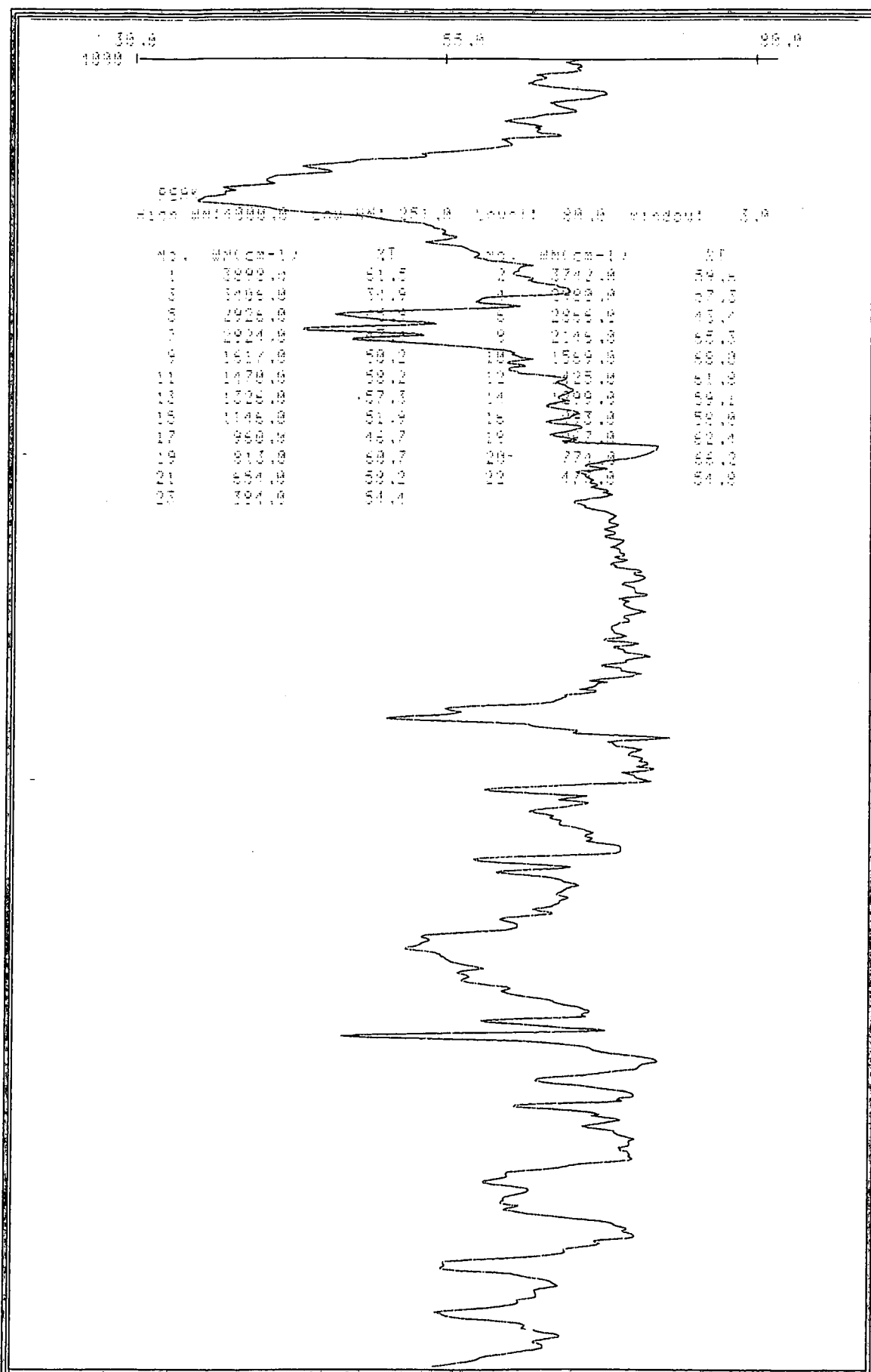


Figure 45 : IR spectrum of the complex $[\text{Rh}(\text{Cl})(\text{cod})]_2$.

4. Synthesis of [M(bpt-NH)(cod)] and [M(bpt)(cod)].

A general synthetic route for the preparation of the studied complexes was derived from work done by Oro et al^{140,141} and can be summarised schematically as shown in Figure 46.

In all cases, the ligand was deprotonated by treating it with a slight excess of KOH. This resulted in a more nucleophilic ligand than the neutral counterpart. The [M(Cl)(cod)]₂ dimer (M = Rh, Ir) was added in stoichiometric amounts to the solution containing the deprotonated ligand. This resulted in the breaking of the metal-chloride bond, yielding the studied complexes and KCl as by-product which was filtered off.

The experimental procedure for each of the four prepared complexes will be discussed individually. For each of the four procedures the MeOH and dichloromethane (DCM) used was deoxygenated by vigorously bubbling nitrogen for half and hour through the solvent.

a) Synthesis of [Ir(bpt)(cod)].

KOH (0.0180g, 0.3209mmol) was dissolved in MeOH (3.2cm³) in a 100cm³ two-neck flask under a nitrogen atmosphere. This resulted in a 0.1M KOMe solution. 3,5-bis(pyridin-2-yl)-1,2,4-triazole (hbpt)

¹⁴⁰ Garcia, M.P.; Manero, J.A.; Oro, L.A.; Aperda, M.C.; Cano, F.H.; Haasnoot, J.G.; Prins, R.; Reedijk, J., *Inorganica Chimica Acta*, **122**, 235 (1986)

¹⁴¹ Garcia, M.P.; Martin, M; Oro, L.A., *Inorganica Chimica Acta*, **191**, 221 (1992)

(0.0665g, 0.2978mmol) was added to the prepared KOH-methanol solution and stirred until dissolved.

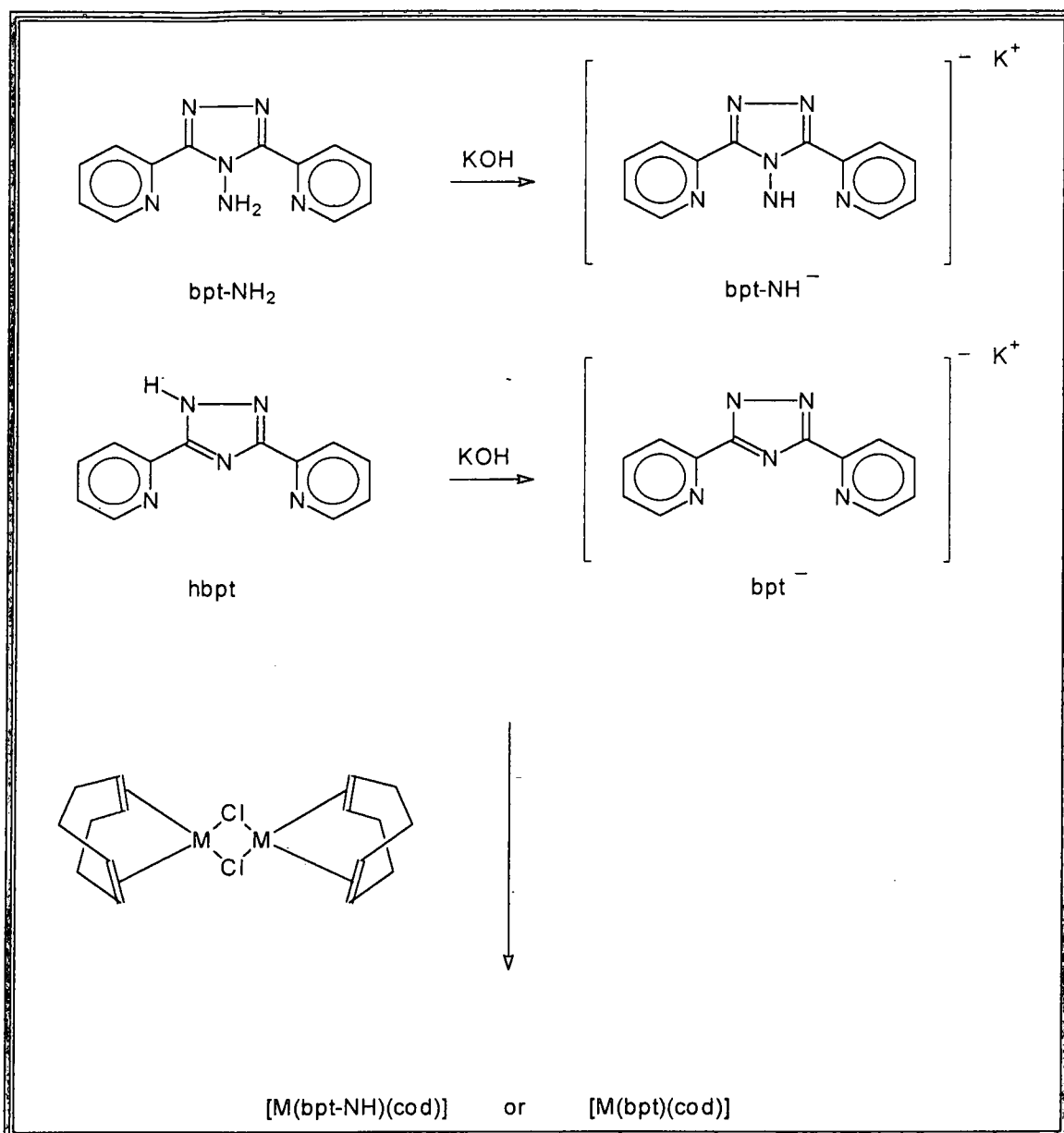


Figure 46 : Synthetic route of the complexes $[\text{M}(\text{bpt-NH})(\text{cod})]$ and $[\text{M}(\text{bpt})(\text{cod})]$ ($\text{M} = \text{Ir}(\text{I})$ or $\text{Rh}(\text{I})$).

$[\text{Ir}(\text{Cl})(\text{cod})]_2$ (0.1g, 0.1489mmol) was dissolved in DCM (4.3cm^3) in a 100cm^3 two-neck flask under a nitrogen atmosphere. The solution containing the deprotonated ligand (bpt^-) was transferred to this solution using a syringe. The reaction was kept under nitrogen until all the solvent evaporated.

The formed red solid was again dissolved in deoxygenated DCM. This solution was then filtered through a fritted glass funnel packed with celite (previously washed with deoxygenated DCM) whilst maintaining a vigorous stream of nitrogen through an inverted funnel covering the filter apparatus. This removed the formed KCl and other insoluble impurities. The red solution was evaporated under nitrogen until dry and the final product was kept stored under nitrogen since decomposition occurs within a few days when left in air. (Yield 0.105g, 67.4%)

^1H NMR in CDCl_3 : **Figure 47** :

For bpt = δ 8.7d(1); 8.19dd(2); 7.97t(1); 7.89d(1);
7.72td(1); 7.23m(2)

For cod = δ 5.0(2); 3.92(2); 2.38(4); 1.88(4)

IR_{KBr} : **Figure 48** : $\nu(\text{C}=\text{C}) = 1635, 1476, 1449, 1428 \text{ cm}^{-1}$

Elemental analysis (%): found(calculated in brackets) :

C = 43.88(45.97); H = 3.80(3.86); N = 12.66(13.40);

Ir = 31.4(36.78)

b) Synthesis of [Ir(bpt-NH)(cod)].

KOH (0.0180g, 0.3209mmol) was dissolved in MeOH (3.2cm^3) in a 100cm^3 two-neck flask under a nitrogen atmosphere. This resulted in a 0.1M KOMe solution. 4-Amino-3,5-bis(pyridin-2-yl)-1,2,4-triazole (bpt-NH₂) (0.0709g, 0.2978mmol) was added to the prepared KOH-methanol solution and stirred until dissolved. $[\text{Ir}(\text{Cl})(\text{cod})]_2$ (0.1g, 0.1489mmol) was dissolved in DCM (3cm^3) in a

100cm³ two-neck flask under a nitrogen atmosphere. The solution containing the deprotonated ligand (bpt-NH⁻) was transferred to this solution using a syringe. The reaction was kept under nitrogen until all the solvent evaporated.

The formed orange solid was again dissolved in deoxygenated DCM. This solution was then filtered under nitrogen as described in the previous procedure. The orange solution was evaporated under nitrogen until dry. (Yield: 0.094g, 58.6 %)

¹H NMR in CDCl₃: **Figure 49** :

For NH = δ 10.92s(1)

For pyridine rings = δ 7.1 – 9.2

For cod = δ 4.17(2); 3.4(2); 2.4(4); 1.92(4)

IR_{KBr}: **Figure 50** : ν(N-H) = 3190 cm⁻¹

ν(C=C) = 1593, 1566, 1494, 1461 cm⁻¹

Elemental analysis (%): found(calculated in brackets) :

C = 44.21(44.68); H = 3.91(3.94); N = 18.02(15.63);

Ir = 24.0(35.75)

c) Synthesis of [Rh(bpt)(cod)].

KOH (0.0180g, 0.3209mmol) was dissolved in MeOH (3.2cm³) in a 100cm³ two-neck flask under a nitrogen atmosphere. This resulted in a 0.1M KOMe solution. 3,5-bis(pyridin-2-yl)-1,2,4-triazole (hbpt) (0.0665g, 0.2978mmol) was added to the prepared KOH-methanol solution and stirred until dissolved. [Rh(Cl)(cod)]₂ (0.075g,

0.1527mmol) was dissolved in DCM (3cm³) in a 100cm³ two-neck flask under a nitrogen atmosphere. The solution containing the deprotonated ligand (bpt⁻) was transferred to this solution using a syringe. The reaction mixture was stirred for 3 hours after which diethyl ether was added to precipitate the product. The solution was centrifuged and the formed orange solid was again dissolved in deoxygenated DCM. This solution was then filtered under nitrogen as described in the previous procedure and evaporated under nitrogen. (Yield: 0.096g, 74.4 %)

¹H NMR in CDCl₃: **Figure 51** :

For bpt⁻ = δ 8.7(1); 8.23(2); 7.88(1); 7.73(1); 7.62(1);
7.25(2)

For cod = δ 4.64(4); 2.42(8)

IR_{KBr}: **Figure 52** : ν(C=C) = 1614, 1593, 1569, 1530 cm⁻¹

Elemental analysis (%) : found(calculated in brackets) :

C = 51.52(55.44); H = 4.47(4.65); N = 16.05(16.16);

Rh = 17.9(23.75)

A literature cited analysis of [Rh(bpt)(cod)] for comparison¹⁴¹:

C = 54.2; H = 4.6; N = 15.9

d) Synthesis of [Rh(bpt-NH)(cod)].

KOH (0.0180g, 0.3209mmol) was dissolved in MeOH (3.2cm³) in a 100cm³ two-neck flask under a nitrogen atmosphere. This resulted in a 0.1M KOMe solution. 4-Amino-3,5-bis(pyridin-2-yl)-1,2,4-triazole (bpt-NH₂) (0.0709g, 0.2978mmol) was added to the

prepared KOH-methanol solution and stirred until dissolved. $[\text{Rh}(\text{Cl})(\text{cod})]_2$ (0.075g, 0.1527mmol) was dissolved in DCM (3cm^3) in a 100cm^3 two-neck flask under a nitrogen atmosphere. The solution containing the deprotonated ligand (bpt-NH⁻) was transferred to this solution using a syringe. The reaction mixture was stirred for 3 hours after which diethyl ether was added to precipitate the product. The solution was centrifuged and the formed orange solid was again dissolved in deoxygenated DCM. This solution was then crystallised and filtered under nitrogen as described in the previous procedure and evaporated under nitrogen. (Yield: 0.091g, 68.2 %)

¹H NMR in CDCl_3 : **Figure 53** :

For NH⁻ = δ 9.16(1)

For pyridine rings = δ 7.1 – 8.9

For cod = δ 4.35(4); 2.2(8)

IR_{KBr} : **Figure 54** : $\nu(\text{C}=\text{C}) = 1620, 1593, 1566 \text{ cm}^{-1}$

Elemental analysis (%) : found(calculated in brackets) :

C = 50.29(53.58); H = 4.61(4.72); N = 17.25(18.75);

Rh = 19.4(22.95)

These results can also be compared from a literature citation analysis of $[\text{Rh}(\text{bpt-NH})(\text{cod})]^{140}$:

C = 53.08; H = 4.57; N = 18.25

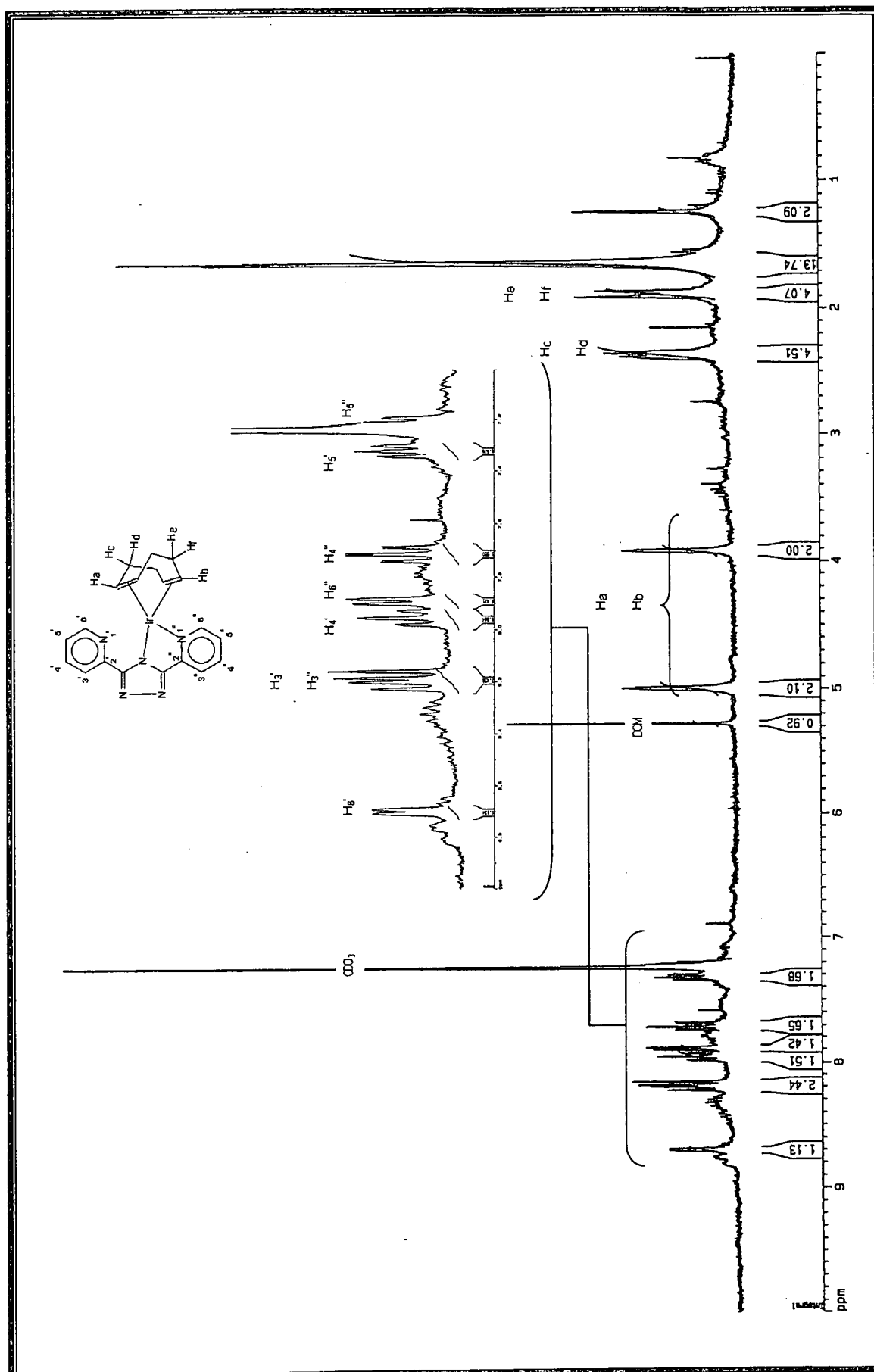


Figure 47 : NMR spectrum of the complex [Ir(bpt)(cod)].

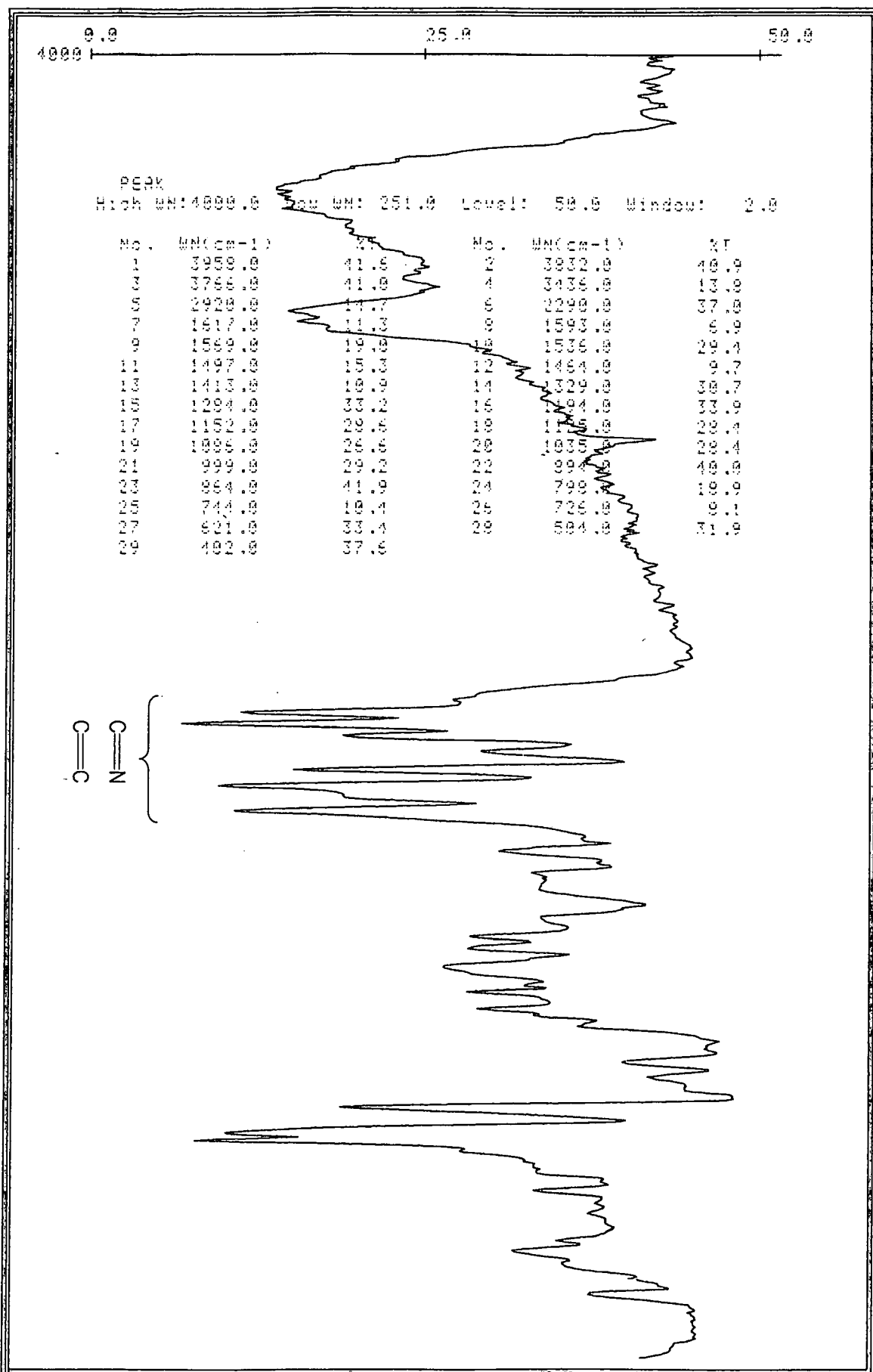


Figure 48 : IR spectrum of the complex [Ir(bpt)(cod)].

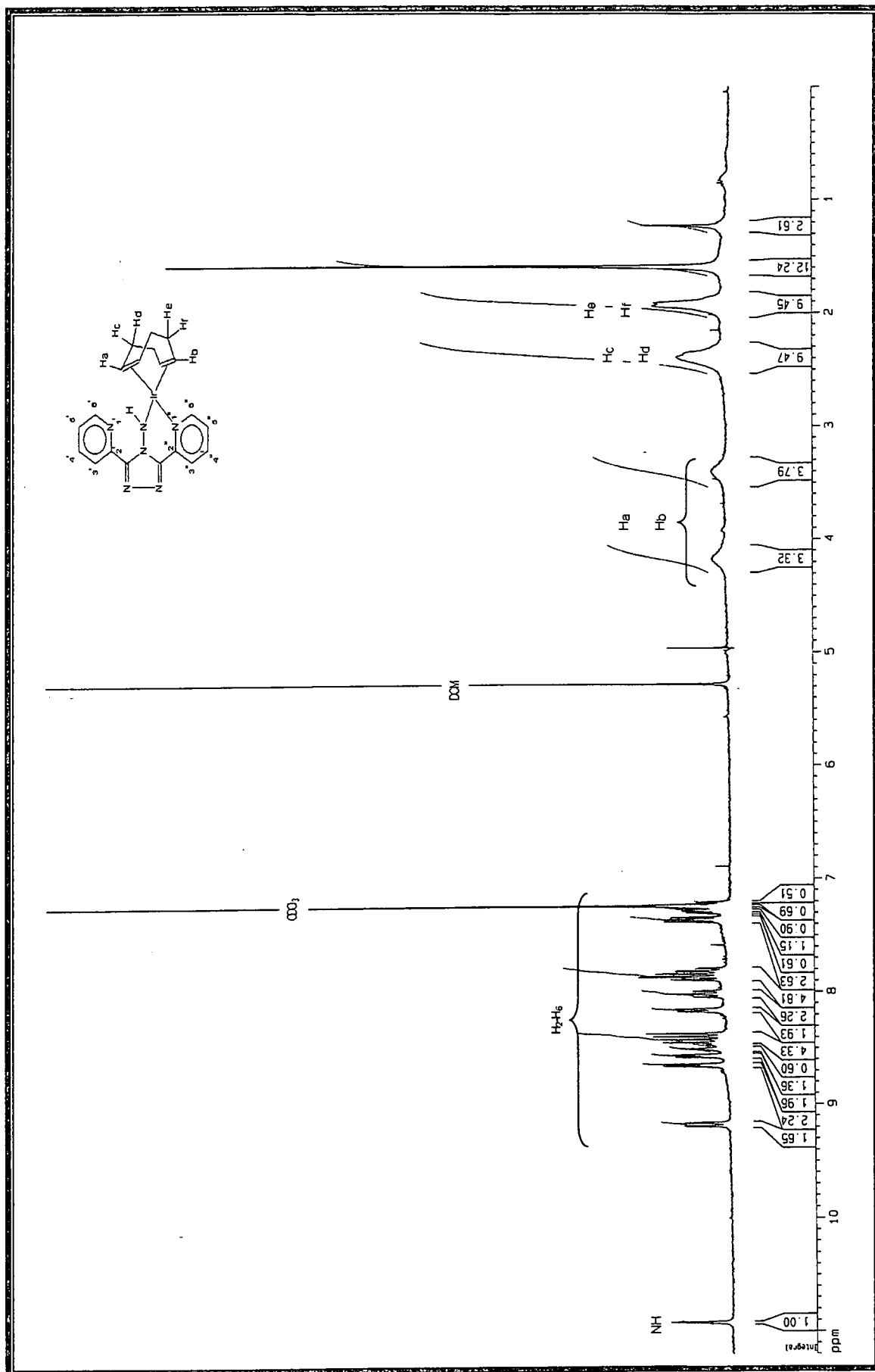


Figure 49 : NMR spectrum of the complex [Ir(bpt-NH)(cod)].

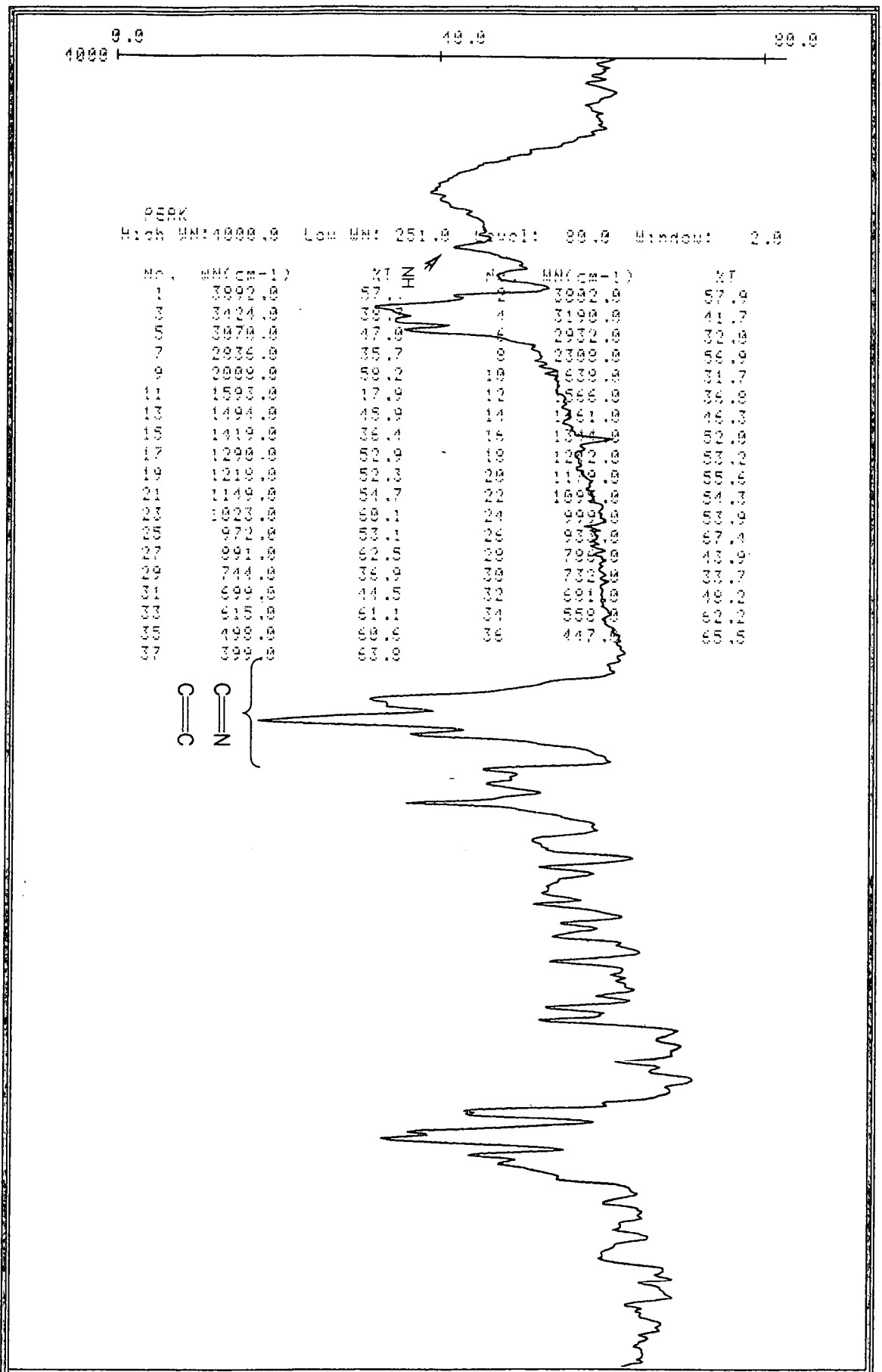


Figure 50 : IR spectrum of the complex [Ir(bpt-NH)(cod)].

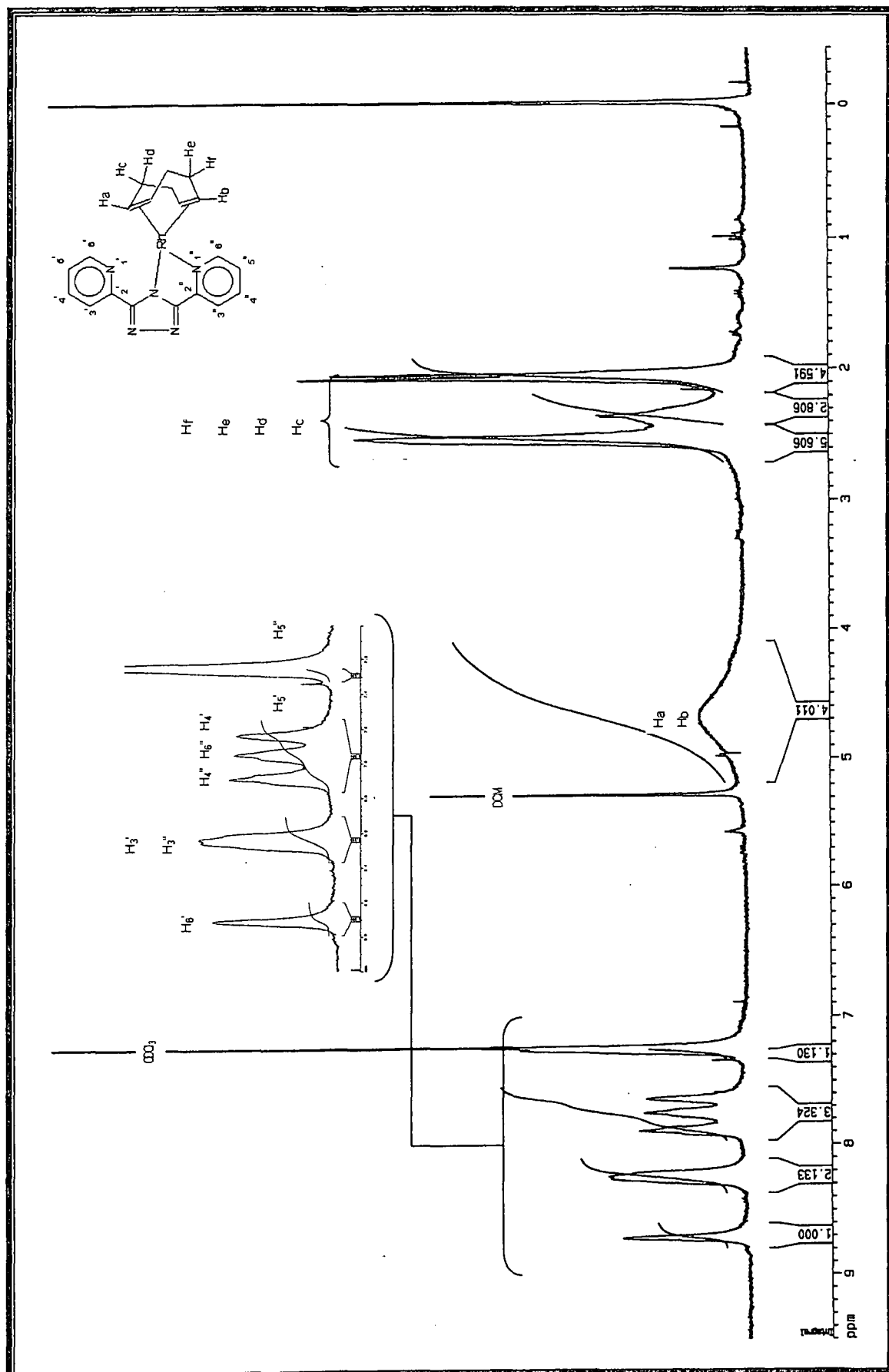


Figure 51 : NMR spectrum of the complex [Rh(bpt)(cod)].

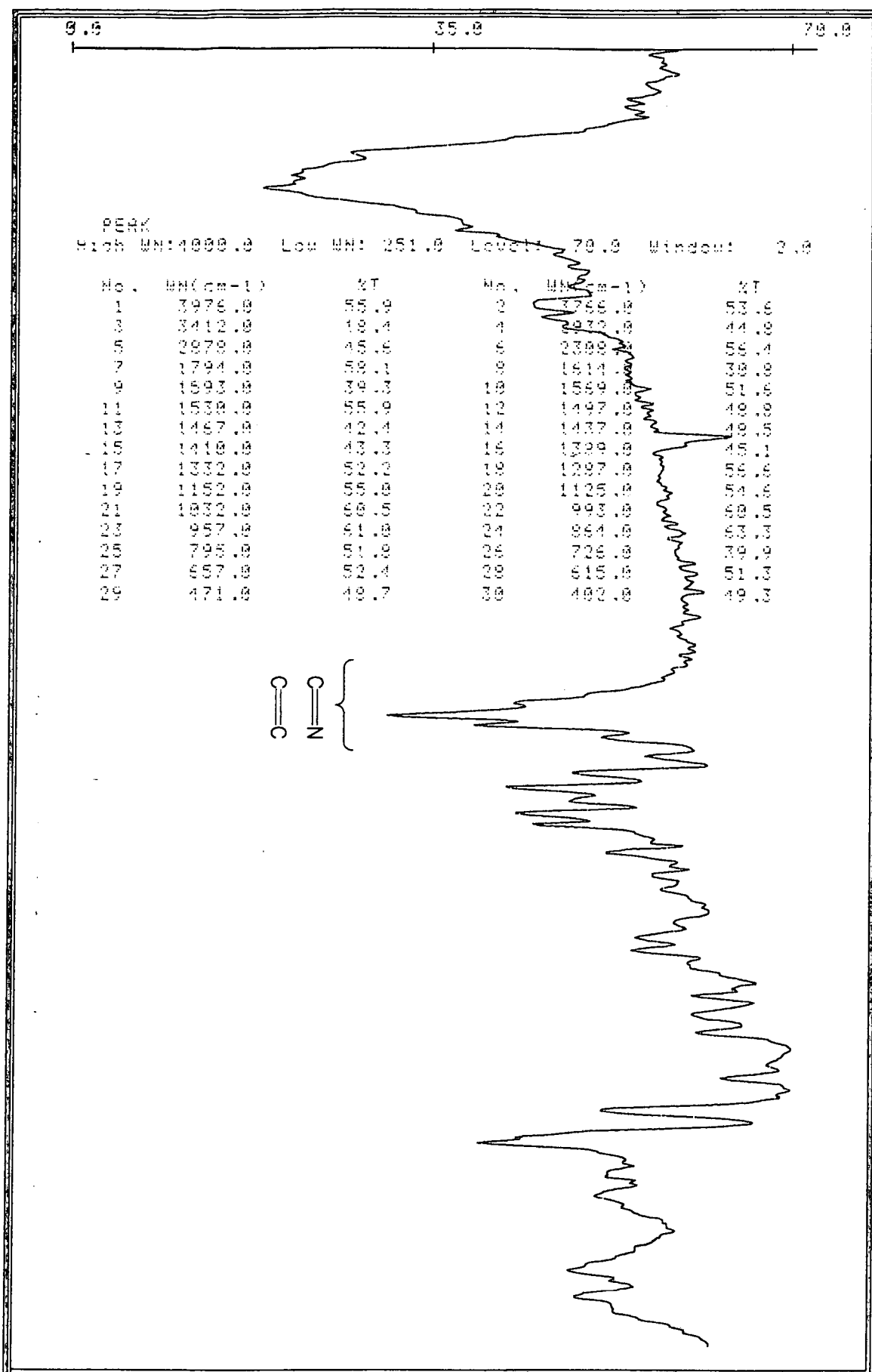


Figure 52 : IR spectrum of the complex [Rh(bpt)(cod)].

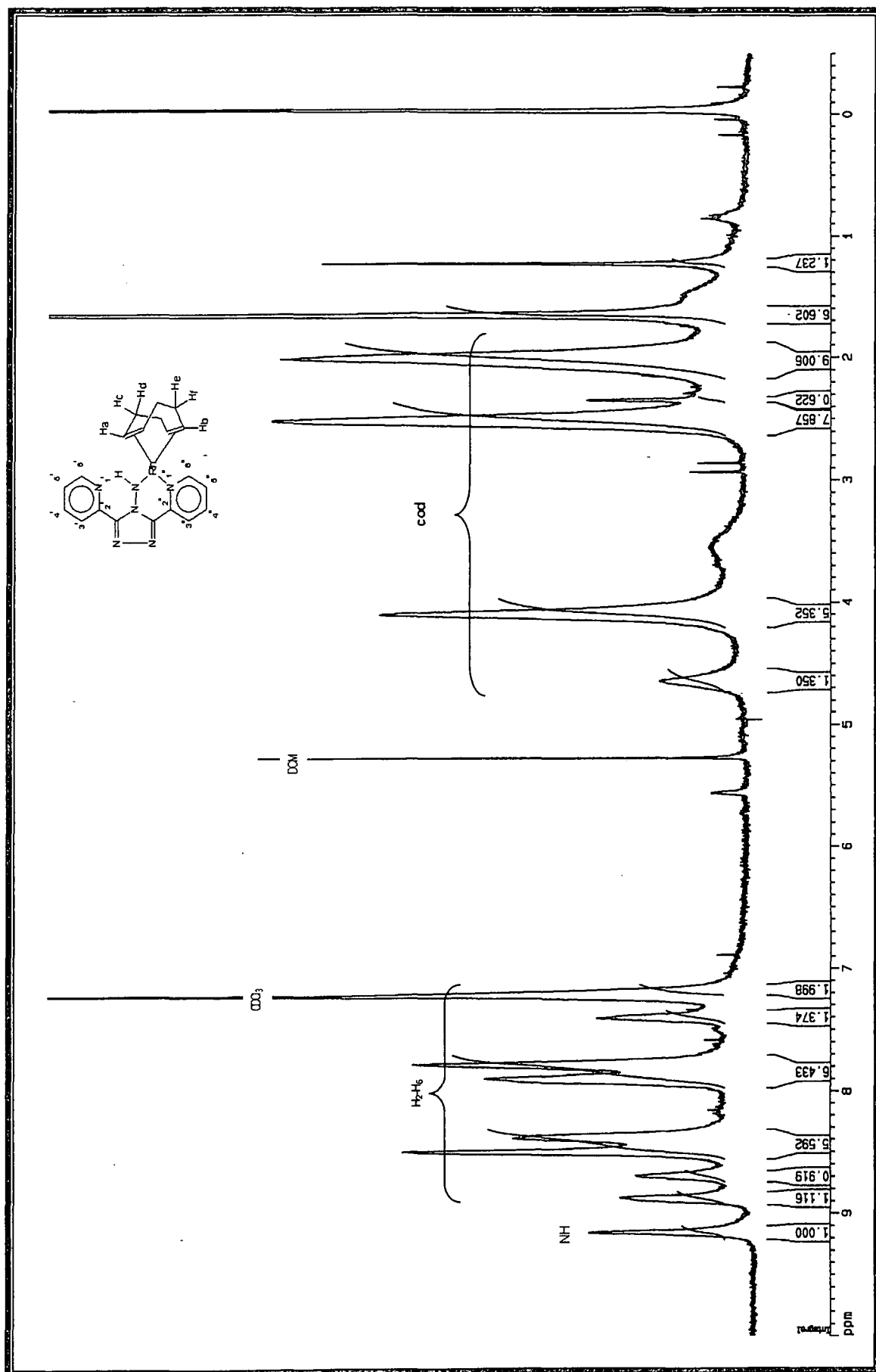


Figure 53 : NMR spectrum of the complex [Rh(bpt-NH)(cod)].

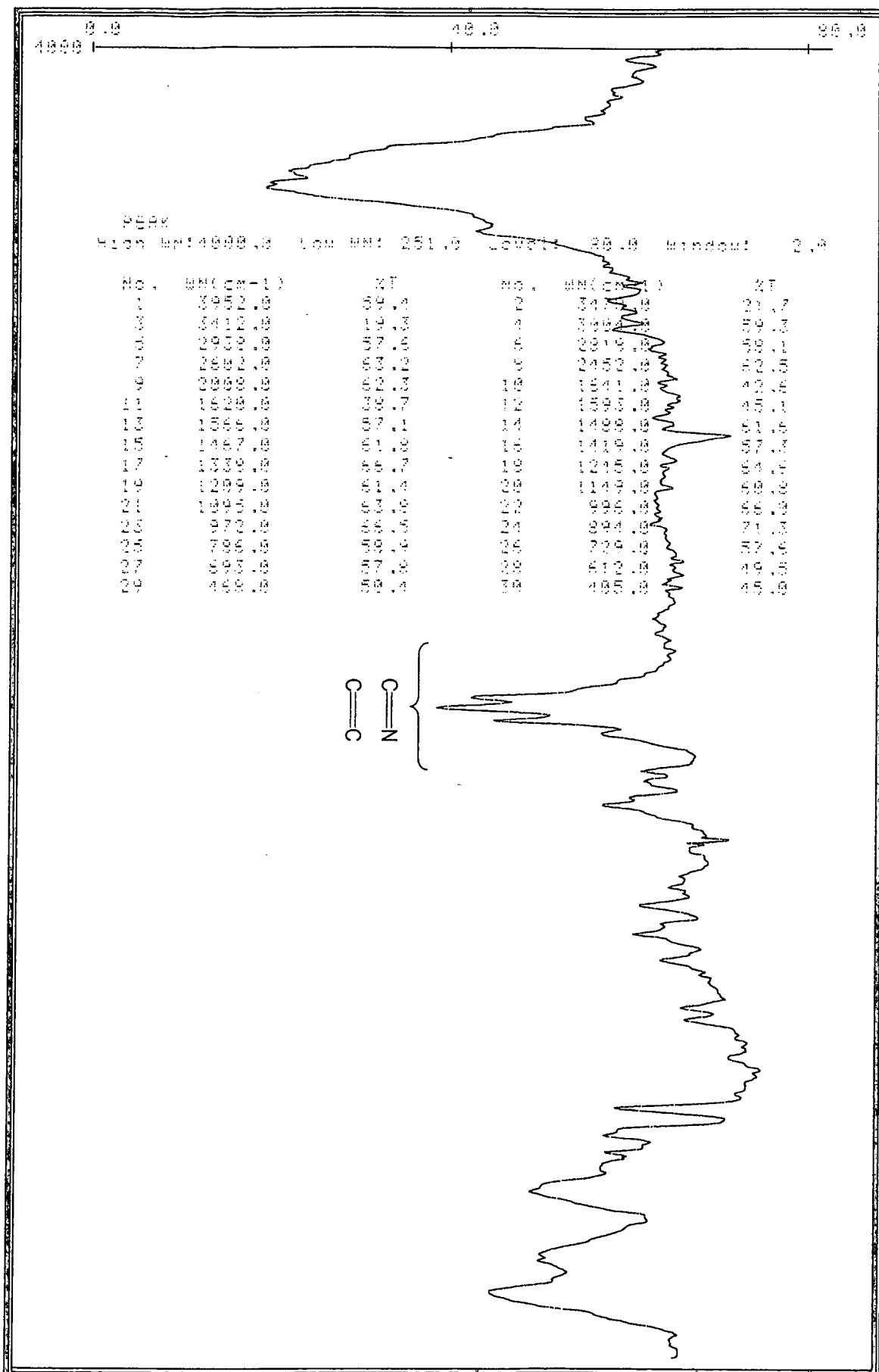


Figure 54: IR spectrum of the complex [Rh(bpt-NH)(cod)].

5. Synthesis of $[\text{M}(\text{bpt-NH})(\text{cod})(\text{CH}_3)(\text{I})]$ and $[\text{M}(\text{bpt})(\text{cod})(\text{CH}_3)(\text{I})]$.

The oxidative addition products of the complexes studied were also isolated and characterised. The procedure for synthesising the complexes was derived from the kinetic results discussed in **Chapter 4**. The complex was kept at the same temperature and an excess amount of CH_3I added. The same solvent was used and from the kinetic results in a realistic reaction time was established for each of the complexes.

Each of the procedures used for the individual complexes are discussed in more detail in the following paragraphs. In each of the procedures the reaction was conducted under a nitrogen atmosphere and deoxygenated solvents were used.

a) Synthesis of $[\text{Ir}(\text{bpt})(\text{cod})(\text{CH}_3)(\text{I})]$.

$[\text{Ir}(\text{bpt})(\text{cod})]$ (0.015g, 0.026mmol) was dissolved in deoxygenated acetone (10cm^3) kept in a water bath at 30°C . An excess of CH_3I (2.6mmol) was added to the solution and the mixture was stirred for 30 min. Diethyl ether was added to precipitate the product and the mixture was centrifuged. The collected solid was dried overnight in a vacuum desiccator over P_2O_5 . (Yield: 0.0135g, 72%)

^1H NMR in CDCl_3 : **Figure 55**:

For pyridine rings = δ 7.1 – 8.8

For cod = δ 2.1 – 5.85

IR_{KBr} : **Figure 56**: $\nu(\text{C}=\text{C}) = 1620, 1500 \text{ cm}^{-1}$

Elemental analysis (%) : found(calculated in brackets) :

C = 35.85(37.96); H = 3.62(3.48); N = 9.11(10.54);

Ir = 25.0(28.92)

b) Synthesis of [Ir(bpt-NH)(cod)(CH₃)(I)].

[Ir(bpt-NH)(cod)] (0.015g, 0.0256mmol) was dissolved in deoxygenated DCM (10cm³) kept in a water bath at 30°C. An excess of CH₃I (2.56mmol) was added to the solution and the mixture was stirred for 30min. Diethyl ether was added to precipitate the product and the mixture was centrifuged. The collected solid was dried overnight in a vacuum desiccator over P₂O₅. (Yield: 0.010g, 53.7%)

¹H NMR in CDCl₃ : **Figure 57** :

For pyridine rings = δ 7.1 – 8.8

For cod = δ 2.1 – 5.8

IR_{KBr} : **Figure 58** : ν(C=C) = 1620, 1593 cm⁻¹

Elemental analysis (%) : found(calculated in brackets) :

C = 36.74(37.12); H = 3.41(3.56); N = 12.77(12.37);

I = 11.16(18.67); Ir = 25.5(28.28)

c) Synthesis of [Rh(bpt)(cod)(CH₃)(I)].

[Rh(bpt)(cod)] (0.015g, 0.031mmol) was dissolved in deoxygenated acetone (10cm³) kept in a water bath at 30°C. An excess of CH₃I (3.12mmol) was added to the solution and the

mixture was stirred for 30min. Diethyl ether was added to precipitate the product and the mixture was centrifuged. The collected solid was dried overnight in a vacuum desiccator over P_2O_5 . (Yield: 0.0155g, 79.8%)

1H NMR in $CDCl_3$: **Figure 59** :

For pyridine rings = δ 7.1 – 8.9

For cod = δ 2.1 – 4.7

IR_{KBr} : **Figure 60** : $\nu(C=C) = 1614 - 1497\text{ cm}^{-1}$

Elemental analysis (%) : found(calculated in brackets) :

C = 44.67(43.85); H = 4.08(4.02); N = 13.12(12.17);

I = 13.60(22.06); Rh = 14.1(17.89)

d) Synthesis of $[Rh(bpt-NH)(cod)(CH_3)(I)]$.

$[Rh(bpt-NH)(cod)]$ (0.015g, 0.030mmol) was dissolved in deoxygenated DCM (10cm^3) kept in a water bath at 30°C . An excess of CH_3I (3.03mmol) was added to the solution and the mixture was stirred for 30min. Diethyl ether was added to precipitate the product and the mixture was centrifuged. The collected solid was dried overnight in a vacuum desiccator over P_2O_5 . (Yield: 0.0173g, 89.6%)

1H NMR in $CDCl_3$: **Figure 61** :

For pyridine rings = δ 7.1 – 8.8

For cod = δ 2.05 – 4.6

IR_{KBr} : **Figure 62** : $\nu(\text{C}=\text{C}) = 1437 \text{ cm}^{-1}$

Elemental analysis (%) : found(calculated in brackets) :

C = 45.97(42.73); H = 4.31(4.10); N = 15.06(14.24);

I = 13.67(21.50); Rh = 16.2(17.43)

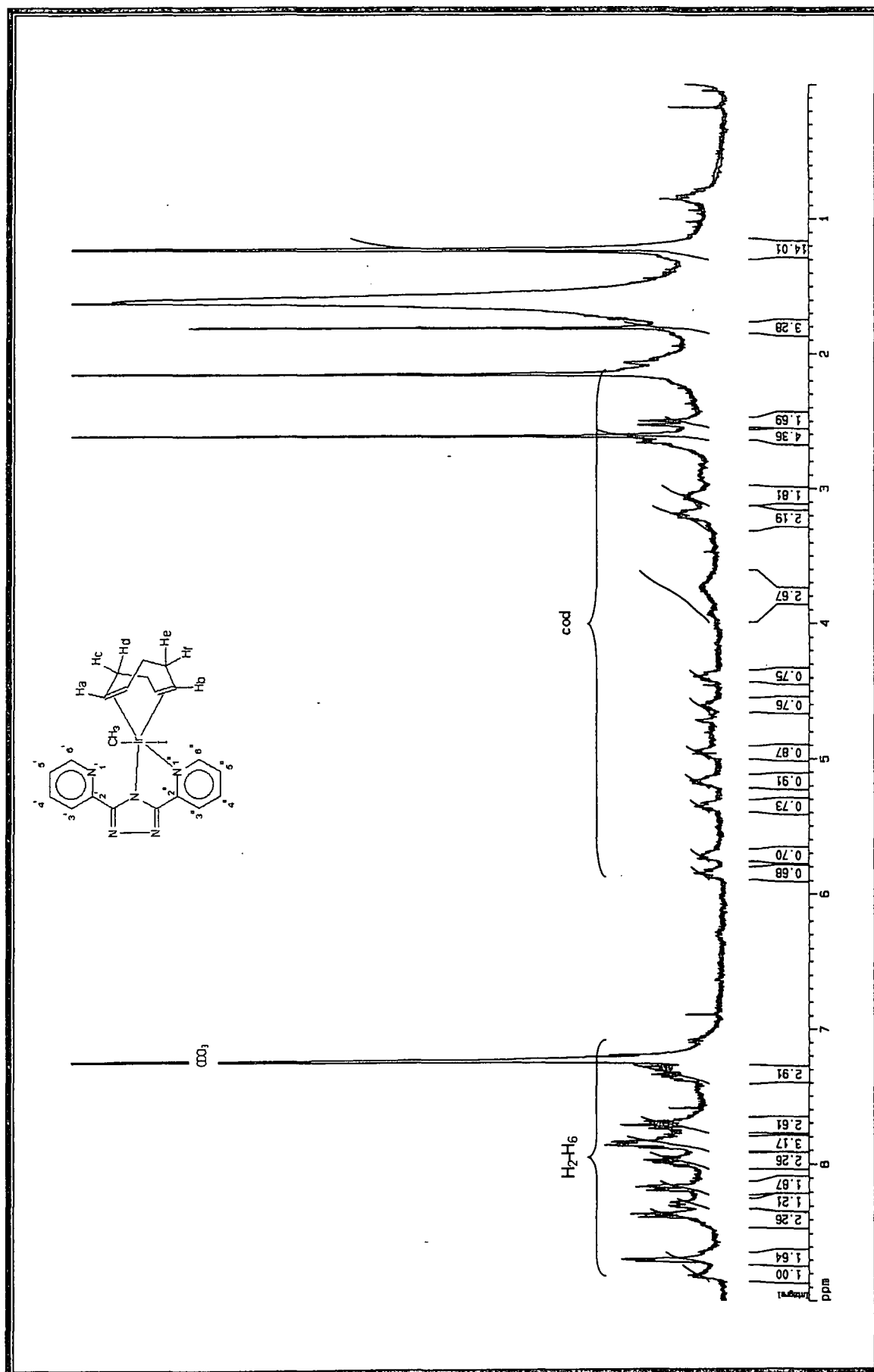


Figure 55 : NMR spectrum of the complex [Ir(bpt)(cod)(CH₃)(I)].

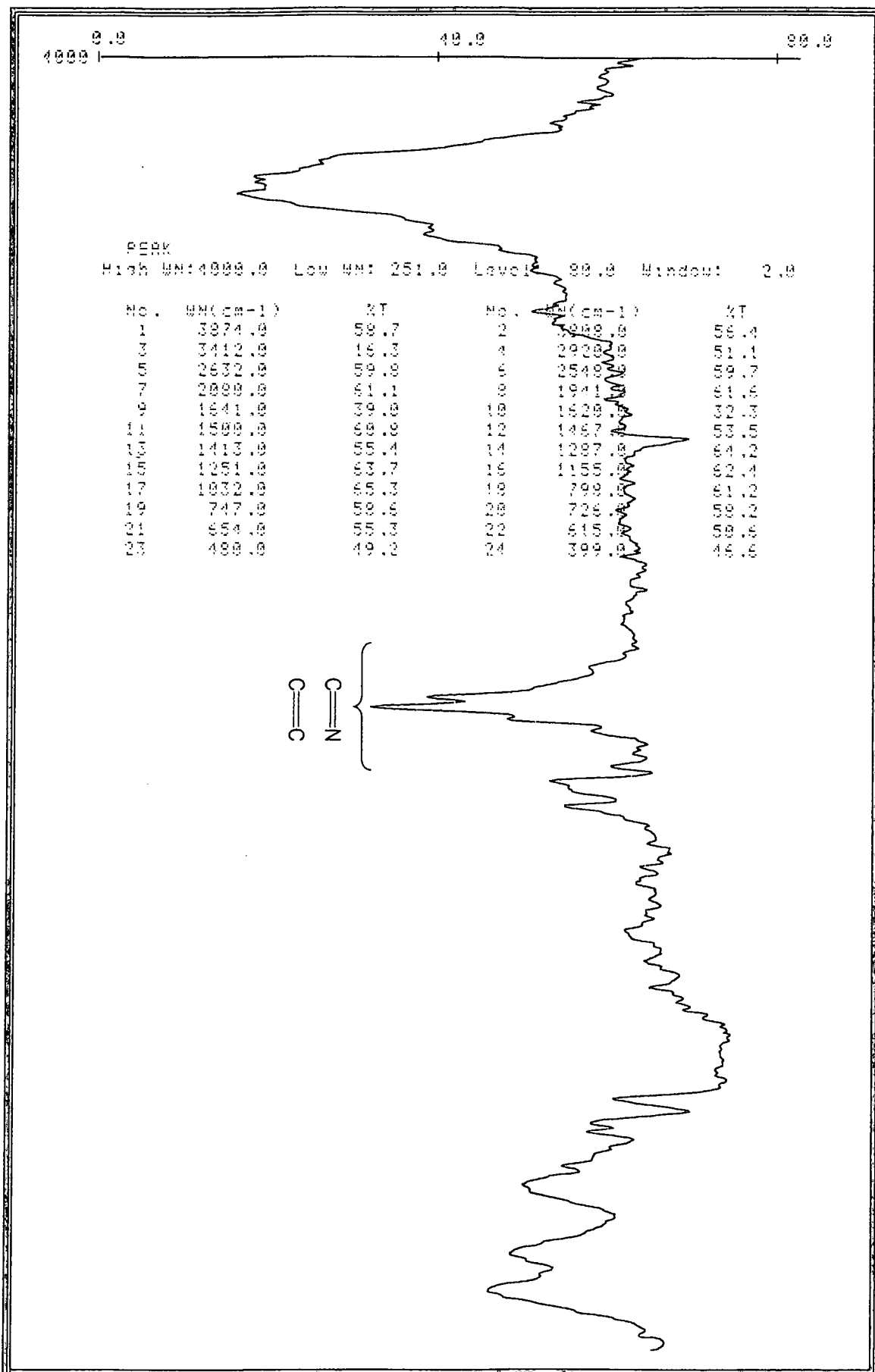


Figure 56 : IR spectrum of the complex [Ir(bpt)(cod)(CH₃)(I)].

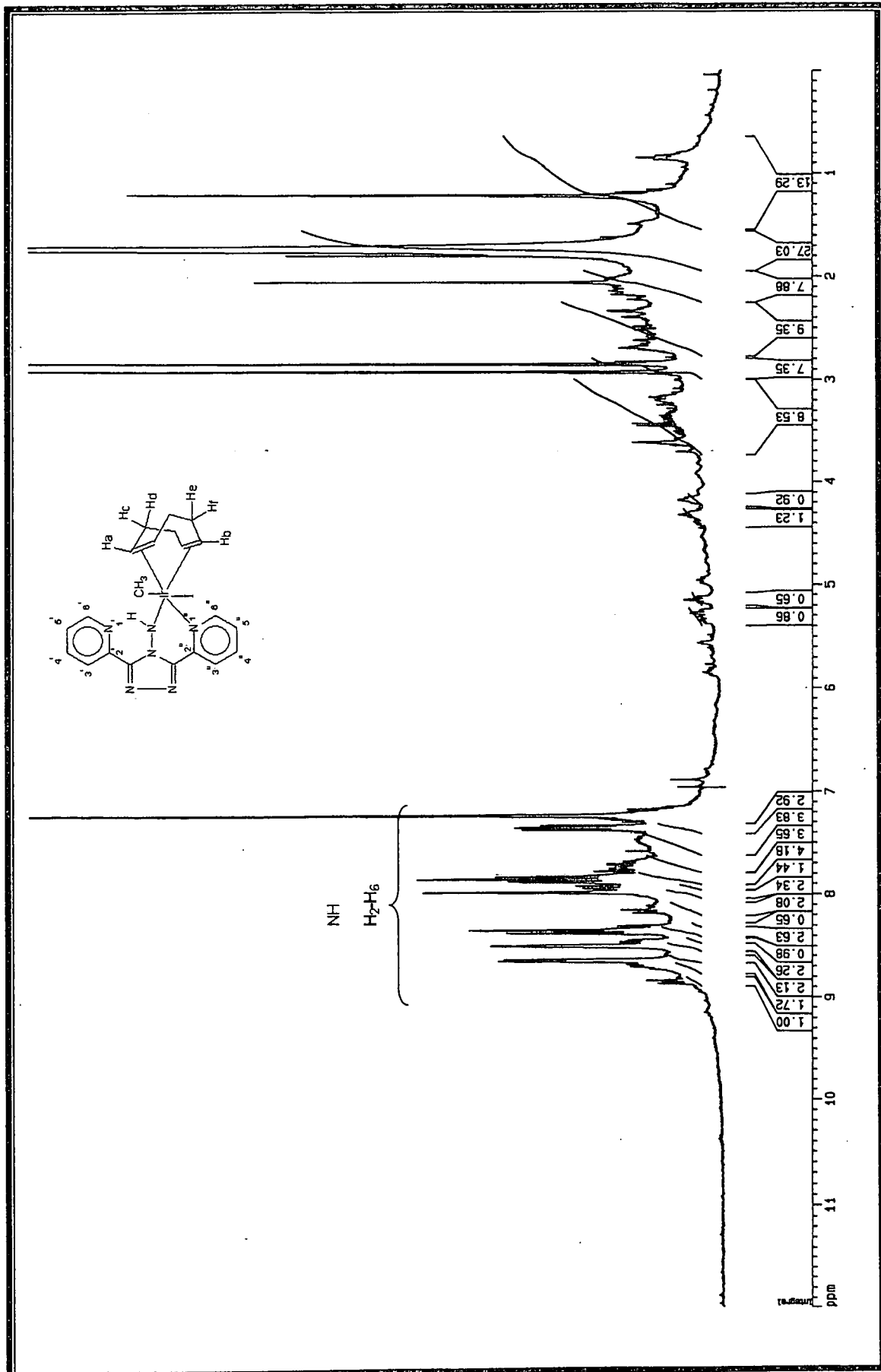


Figure 57 : NMR spectrum of the complex [Ir(bpt-NH)(cod)(CH₃)(I)].

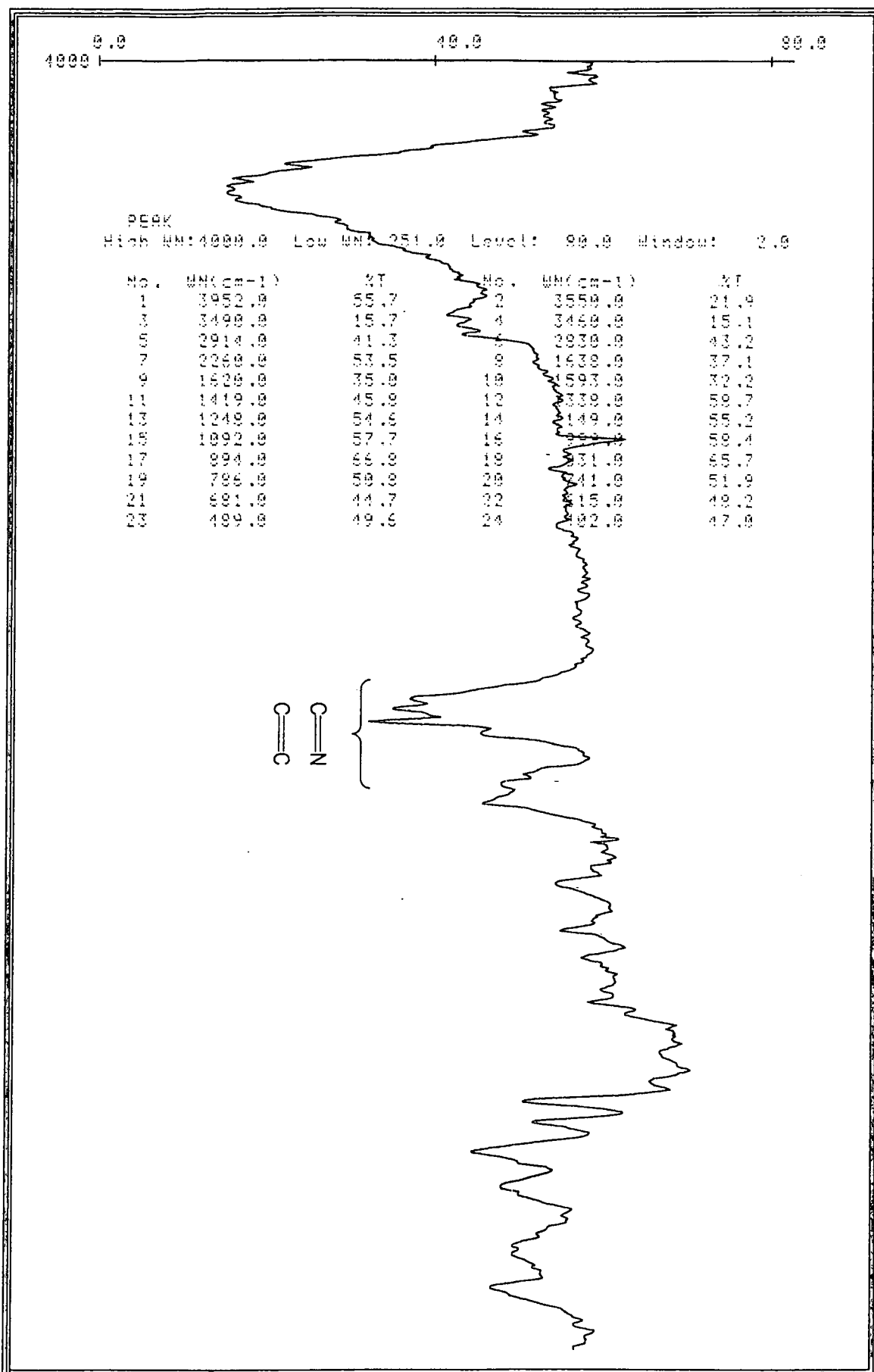


Figure 58 : IR spectrum of the complex $[\text{Ir}(\text{bpt-NH})(\text{cod})(\text{CH}_3)(\text{I})]$.

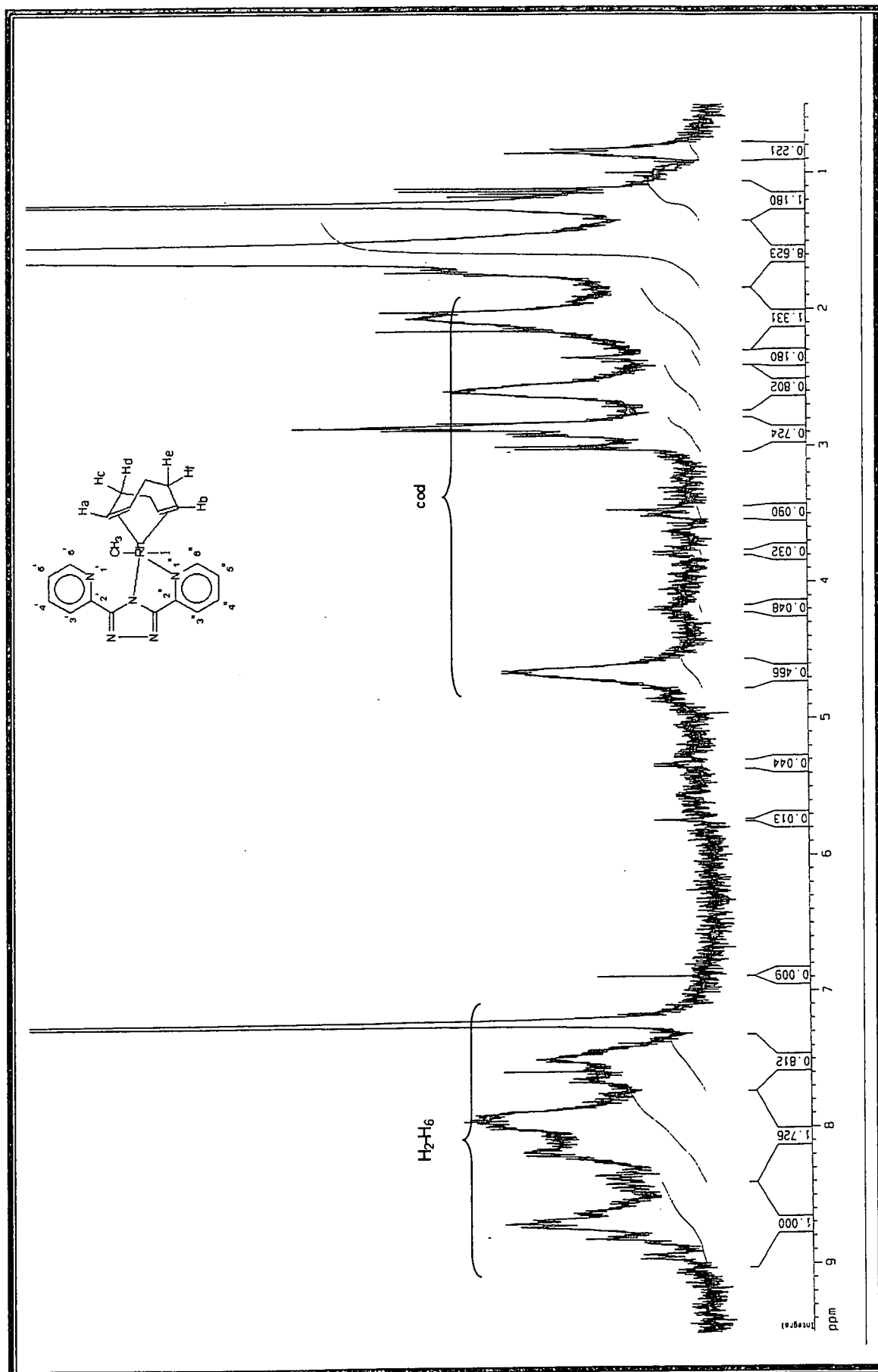


Figure 59: NMR spectrum of the complex [Rh(bpt)(cod)(CH₃)(I)].

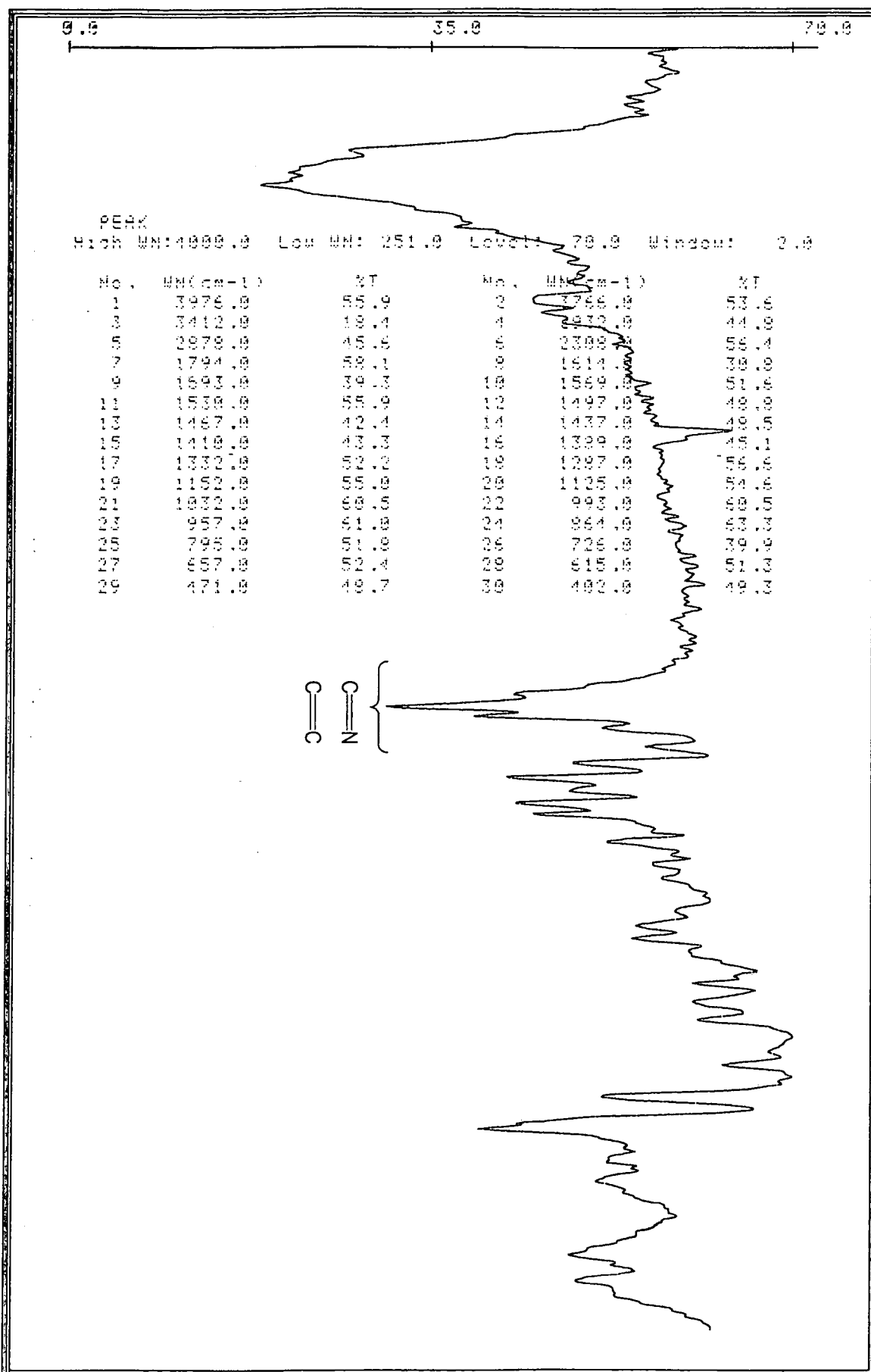


Figure 60 : IR spectrum of the complex $[\text{Rh}(\text{bpt})(\text{cod})(\text{CH}_3)(\text{I})]$.

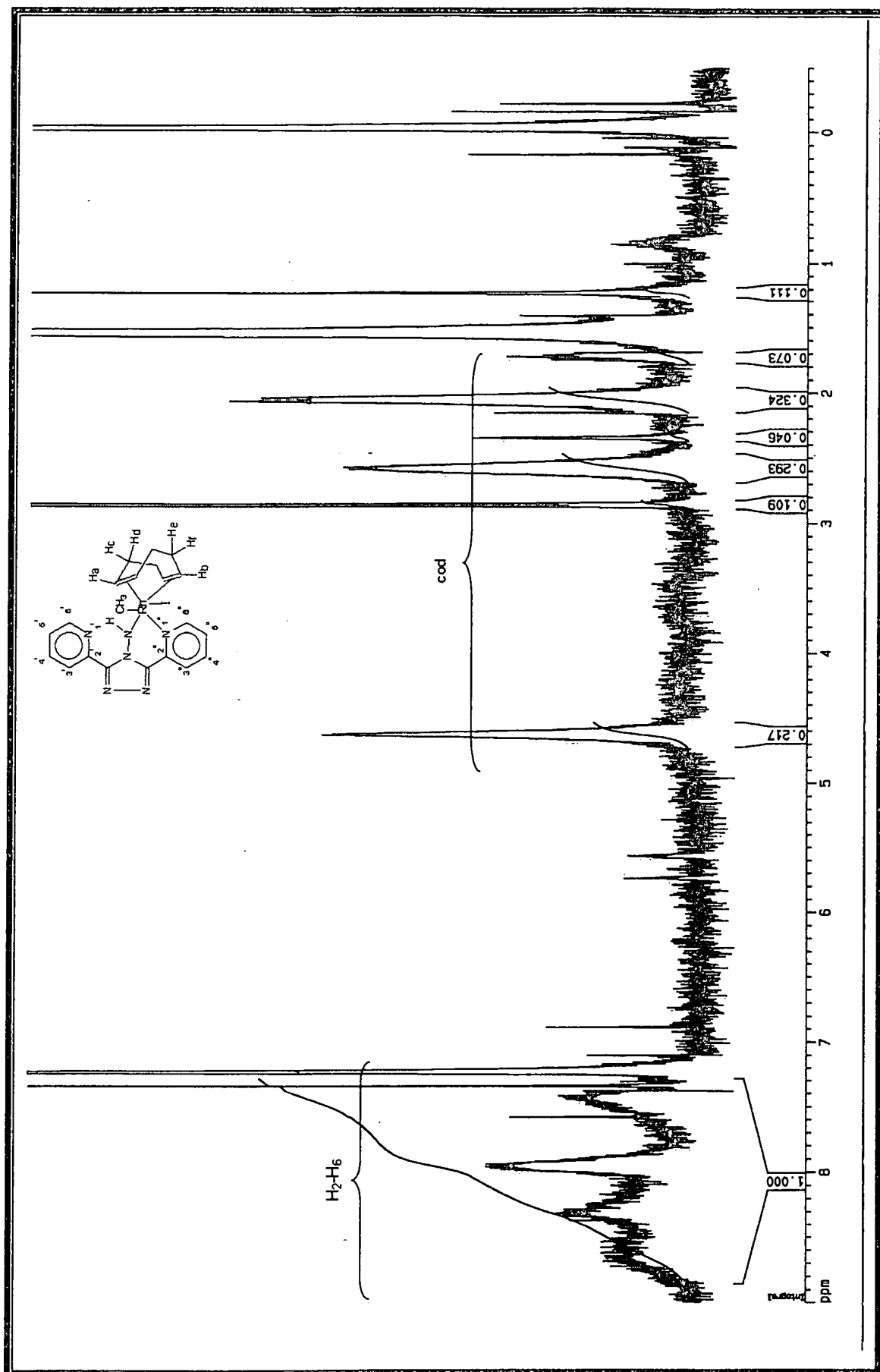


Figure 61 : NMR spectrum of the complex [Rh(bpt-NH)(cod)(CH₃)(I)].

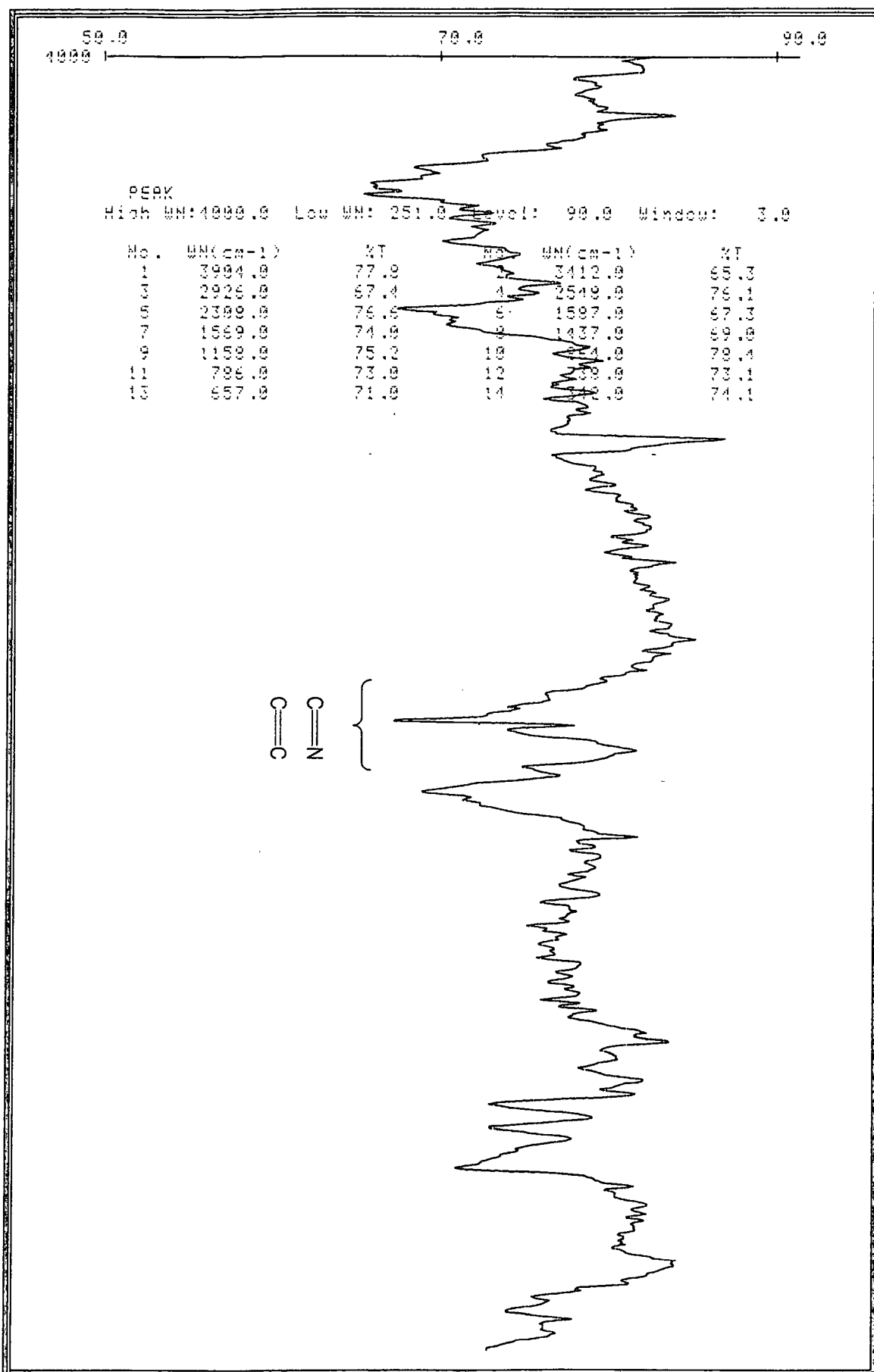


Figure 62 : IR spectrum of the complex $[\text{Rh}(\text{bpt-NH})(\text{cod})(\text{CH}_3)(\text{I})]$.

6. Discussion.

Although the elemental analyses are within acceptable range for the C, H and N analyses, the metal analyses are lower than expected. It is important to notice that the total analysis only account for approximately 90% for each of the complexes. The other 10% may be assigned to organic impurities, aerial oxidation or traces of other impurities in the starting materials. Further analysis indicated the presence of approximately 3% chloride, which suggests that not all the chloride was removed during the filtration step. In typical C, H and N analyses of for example $[\text{Rh}(\text{bpt})(\text{cod})]^{141}$ or $[\text{Rh}(\text{bpt-NH})(\text{cod})]^{140}$ it can be seen that our C, H and N values are within experimental error comparable but not the heavier elements. We therefore suspect that the analytical results of Canadian Microanalytical Service for the heavier elements are not up to standard – a question that will only be solved with another analytical laboratory's results for benchmarking.

However, studying the ratio between nitrogen and metal values (**Table 15**), it can be safely assumed that the complexes are monomeric with the metal bonded to the bidentate ligand in a 1:1 ratio. The only exception is that of $[\text{Ir}(\text{bpt-NH})(\text{cod})]$ where the ratio almost seems to be 2:1 (bidentate ligand:metal). From this a series of complexes such as $[\text{Ir}(\text{bpt-NH}_2)(\text{cod})]^+\text{bpt-NH}^-$ can be postulated. What exactly the correct formulation is, is not known and requires further investigation into this complex.

Table 15 : Summary of the ratio between nitrogen (in the bidentate ligand) and the metal used in the studied complexes.

Complex	%N	%Metal	Ratio (N:Metal)	Ratio (N:Metal) Expected
[Ir(bpt)(cod)]	12.66	31.2	5.5:1	5:1
[Ir(bpt-NH)(cod)]	18.02	24.0	10.3:1	6:1
[Ir(bpt)(cod)(Me)(I)]	9.11	25.0	5:1	5:1
[Ir(bpt-NH)(cod)(Me)(I)]	12.77	25.4	6.9:1	6:1
[Rh(bpt)(cod)]	16.05	17.9	6.5:1	5:1
[Rh(bpt-NH)(cod)]	17.25	19.4	6.5:1	6:1
[Rh(bpt)(cod)(Me)(I)]	13.12	14.1	6.7:1	5:1
[Rh(bpt-NH)(cod)(Me)(I)]	15.06	16.2	6.7:1	6:1

Chapter 4

The oxidative addition kinetics of CH_3I with $[\text{M}(\text{LL}')(\text{cod})]$ complexes.

1. Introduction.

As discussed in **Chapter 2** there are a number of factors influencing the rate as well as the mechanism of oxidative addition reactions.

The rate of oxidative addition between CH_3I and $[\text{M}(\text{LL}')(\text{cod})]$ (where $\text{M} = \text{Ir}$ or Rh and $\text{LL}' = \text{bpt-NH}$ or bpt) was studied and a number of factors were varied to determine their influence on the reaction. These variations included:

- i) The metal atom used (Rh or Ir).
- ii) The bidentate ligand.
- iii) The polarity of the solvent.
- iv) The temperature of the reaction mixture.
- v) The concentrations of the reacting substances.

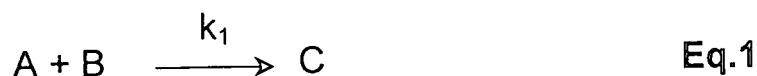
2. Theoretical Principles.

In this section, the relevant rate expressions and kinetic principles,

as well as activation parameters are briefly discussed to give some background information.

a) Basic concepts.

The rate of a reaction nearly always depends upon reactant and for reversible reactions, product concentrations. The interpretation of kinetic data is largely based on an empirical finding called the Law of Mass Action, which states that in dilute solutions the rate of a one-step reaction is proportional to the powers of their stoichiometric coefficients, and independent of other concentrations and reactions¹⁴⁴. Thus for a bimolecular reaction:



the rate of the reaction can be written as:

$$R = k_1[A]^a[B]^b \quad \text{Eq.2}$$

with k_1 being a proportionality constant (rate constant) that relates the rate of change to the reagent concentrations and a and b are called the order of the reaction with respect to A and B respectively. The values of a and b can be determined experimentally by using pseudo-first order conditions where $[B] \gg [A]$, whence Eq.2 reduces to:

$$R = k_{\text{obs}}[A]^a \quad \text{Eq.3}$$

with the observed pseudo-first order rate constant being:

¹⁴⁴ Hammett, L.P., *J. Chem. Educ.*, 43, 464 (1966)

$$k_{\text{obs}} = k_1[B]^b \quad \text{Eq.4}$$

Pseudo-first order conditions (with [B] at least 10 times in excess of [A]) resulting in Eq.4 helps in obtaining the rate constant by determining k_{obs} at different concentrations of B. Under equilibrium conditions for Eq.1, with k_{-1} the reverse rate constant, it can be shown (proof of this in Addendum A) that:

$$k_{\text{obs}} = k_1[B] + k_{-1} \quad \text{Eq.5}$$

whence k_1 and k_{-1} can be determined from the slope and intercept of the linear plot of this equation.

An integration of Eq.2 between time = 0 and t respectively gives the following equation (expressed in terms of C in Eq.1):

$$[C]_t = [C]_0 e^{-k_1 t} \quad \text{Eq.6}$$

Using the Beer-Lambert's law, $A = \epsilon cl$, and with ϵ and l as constants, the absorbance is directly proportional to concentration:

$$[C]_0 \propto A_0 - A_\infty \quad \text{Eq.7}$$

$$[C]_t \propto A_t - A_\infty \quad \text{Eq.8}$$

with A_0 = absorption at time zero

A_t = absorption at time t

A_∞ = absorption at time infinity

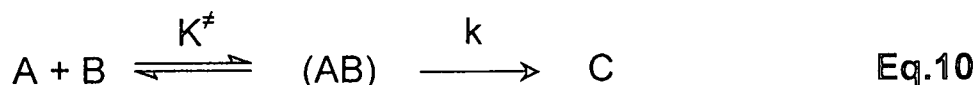
Incorporating Eq.7 and Eq.8 into Eq.6 (with $\frac{[C]_t}{[C]_0} = \frac{A_\infty - A_t}{A_\infty - A_0}$) and then manipulating it, the following equation results:

$$A_t = A_\infty - (A_\infty - A_0)e^{-k_{\text{obs}}t} \quad \text{Eq.9}$$

Infinity is the time at which the reaction is complete for all practical reasons and k_{obs} can then be determined by a least squares fit utilizing absorbance vs time data for the first order reaction.

b) Activation enthalpy and entropy.¹⁴⁵

The transition state theory states that an activated complex or transition state is in equilibrium (K^\ddagger = equilibrium constant) with the reagents before the reaction takes place and that the rate is given by the decomposition rate (k) of the activated complex to yield the products:



The rate of which is given by:

$$k = \frac{k_B T}{h} K^\ddagger \quad \text{Eq.11}$$

where k_B = Boltzmann's and h = Planck's constants.

From basic thermodynamics it follows that:

¹⁴⁵ Frost, A.F.; Pearson, R.G.; *Kinetics and Mechanism*, John Wiley and Sons, New York (1953)

$$K^\ddagger = e^{\frac{-\Delta G^{0\ddagger}}{RT}} \quad \text{Eq.12}$$

with $\Delta G^{0\ddagger}$ = standard free energy change and R = universal gas constant.

Substituting Eq.12 into Eq.11 and the fact that $\Delta G^\circ = \Delta H^\circ - T\Delta S^\circ$ yields Eq.13 known as the Eyring equation.

$$k = T \frac{k_B}{h} e^{\left(\frac{\Delta S^\ddagger}{R}\right) \left(\frac{\Delta H^\ddagger}{RT}\right)} \quad \text{Eq.13}$$

Eq.13 is generally written in a logarithmic form as shown in Eq.14 below

$$\ln\left(\frac{k}{T}\right) = \ln\left(\frac{k_B}{h}\right) + \left(\frac{\Delta S^\ddagger}{R}\right) - \left(\frac{\Delta H^\ddagger}{RT}\right) \quad \text{Eq.14}$$

The graph of $\ln\frac{k}{T}$ vs $\frac{1}{T}$ will have a slope of $-\frac{\Delta H^\ddagger}{RT}$, with ΔH^\ddagger = standard enthalpy change of activation and the y-intercept yielding $\frac{\Delta S^\ddagger}{R} + \ln\left(\frac{k_B}{h}\right)$, with ΔS^\ddagger = standard entropy change of activation.

3. Experimental

The ligands (bpt-NH₂ and hbpt), the starting metal complexes, [M(Cl)(cod)]₂, and the studied complexes ([M(bpt)(cod)] and [M(bpt-NH)(cod)]) were synthesised as described in chapter 3.

The CH₃I used for this study was bought from Merck and stabilized with silver foil preventing decomposition to iodine. Care was taken when handling CH₃I since it is highly volatile and carcinogenic. It was only used in well-ventilated rooms and contact with skin was avoided.

All the solvents used in the kinetic studies were of analytical quality. The solvents were purified and dried using purification methods described in **Addendum B**.

The stability of each of the complexes was tested in the various solvents used. It was found that under inert atmosphere the complexes showed slow reactions with the solvent. When an excess amount of CH₃I was added under these conditions, faster reactions than the decomposition in solvent were obtained and from these a suitable wavelength was deducted to study the reaction. These wavelengths are given at each section of kinetic data discussed later on. As an example, one of these preliminary investigatory spectra is included (**Figure 63**). **Figure 63(a)** is the spectrum of [Rh(bpt-NH)(cod)] in DCM scanned hourly, while **Figure 63(b)** is the same complex with CH₃I added but scanned every 30 min. One can see that the oxidative addition with CH₃I is

already completed in less than 30 min since no further reaction is detected.

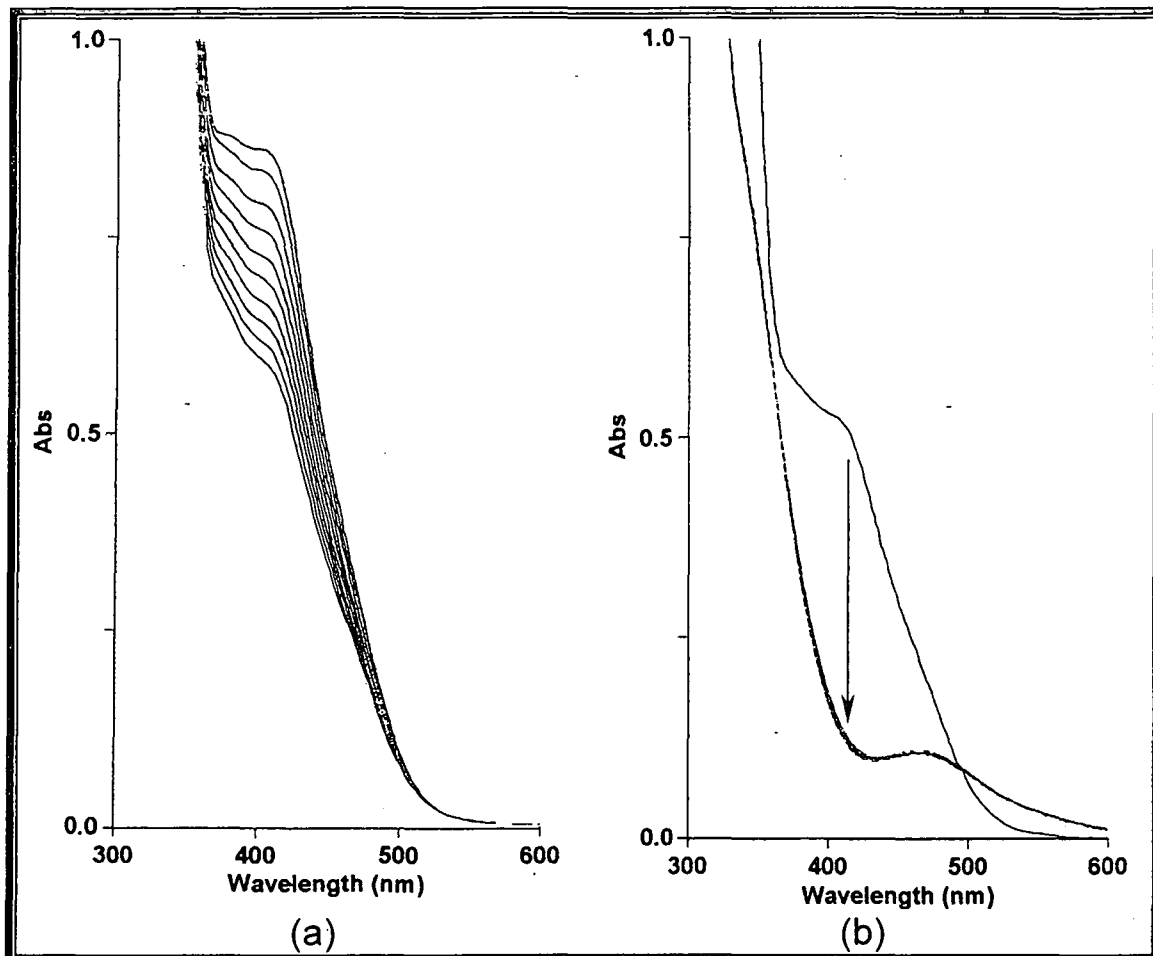


Figure 63 : Spectrums of the decomposition of $\text{Rh}(\text{bpt-NH})(\text{cod})$ in DCM (a) and the reaction with CH_3I (b).

Reactions were followed using a Cary-50 double beam spectrophotometer in a thermostatically controlled cell holder ($\pm 0.1^\circ\text{C}$) The cell holder has a capacity of 18 cells.

During the kinetic investigations temperature and concentration variations were carried out at room temperature to determine the activation enthalpy and entropy for each of the reactions in different solvents. These activation parameters were calculated with the aid of Eq.14. All reactions were carried out under pseudo-

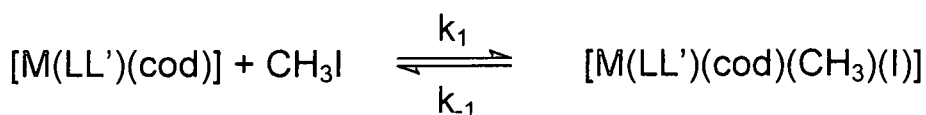
first order conditions where the concentration of the CH_3I was at least ten times that of the metal complex concentration.

The CH_3I solutions used during the concentration variations were prepared as follow: the solvent ($\pm 7\text{cm}^3$) was poured into a 10cm^3 volumetric flask and zeroed on a balance. The CH_3I was added dropwise using a glass syringe until the approximate desired mass was reached. The exact mass of CH_3I was noted and the volumetric flask was then made up to volume as soon as possible. Use of this method limited the evaporation of CH_3I to a minimum and the concentrations were calculated from the accurate mass used.

The mathematical calculations of the kinetic investigations were done on a desktop computer using a least squares program (Micromath Scientis for Windows). The observed pseudo-first order rate constant k_{obs} was calculated from the absorbance-time data with the aid of Eq.9.

4. Kinetic Results.

The oxidative reaction between CH_3I and $[\text{M}(\text{LL}')(\text{cod})]$ ($\text{M} = \text{Ir}, \text{Rh}$ and $\text{LL}' = \text{bpt}^-, \text{bpt-NH}^-$) can be presented as follow:



The rate law for the second-order reversible kinetics would be given by :

The rate law for the second-order reversible kinetics would be given by :

$$R = k_1[M(LL')(cod)][CH_3I] - k_{-1}[M(LL')(cod)(CH_3)(I)]$$

This rate law can be simplified by substantially increasing [CH₃I] (pseudo-first order conditions). With the use of **Eq. 5** we can then assign

$$k_{obs} = k_1[CH_3I] + k_{-1}$$

as the new constant, which is the observed reaction rate.

From a graph of k_{obs} against [CH₃I] the values of k_1 and k_{-1} can be obtained. In all the studied cases a zero intercept (within experimental error) was found. This implies that the reverse reaction is of limited extent or does not occur at all. The value of k_{-1} can thus be omitted, simplifying the rate law to:

$$R = k_1[CH_3I][M(LL')(cod)]$$

For comparative purposes, the calculated values of k_{-1} are included in the tabulated data.

a) Kinetic investigation of the oxidative addition between CH₃I and [Ir(bpt)(cod)].

The oxidative reaction between CH₃I and [Ir(bpt)(cod)] in acetone was done under pseudo-first order conditions. This yielded a linear graph when k_{obs} was plotted against [CH₃I] (**Figure 64**). The values

for k_1 and k_{-1} can be calculated from Eq.5, which is the slope and intercept of Figure 64.

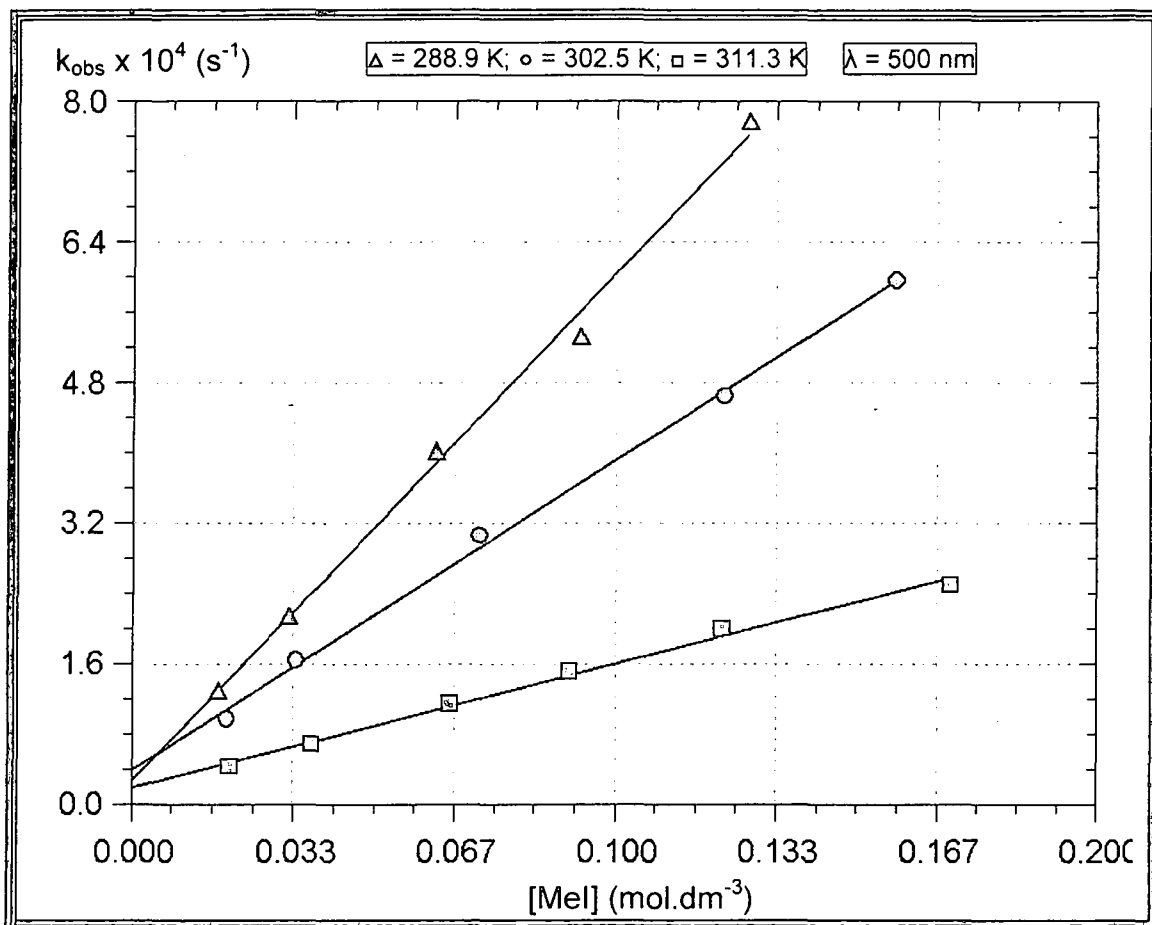


Figure 64 : Plot of k_{obs} against $[\text{Mel}]$ for the oxidative addition between CH_3I and $[\text{Ir}(\text{bpt})(\text{cod})]$ in acetone.

The reaction was performed at three temperatures to determine the activation parameters of the reaction as well. The values of ΔH^\ddagger and ΔS^\ddagger were calculated from this with the use of Eq.14 as $42.8(6) \text{ kJ}\cdot\text{mol}^{-1}$ and $-150(2) \text{ JK}^{-1}\text{mol}^{-1}$ respectively. The complete set of kinetic data for this reaction is given in Addendum A (Table 18).

b) Kinetic investigation of the oxidative addition between CH_3I and $[\text{Ir}(\text{bpt-NH})(\text{cod})]$.

The oxidative reaction between CH_3I and $[\text{Ir}(\text{bpt-NH})(\text{cod})]$ in benzene was done under pseudo-first order conditions. This yielded a linear graph when k_{obs} was plotted against $[\text{CH}_3\text{I}]$ (Figure 65). The values for k_1 and k_{-1} can be calculated from Eq.5, which is the slope and intercept of Figure 65.

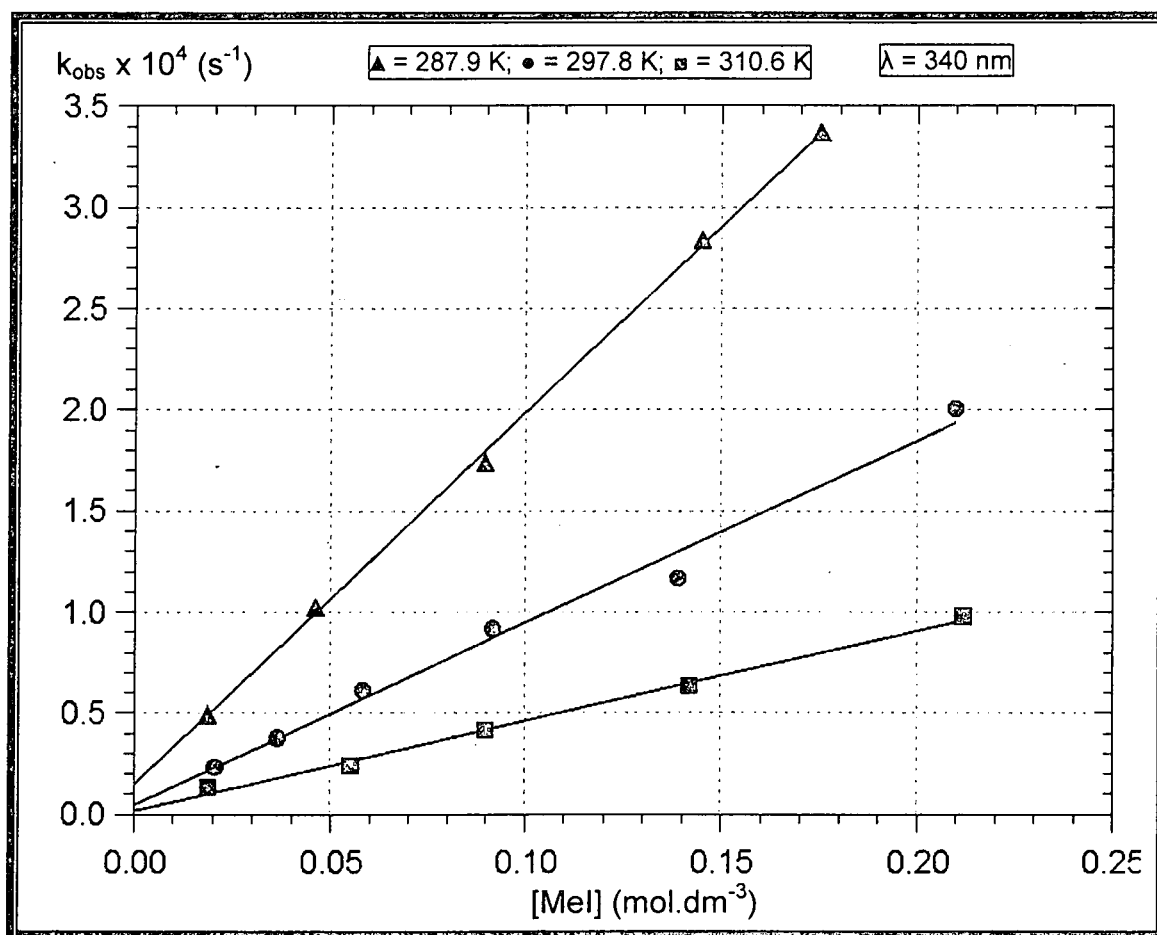


Figure 65 : Plot of k_{obs} against $[\text{MeI}]$ for the oxidative addition between CH_3I and $[\text{Ir}(\text{bpt-NH})(\text{cod})]$ in benzene.

The reaction was performed at three temperatures to determine the activation parameters of the reaction as well. The values of ΔH^\ddagger and ΔS^\ddagger were calculated from this with the use of Eq.14 as

42(2) kJ.mol⁻¹ and -162(8) JK⁻¹mol⁻¹ respectively. The complete set of kinetic data for this reaction is given in Addendum A (Table 19).

The reaction was also conducted in DCM showing the same linear relationship (Figure 66).

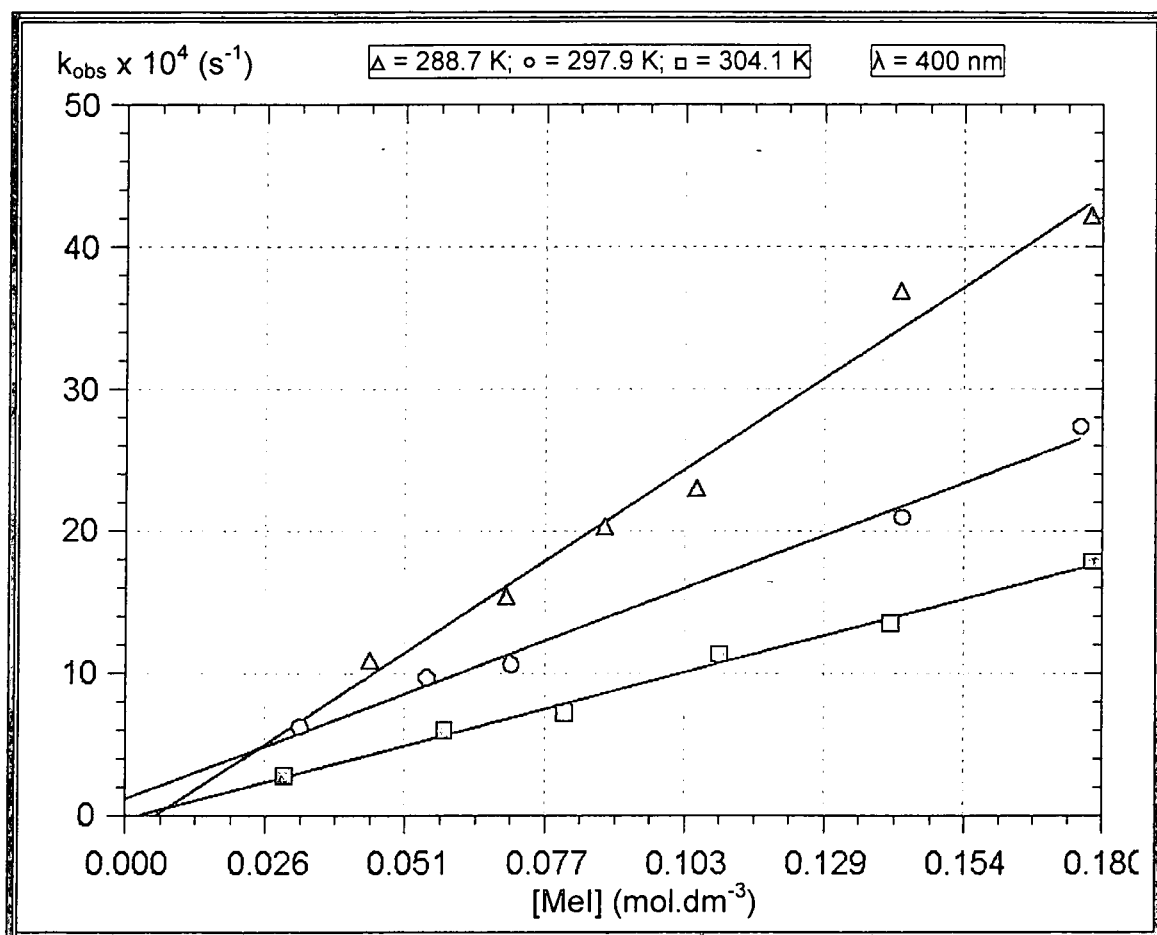


Figure 66 : Plot of k_{obs} against $[\text{Mel}]$ for the oxidative addition between CH_3I and $[\text{Ir}(\text{bpt-NH})(\text{cod})]$ in DCM.

The reaction was preformed at three temperatures to determine the activation parameters of the reaction as well. The values of ΔH^\ddagger and ΔS^\ddagger were calculated from this with the use of Eq.14 as 46(12) kJ.mol⁻¹ and -123(42) JK⁻¹mol⁻¹ respectively. The complete

set of kinetic data for this reaction is given in **Addendum A (Table 20)**.

c) Kinetic investigation of the oxidative addition between CH_3I and $[\text{Rh}(\text{bpt})(\text{cod})]$.

The oxidative reaction between CH_3I and $[\text{Rh}(\text{bpt})(\text{cod})]$ in acetone was done under pseudo-first order conditions. This yielded a linear graph when k_{obs} was plotted against $[\text{CH}_3\text{I}]$ (**Figure 67**). The values for k_1 and k_{-1} can be calculated from **Eq.5**, which is the slope and intercept of **Figure 67**.

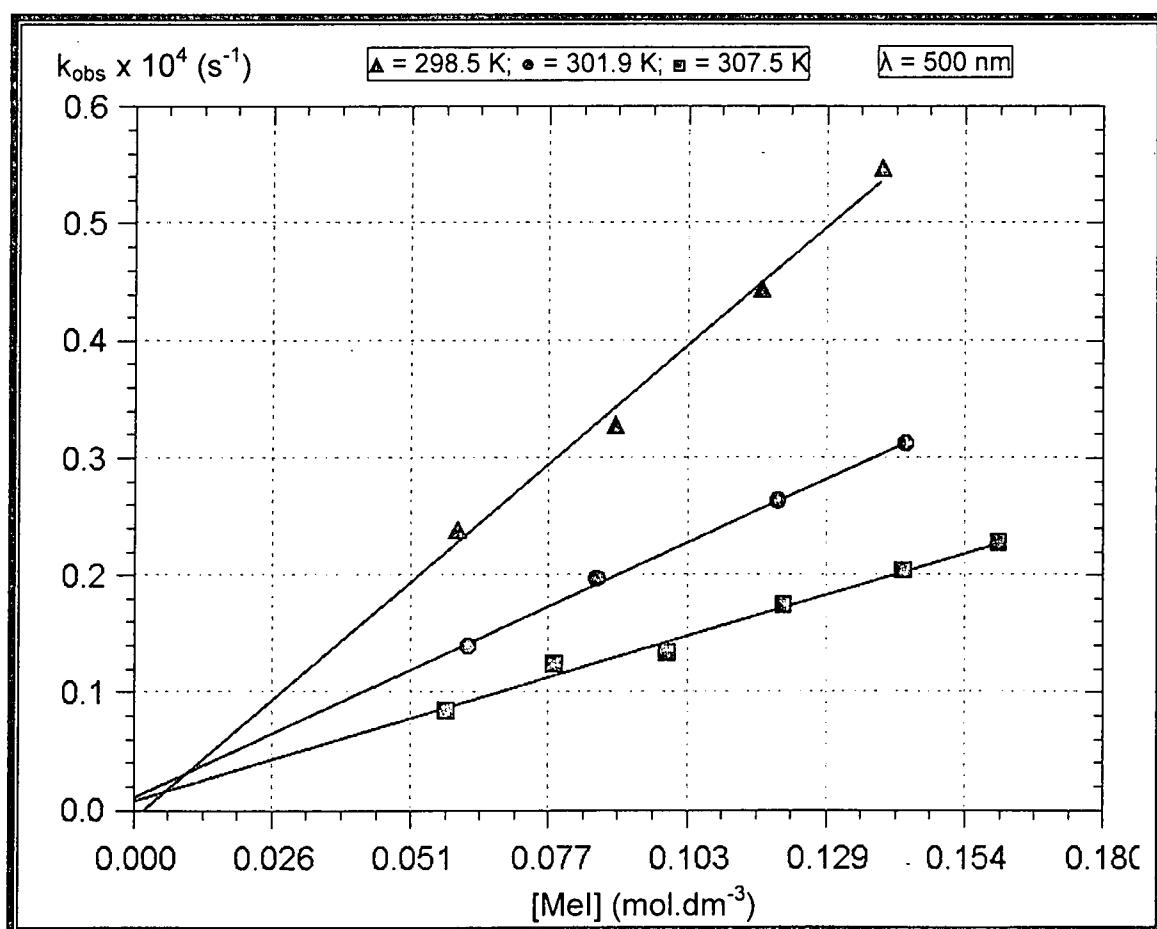


Figure 67 : Plot of k_{obs} against $[\text{MeI}]$ for the oxidative addition between CH_3I and $[\text{Rh}(\text{bpt})(\text{cod})]$ in acetone.

The reaction was performed at three temperatures to determine the activation parameters of the reaction as well. The values of ΔH^\ddagger and ΔS^\ddagger were calculated from this with the use of Eq.14 as 40(8) kJ.mol⁻¹ and -131(6) JK⁻¹mol⁻¹ respectively. The complete set of kinetic data for this reaction is given in Addendum A (Table 21).

d) Kinetic investigation of the oxidative addition between CH₃I and [Rh(bpt-NH)(cod)].

The oxidative reaction between CH₃I and [Rh(bpt-NH)(cod)] in benzene was done under pseudo-first order conditions. This yielded a linear graph when k_{obs} was plotted against [CH₃I] (Figure 68). The values for k_1 and k_{-1} can be calculated from Eq.5, which is the slope and intercept of Figure 68.

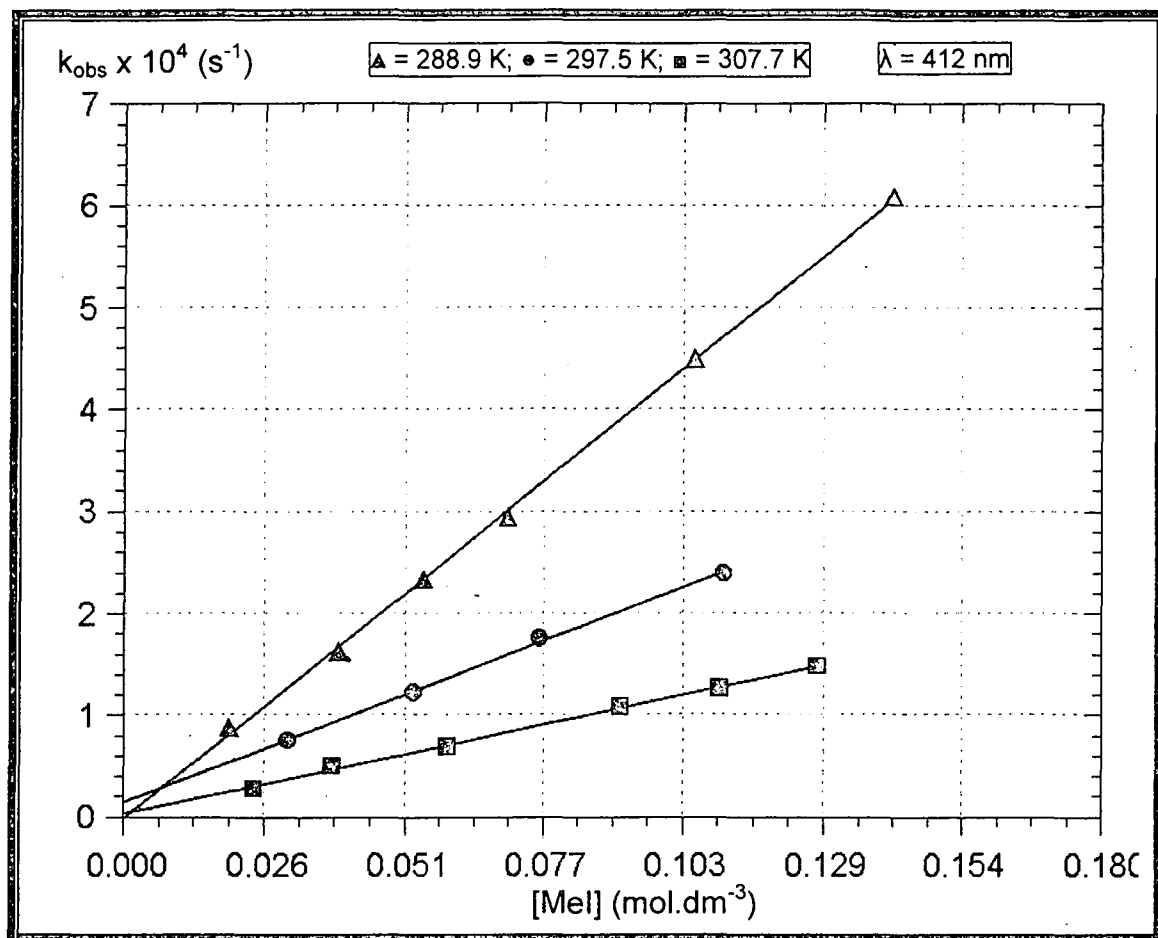


Figure 68 : Plot of k_{obs} against $[\text{MeI}]$ for the oxidative addition between CH_3I and $[\text{Rh}(\text{bpt-NH})(\text{cod})]$ in benzene.

The reaction was performed at three temperatures to determine the activation parameters of the reaction as well. The values of ΔH^\ddagger and ΔS^\ddagger were calculated from this with the use of **Eq.14** as $51(2) \text{ kJ.mol}^{-1}$ and $-124(7) \text{ JK}^{-1}\text{mol}^{-1}$ respectively. The complete set of kinetic data for this reaction is given in **Addendum A (Table 22)**.

The reaction was also conducted in DCM showing the same linear relationship (**Figure 69**).

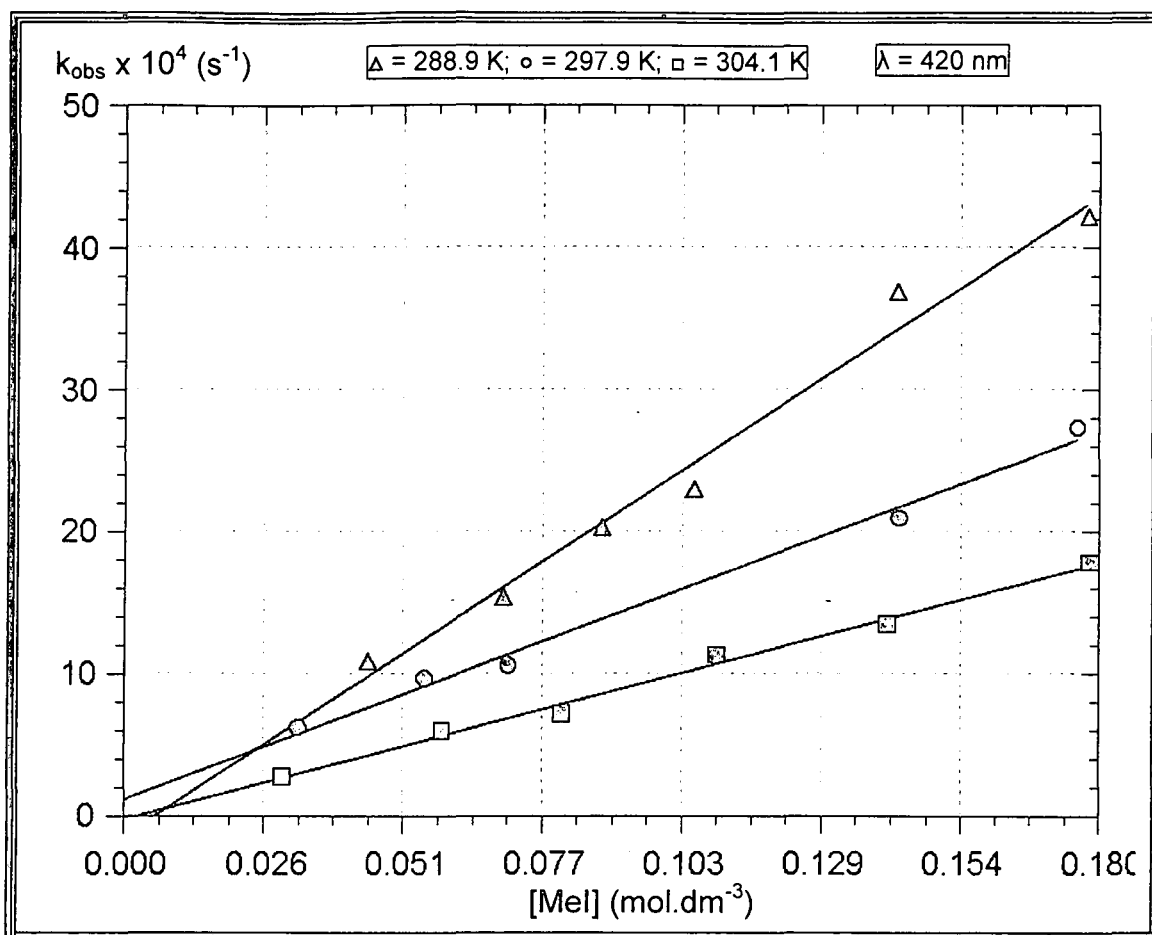


Figure 69 : Plot of k_{obs} against $[\text{Mel}]$ for the oxidative addition between CH_3I and $[\text{Rh}(\text{bpt-NH})(\text{cod})]$ in DCM.

The reaction was performed at three temperatures to determine the activation parameters of the reaction as well. The values of ΔH^\ddagger and ΔS^\ddagger were calculated from this with the use of Eq.14 as $37(4) \text{ kJ.mol}^{-1}$ and $-152(14) \text{ JK}^{-1}\text{mol}^{-1}$ respectively. The complete set of kinetic data for this reaction is given in Addendum A (Table 23).

5. Discussion

A compilation of the kinetic results is shown in **Table 16**.

Table 16 : Summary of the kinetic data for the oxidative addition between CH₃I and [M(bpt)(cod)] (M = Rh, Ir) in different solvents and temperatures.

Complex	Solvent	Temp. (K)	$k_1 \times 10^2$ (M ⁻¹ .s ⁻¹)	$k_{-1} \times 10^4$ (s ⁻¹)	ΔH^\ddagger kJ.mol ⁻¹	ΔS^\ddagger JK ⁻¹ .mol ⁻¹
[Ir(bpt)(cod)]	Act	288.9	0.141(6)	1.8(5)	42.8(6)	-150(2)
		302.5	0.35(1)	0.4(1)		
		311.3	0.58(2)	0.3(1)		
[Ir(bpt-NH)(cod)]	Bz	287.9	0.044(2)	0.02(2)	42(2)	-162(8)
		297.8	0.092(5)	0.03(6)		
		310.6	0.184(3)	0.15(3)		
[Ir(bpt-NH)(cod)]	DCM	288.7	1.00(5)	0.2(5)	46(12)	-123(42)
		297.9	1.44(7)	1.1(8)		
		304.1	2.5(2)	-1(2)		
[Rh(bpt)(cod)]	Act	298.5	0.0136(8)	0.008(9)	40(8)	-131(6)
		301.9	0.021(2)	0.01(2)		
		307.5	0.039(3)	-0.01(3)		
[Rh(bpt-NH)(cod)]	Bz	288.5	0.114(3)	0.03(2)	51(2)	-124(7)
		297.5	0.21(2)	0.01(2)		
		307.7	0.429(6)	-0.01(5)		
[Rh(bpt-NH)(cod)]	DCM	288.9	1.23(3)	1.3(3)	37(4)	-152(14)
		297.9	2.20(3)	0.4(3)		
		303.9	2.9(1)	2(2)		

Careful inspection of the data in this table revealed a number interesting facts about the oxidative addition kinetics of the complexes studied. These are discussed in more detail in the following paragraphs.

a) The influence of the solvent.

A number of solvents tested showed different side reactions even with the use of inert atmosphere conditions and purified solvents. However, a few showed satisfactory results and deductions can still be made from this. Both iridium and rhodium analogues with

the bpt-NH deprotonated ligand were studied in two solvents of different polarities. There is an increase of approximately a factor 10 for both metals as the solvent is changed from benzene ($\epsilon = 2.3$) to DCM ($\epsilon = 9.1$). Thus the solvent polarity has an influence on the rate of oxidative addition, proving that the solvent's function is to promote the charge separation in the transition state as those indicated in Chapter 2 Figure 15(a) and (b).

As previously mentioned, the values for k_{-1} are zero within experimental error, indicating that there is no reverse reaction or at best, a negligible contribution from this term in Eq.5.

b) The influence of the bidentate ligands and the metal atom.

The bidentate ligands hbpt and bpt-NH₂ influence the metal complexes differently by their varied donating abilities through the N-donor atoms to the metal atom. The complexes of the bpt⁻ ligand is slower than those of the bpt-NH⁻, despite the fact that acetone is a more polar solvent ($\epsilon = 20.7$) than DCM ($\epsilon = 9.1$). In line with this it is expected that coordination through the -NH⁻-group to the metal will invoke a better Lewis base for the metal center in such a complex. Only when a less polar solvent like benzene ($\epsilon = 2.3$) is used, the rate of the bpt⁻ complex is faster, and only for the iridium analogue.

The difference in the reaction rates for the bidentate ligands is also more prominent in the rhodium analogues, where there is a two-order difference between the ones in acetone and DCM, compared

to the 4 – 7 factor difference for the iridium analogues. This difference is smaller when comparing the benzene kinetics to the acetone kinetics, due to solvent effects discussed in the previous part.

An interesting discrepancy can be noticed when comparing the rates for the two metal atoms. For the bpt^- ligand the iridium analogue is more reactive, while the opposite is noticed for the bpt-NH^- ligand. The answer to this is not obvious and requires further investigation of the complexes. A possible reason might be the fact that bpt-NH^- has the possibility to act as either a 5- or 6-membered bidentate ligand as seen in **Figure 70**. While it may form a 5-membered ring complex with iridium, the analogous ring complex with rhodium might not have been possible, or *vice versa*. This could change the kinetic rate significantly.

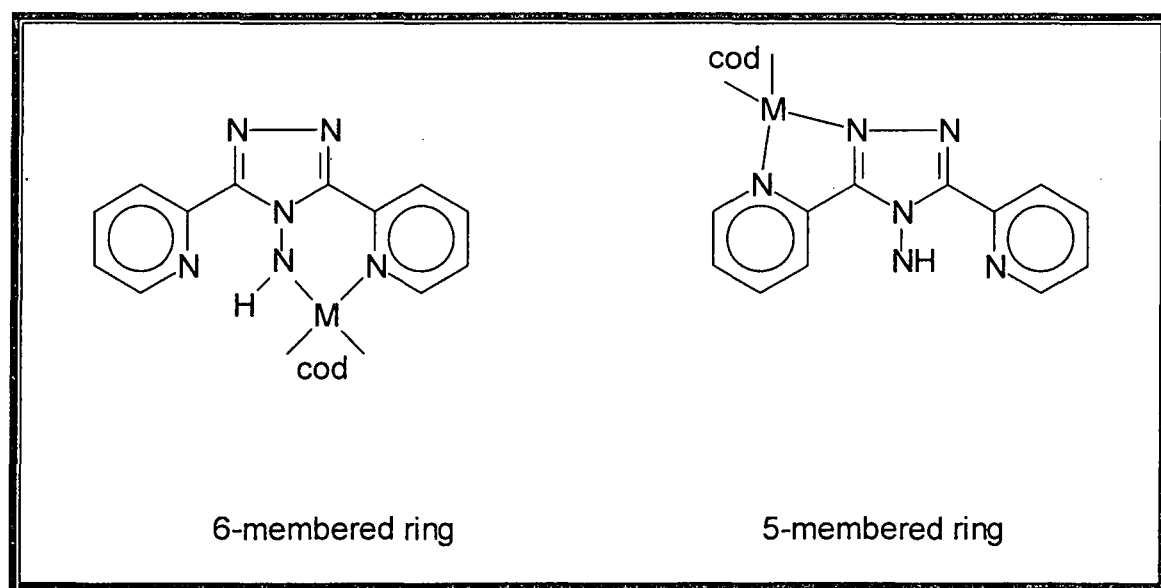


Figure 70: Possible rearrangement of the bonding sites of bpt-NH^- to a metal atom.

Although a lot of work was done by our group to determine the effect of ring size on the rate of oxidative addition, there is still not a definitive answer on this as seen from **Table 17**.

Also included in this table are the kinetic data for the studied iridium complexes to compare them to other similar complexes studied by our group. The complexes are comparable to the S-O-donor atom complexes when done in the correct solvent. It should be noted that not only the donor atoms play an important role, but the groups bonded to it as well.

Table 17 : Summary of the kinetic data for the oxidative addition between CH_3I and $[\text{Ir}(\text{LL}')(\text{cod})]$ with different solvents and ring sizes.

Complex	Donor atoms	Ring size	$k_1 \times 10^2$ ($\text{M}^{-1}, \text{s}^{-1}$)	Solvent
$[\text{Ir}(\text{macsm})(\text{cod})]$	S-N	6	2.84(7)	acetonitrile
$[\text{Ir}(\text{AnMetha})(\text{cod})]$	S-O	5	2.69(6)	nitromethane
$[\text{Ir}(\text{hpt})(\text{cod})]$	S-O	5	2.2(2)	nitromethane
$[\text{Ir}(\text{bpt-NH})(\text{cod})]$	N-N	5/6	1.44(7)	dichloromethane
$[\text{Ir}(\text{sacac})(\text{cod})]$	S-O	6	0.52(3)	acetonitrile
$[\text{Ir}(\text{tfaa})(\text{cod})]$	O-O	6	0.44(2)	acetonitrile
$[\text{Ir}(\text{cupf})(\text{cod})]$	O-O	5	0.217(7)	acetonitrile
$[\text{Ir}(\text{AnMetha})(\text{cod})]$	S-O	5	0.943(10)	acetone
$[\text{Ir}(\text{hpt})(\text{cod})]$	S-O	5	0.693(17)	acetone
$[\text{Ir}(\text{sacac})(\text{cod})]$	S-O	6	0.34(2)	acetone
$[\text{Ir}(\text{bpt})(\text{cod})]$	N-N	5	0.35(1)	acetone
$[\text{Ir}(\text{bpt-NH})(\text{cod})]$	N-N	5/6	0.0919(4)	benzene

c) The implication of the activation parameters.

The activation parameters in Table 16 can be used to determine the type of transition state for the reactions involved. The values

OXIDATIVE ADDITION KINETICS OF CH₃I WITH [M(LL')(cod)] COMPLEXES

are characterised by positive values for ΔH^\ddagger and relative large negative values for ΔS^\ddagger . This indicates that bond formation plays an important role on the formation of the transition state in an associative mechanism.

Addendum A

Supplementary kinetic aspects.

a) Kinetic data.

Table 18 : Kinetic results for the oxidative addition between CH_3I and $[\text{Ir}(\text{bpt})(\text{cod})]$ in acetone at different temperatures.

Temperature (K)	$[\text{CH}_3\text{I}]$ ($\text{mol}\cdot\text{dm}^{-3}$)	$k_{\text{obs}} \times 10^4$ (s^{-1})	$k_1 \times 10^2$ ($\text{M}^{-1}\cdot\text{s}^{-1}$)	$k_{-1} \times 10^4$ (s^{-1})
288.9	0.0202	0.4223(4)	0.141(6)	1.8(5)
	0.0370	0.6863(6)		
	0.0657	1.142(1)		
	0.0905	1.503(2)		
	0.1221	1.994(4)		
	0.1693	2.491(6)		
302.5	0.0196	0.961(1)	0.35(1)	0.4(1)
	0.0338	1.633(3)		
	0.0717	3.055(5)		
	0.1224	4.64(2)		
	0.1582	5.96(3)		
311.3	0.0177	1.287(2)	0.58(2)	0.3(1)
	0.0322	2.142(6)		
	0.0627	4.02(2)		
	0.0913	5.33(3)		
	0.1276	7.78(6)		

ADDENDUM A

Table 19 : Kinetic results for the oxidative addition between CH₃I and [Ir(bpt-NH)(cod)] in benzene at different temperatures.

Temperature (K)	[CH ₃ I] (mol.dm ⁻³)	k _{obs} × 10 ⁴ (s ⁻¹)	k ₁ × 10 ² (M ⁻¹ .s ⁻¹)	k ₋₁ × 10 ⁴ (s ⁻¹)
287.9	0.0190	0.131(1)	0.044(2)	0.02(2)
	0.0552	0.234(1)		
	0.0899	0.412(2)		
	0.1419	0.629(4)		
	0.2120	0.976(4)		
297.8	0.0206	0.228(1)	0.092(5)	0.03(6)
	0.0364	0.372(1)		
	0.0583	0.608(3)		
	0.0917	0.912(6)		
	0.1390	1.16(1)		
310.6	0.0187	0.493(1)	0.184(3)	0.15(3)
	0.0459	1.019(2)		
	0.0896	1.739(9)		
	0.1448	2.834(1)		
	0.1752	3.37(2)		

Table 20 : Kinetic results for the oxidative addition between CH₃I and [Ir(bpt-NH)(cod)] in DCM at different temperatures.

Temperature (K)	[CH ₃ I] (mol.dm ⁻³)	k _{obs} × 10 ⁴ (s ⁻¹)	k ₁ × 10 ² (M ⁻¹ .s ⁻¹)	k ₋₁ × 10 ⁴ (s ⁻¹)
288.7	0.0291	2.72(2)	1.00(5)	-0.2(5)
	0.0586	5.93(3)		
	0.0807	7.10(7)		
	0.1093	11.29(8)		
	0.1407	13.40(1)		
297.9	0.1782	17.80(2)	1.44(7)	1.1(8)
	0.0320	6.18(4)		
	0.0554	9.61(7)		
	0.0710	10.5(1)		
	0.1429	20.9(3)		
304.1	0.1760	27.3(3)	2.5(2)	-1(2)
	0.0448	10.87(8)		
	0.0699	15.4(2)		
	0.0880	20.3(2)		
	0.1049	23(3)		
	0.1425	36.9(4)		
	0.1778	42.2(6)		

SUPPLEMENTARY KINETIC ASPECTS

Table 21 : Kinetic results for the oxidative addition between CH_3I and $[\text{Rh}(\text{bpt})(\text{cod})]$ in acetone at different temperatures.

Temperature (K)	$[\text{CH}_3\text{I}]$ ($\text{mol}\cdot\text{dm}^{-3}$)	$k_{\text{obs}} \times 10^4$ (s^{-1})	$k_1 \times 10^2$ ($\text{M}^{-1}\cdot\text{s}^{-1}$)	$k_{-1} \times 10^4$ (s^{-1})
298.5	0.0581	0.0845(3)	0.0136(8)	0.008(9)
	0.0782	0.1241(6)		
	0.0991	0.1332(3)		
	0.1208	0.1743(4)		
	0.1429	0.2035(3)		
	0.1606	0.2274(4)		
301.9	0.0621	0.1391(3)	0.021(2)	0.01(2)
	0.0860	0.1963(2)		
	0.1197	0.263(2)		
	0.1432	0.3121(4)		
307.5	0.0599	0.2387(7)	0.039(3)	-0.01(3)
	0.0893	0.3282(4)		
	0.1166	0.4438(5)		
	0.1388	0.5470(4)		

Table 22 : Kinetic results for the oxidative addition between CH_3I and $[\text{Rh}(\text{bpt-NH})(\text{cod})]$ in benzene at different temperatures.

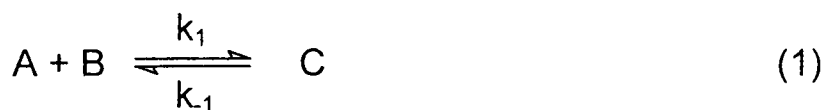
Temperature (K)	$[\text{CH}_3\text{I}]$ ($\text{mol}\cdot\text{dm}^{-3}$)	$k_{\text{obs}} \times 10^4$ (s^{-1})	$k_1 \times 10^2$ ($\text{M}^{-1}\cdot\text{s}^{-1}$)	$k_{-1} \times 10^4$ (s^{-1})
288.9	0.0237	0.2762(4)	0.114(3)	0.03(2)
	0.0380	0.5006(5)		
	0.0592	0.689(1)		
	0.0913	1.079(2)		
	0.1095	1.266(3)		
	0.1273	1.481(3)		
297.5	0.0299	0.753(2)	0.21(2)	0.01(2)
	0.0530	1.223(3)		
	0.0764	1.751(5)		
	0.1102	2.394(8)		
307.7	0.0191	0.881(1)	0.429(6)	-0.01(5)
	0.0391	1.630(3)		
	0.0547	2.332(4)		
	0.0704	2.945(6)		
	0.1048	4.50(2)		
	0.1413	6.09(3)		

Table 23 : Kinetic results for the oxidative addition between CH_3I and $[\text{Rh}(\text{bpt-NH})(\text{cod})]$ in DCM at different temperatures.

Temperature (K)	$[\text{CH}_3\text{I}]$ ($\text{mol}\cdot\text{dm}^{-3}$)	$k_{\text{obs}} \times 10^4$ (s^{-1})	$k_1 \times 10^2$ ($\text{M}^{-1}\cdot\text{s}^{-1}$)	$k_{-1} \times 10^4$ (s^{-1})
288.9	0.0292	4.83(1)	1.23(3)	-1.3(3)
	0.0588	8.54(3)		
	0.0722	9.97(4)		
	0.1094	15.4(6)		
	0.1436	19.0(1)		
	0.1936	25.0(1)		
297.9	0.0418	9.64(3)	2.20(3)	0.4(3)
	0.0530	12.04(5)		
	0.0722	16.54(6)		
	0.1085	23.6(1)		
	0.1435	32.3(1)		
	0.1752	38.9(2)		
303.9	0.0292	9.89(3)	2.9(1)	2(2)
	0.0588	21.26(9)		
	0.0722	23.0(1)		
	0.1094	30.8(2)		
	0.1436	43.9(2)		
	0.1936	58.1(2)		

b) Mathematical proof of Eq.5 in Chapter 4.

Consider the reaction



The rate of this reaction can be expressed as

$$-\frac{d[\text{A}]}{dt} = \frac{d[\text{C}]}{dt} = k_1[\text{A}][\text{B}] - k_{-1}[\text{C}] \quad (2)$$

where $[\text{A}]$ = concentration of reactant A
 $[\text{B}]$ = concentration of reactant B
 $[\text{C}]$ = concentration of product C

Under pseudo-first order conditions where $[B] \gg [A]$, equation 2 simplifies to

$$-\frac{d[A]}{dt} = \frac{d[C]}{dt} = k'_1[A] - k_{-1}[C] \quad (3)$$

where $k'_1 = k_1[B]$

If the reaction reaches equilibrium, the following equation would be true

$$-\frac{d[A]_{\text{eq}}}{dt} = \frac{d[C]_{\text{eq}}}{dt} = 0 \quad (4)$$

where $[A]$ = concentration of reactant A at equilibrium
 $[C]$ = concentration of product C at equilibrium

From equation 4 and 2 we get

$$\frac{k'_1}{k_{-1}} = \frac{[C]_{\text{eq}}}{[A]_{\text{eq}}} \quad (5)$$

If the initial concentration of A is given the value of A_0 we can manipulate equation 5 to

$$\frac{k'_1}{k_{-1}} = \frac{[A]_0 - [A]_{\text{eq}}}{[A]_{\text{eq}}}$$

$$[A]_{\text{eq}} = \left(\frac{k_{-1}}{k'_1 + k_{-1}} \right) [A]_0 \quad (6)$$

We also apply this manipulation to equation 3

$$\begin{aligned} \frac{d[A]}{dt} &= -k'_1[A] + k_{-1}([A]_0 - [A]) \\ &= -k'_1[A] + k_{-1}[A]_0 - k_{-1}[A] \\ &= -(k'_1 + k_{-1})[A] + k_{-1}[A]_0 \end{aligned}$$

$$= -(k'_1 + k_{-1}) \left([A] - \frac{k_{-1}}{k'_1 + k_{-1}} [A]_0 \right) \quad (7)$$

From equations 6 and 7 we get

$$\frac{d[A]}{dt} = -(k'_1 + k_{-1})([A] - [A]_{eq}) \quad (8)$$

By grouping the variables in equation 8, we can then integrate to remove the differential signs

$$\begin{aligned} \frac{d[A]}{[A] - [A]_{eq}} &= -(k'_1 + k_{-1}) \\ \int_{[A]_0}^{[A]} \frac{d[A]}{[A] - [A]_{eq}} &= -(k'_1 + k_{-1}) \int_{t=0}^{t=t} dt \\ \ln([A] - [A]_{eq}) \Big|_{[A]_0}^{[A]} &= -(k'_1 + k_{-1}) [t]_{t=0}^{t=t} \\ \ln \left(\frac{[A]_0 - [A]_{eq}}{[A] - [A]_{eq}} \right) &= (k'_1 + k_{-1}) t \end{aligned} \quad (9)$$

The sum of the two constants ($k'_1 + k_{-1}$) is also a constant. By definition this constant is the observed rate, k_{obs} . Thus we have

$$k_{obs} = k'_1 + k_{-1}$$

Therefore

$$k_{obs} = k_1[B] + k_{-1} \quad (10)$$

Addendum B

Purification of Solvents¹⁴⁶

Acetone

The main impurity in acetone is mesityl oxide. Water is removed by leaving 1L of acetone overnight over 400g K_2CO_3 (previously dried at 200 - 300°C). Approximately 100g of finely powdered NaI was then dissolved in 440g of boiling acetone. The solution was cooled in an ice/salt mixture to -8 °C. The crystals of $NaI \cdot 3C_3H_6O$ that formed were filtered off and warmed in a flask to distil the pure acetone.

Benzene

Water, thiophen and olefinic impurities are usually found in benzene. These impurities are removed by shaking 1L of benzene with 150 cm³ concentrated H_2SO_4 . This was repeated until the acid layer remains colorless. The benzene was then successively shaken with water and diluted NaOH to neutralise any remaining acid. The benzene was left overnight in a flask over $CaCl_2$ and fractionally distilled from CaH_2 .

Dichloromethane

Dichloromethane was shaken with small portions of concentrated H_2SO_4 until the acid layer remained colorless. The acid was neutralised by successively shaking it with water and $NaHCO_3$

¹⁴⁶ Perrin, D.D.; Armarego, W.L.F., *Purification of Laboratory Chemicals*, Pergamon Press (1988)

(5%). The dichloromethane was left standing overnight in a flask with CaCl_2 and then fractionally distilled over CaH_2 . Dichloromethane was stored in a dark bottle under an inert atmosphere to prevent decomposition.

Methanol

Methanol was left standing overnight in a flask containing freshly activated molecular sieves. It was then fractionally distilled from CaH_2 .

Summary

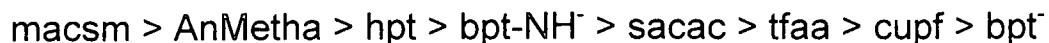
A number of triazolecyclooctadienemetal(I) complexes of the type $[M(LL')(cod)]$ (where $M = Ir$ or Rh and LL' represents the different bidentate N-N'- donor atom ligands, such as $bpt-NH^-$ and bpt^-) as well as their oxidative addition products $[M(LL')(cod)(Me)(I)]$ have been prepared and characterised by IR, 1H NMR and elemental analyses. It was found that in general these complexes are monomeric containing one LL' and cod ligand respectively.

The oxidative addition between CH_3I and the studied metal(I) complexes have been investigated on a UV/Vis spectrophotometer. Under pseudo-first order conditions linear relationships were found indicating second order kinetics. All of the kinetic data had zero intercepts (within experimental error) indicating that no reverse reactions occur. The reactions were carried out in different solvents to study the influence of solvent properties on the reaction rate.

The reactions were also conducted at different temperatures to calculate the activation parameters. These indicated an associative mechanism as what is usually expected from these types of complexes.

The ability of the LL' bidentate ligands to increase the Lewis basicity of the metal center are reflected in the values of the second order rate constants. From this we can compile the

following series indicating the different bidentate ligands' donating capabilities:



The activation ability of the bpt-NH⁻ ligand for oxidative addition to the metal center is better than that of the bpt⁻ ligand given the correct solvent and metal center are chosen. It seems that in the case of the [M(bpt-NH)(cod)] complexes the rhodium analogue is more reactive, while the opposite case is observed for the [M(bpt)(cod)] complexes. Thus the bpt-NH⁻ ligand is the better σ -donor in the rhodium complex, while the bpt⁻ ligand is the better σ -donor in the iridium complex.

Opsomming

'n Aantal triasoolsiklooktadiëenmetaal(I) komplekse van die tipe $[M(LL')(cod)]$ (waar $M = Ir$ of Rh en LL' verskillende bidentate ligande met N-N'-donoratome soos byvoorbeeld $bpt-NH^-$ en bpt^-) sowel as hulle oksidatiewe produkte $[M(LL')(cod)(Me)(I)]$, is berei en gekarakteriseer met behulp van IR, 1H KMR en elementanalises. In die algemeen is die bestudeerde komplekse monomeries met een bidentate ligand en 'n siklooktadiëenmolekuul.

Die oksidatiewe addisie van CH_3I aan die metaal(I) komplekse is bestudeer op 'n UV/Sigbare spektrofotometer. Onder pseudo-eerste-orde kondisies word 'n reglynige verband gevind, kenmerkend van tweede-orde kinetika. Al die kinetiese data het binne eksperimentele fout nulafsnitte wat daarop dui dat geen terugwaartse reaksie plaasvind nie. Die reaksie is ook in verskillende oplosmiddels gedoen om die effek van oplosmiddeleienskappe op die reaksietempo te bestudeer.

Die reaksies is ook by verskillende temperature gedoen om die aktiveringsparameters te bepaal. Die eksperimentele waardes is kenmerkend van 'n assosiatiewe meganisme soos verwag word vir hierdie tipe komplekse.

Die vermoë van die bidentate ligande om die Lewisbasisiteit van die metaalsentrum te verhoog word in die waardes van die tweede-ordetempokonstantes weerspieël en op grond daarvan is die ligande volgens hul doneringsvermoë in die volgende ordereeks geplaas:



Die aktiveringsvermoë van bpt-NH^- vir oksidatiewe addisie van die metaalsentrum is beter as die van die bpt^- ligand, gegewe die korrekte oplosmiddel en metaalsentrum. Dit blyk dat in die geval van die $[\text{M}(\text{bpt-NH})(\text{cod})]$ -komplekse die rodiumanalooq meer reaktief is, terwyl die teenoorgestelde waargeneem word vir $[\text{M}(\text{bpt})(\text{cod})]$ -komplekse. Dus is die bpt-NH^- ligand die beter σ -donor in die rodiumkompleks, terwyl die bpt^- in die iridiumkompleks die beter σ -donor is.

U.O.V.S. BIBLIOTEK